THÈSE

En vue de l'obtention du

DOCTORAT DE L'UNIVERSITÉ DE TOULOUSE

Délivré par :

Université Toulouse 3 Paul Sabatier (UT3 Paul Sabatier)

Cotutelle internationale avec l'Université de Xi'an Jiaotong

Présentée et soutenue par :
Linlin ZHONG

le vendredi 16 juin 2017

Titre :

Influence of copper contamination on thermophysical, radiation, and dielectric breakdown properties of CO2-N2 mixtures as Replacement of SF6 in Circuit Breakers

---

École doctorale et discipline ou spécialité :
ED GEET : Ingénierie des PLASMAS

Unité de recherche :
LAPLACE, UMR 5213

Directeur/trice(s) de Thèse :

Yann CRESSAULT, Maître de Conférences, Université Paul Sabatier, Toulouse, France
Mingzhe RONG, Professeur, Université de Xi'an Jiaotong, Xi'an, China

Jury :
M. Yann CRESSAULT, Maître de Conférences, Université Paul Sabatier, CoDirecteur
M. Mingzhe RONG, Professeur, Université de Xi'an Jiaotong, CoDirecteur
M. Pascal ANDRÉ, Professeur, Université Blaise Pascal - Clermont-Ferrand II, Rapporteur
Mme Zhihong XU, Professeur, Université de Fuzhou, Rapporteur
M. Georges ZISSIS, Professeur, Université Toulouse III - Paul Sabatier, Examinateur
M. Xiaohua WANG, Professeur, Université de Xi'an Jiaotong, Examinateur

AUTHOR : Linlin ZHONG

TITLE : Influence of copper contamination on thermophysical, radiation, and dielectric breakdown properties of CO_2-N_2 **m**ixtures as Replacement of SF_6 in Circuit Breakers

THESIS SUPERVISOR : Yann CRESSAULT

SITE : LAPLACE UMR 5213 CNRS, Université Paul Sabatier, 118 route de Narbonne, Bât. 3R3, 31062 Toulouse Cedex 9

_____

Abstract

Sulfur hexafluoride (SF_6) is a greenhouse gas designated by the Kyoto Protocol because of its extremely high global warming potential (GWP). CO_2, N_2, and their mixtures have the potential to replace SF_6 in certain applications, such as circuit breakers. In these electric apparatus, copper vapour resulting from the heating of electrodes can modify the characteristics of arc plasmas, which must be taken into account when setting up physical models. This dissertation, therefore, investigates the thermodynamic, transport, diffusion, radiation, and dielectric breakdown properties of CO_2-N_2 mixtures contaminated by copper at temperatures of $300 - 30,000$ K and pressures of $0.1 - 16$ bar.

The equilibrium compositions are calculated using the minimization of Gibbs free energy with consideration of condensed species. Copper vapour is found to condense at temperatures below 3000 K. Based on the compositions, the thermodynamic properties, including mass density, specific enthalpy, and specific heat at constant enthalpy, are determined according to their definitions. The Debye-Hückel corrections are also considered in the calculation of compositions and thermodynamic properties.

The transport coefficients (including electrical conductivity, viscosity, thermal conductivity) and combined diffusion coefficients (including the combined ordinary diffusion coefficient, combined electric field diffusion coefficient, combined temperature diffusion coefficient and combined pressure diffusion coefficient) are calculated based on the Chapman-Enskog theory. The newly developed Lennard-Jones like phenomenological model potential is adopted to describe the neutral-neutral and neutral-ion interactions in determining collision integrals.

The net emission coefficients (NEC) of gas mixtures are calculated with considering atomic lines and continuum and molecular bands and continuum. The pressure broadening (Van der Waals broadening and the resonance broadening), Stark broadening, and Doppler broadening are taken into account in the determination of escape factors. The continuum radiation of atoms is described by radiative attachment, radiative recombination, and Bremsstrahlung.

The dielectric breakdown properties (including EEDF, reduced ionization coefficient, reduced electron attachment coefficient, reduced effective ionization coefficient, and reduced critical electric field strength) of hot gas mixtures are calculated based on the two-term approximation of the Boltzmann equation. The interactions, including elastic, excitation, ionization and attachment collisions, between electrons and neutral species are taken into account in solving the Boltzmann equation. The ionization cross sections of Cu_2 and CuO which are unavailable in literatures are calculated using the DM method.

Compared with SF_6-Cu mixtures, CO_2-N_2-Cu mixtures present much different thermophysical, radiation, and dielectric breakdown properties. As an arc quenching gas, CO_2-N_2-Cu mixtures have lower $\rho \cdot C_p$ and thermal conductivity at low temperatures but present higher $\rho \cdot C_p$, thermal conductivity, and NEC in the medium temperature range. As an insulating medium, the hot CO_2-N_2-Cu mixtures have much poorer dielectric strength below 2000 K, whereas above 2000 K, they present better dielectric breakdown performance than SF_6-Cu mixtures.

Keywords

CO_2/N_2/Cu, circuit breakers, high voltage, transport properties, radiation properties, Chapman-Enskog method, Net emission coefficient, dielectric breakdown, SF_6 replacement.

ACKNOWLEDGEMENTS

TABLE OF CONTENTS

1.1 Background and motivation

1.1.1 SF$_6$ replacements

Sulfur hexafluoride (SF$_6$) is a nontoxic, nonflammable and chemically stable gas that is widely used as an arc quenching medium in medium-voltage (MV) and high-voltage (HV) circuit breakers and as an insulating medium in gas-insulated substations (GIS) and gas-insulated lines (GIL). However, SF$_6$ has been designated as one of the six greenhouse gases by the Kyoto Protocol because the global warming potential (GWP) of SF$_6$ is nearly 24000 times higher than that of CO$_2$ over a 100 year interval [1, 2]. Additionally, SF$_6$ decomposes into lower fluorides of sulphur which in turn react with electrodes or gas impurities to form many toxic products, such as sulphur dioxide, hydrofluoric acid and metal fluoride compounds, which are hazardous to maintenance personnel [3, 4]. Finding suitable substitutes to SF$_6$ is therefore an urgent task. Table 1-1 illustrates some potential alternatives.

Over the last few decades, the searching of SF$_6$ replacements have been divided into two directions: one to mix SF$_6$ with different buffer gases, and the other to replace SF$_6$ with completely new gases. In the former way, the buffer gases are always the ones with much lower GWP than SF$_6$, with which to generate various SF$_6$ mixtures, such as SF$_6$-N$_2$ [5-10], SF$_6$-O$_2$ [7], SF$_6$-CO$_2$ [1, 5, 11, 12], SF$_6$-CF$_4$ [13, 14], and SF$_6$-He [15, 16]. The latter way is to find relatively eco-friendly gases, such as some fluorinated compounds (e.g. CF$_4$ [17], CF$_3$I [18-22], C$_3$F$_8$ [2, 23, 24], c-C$_4$F$_8$ [25, 26], C$_5$F$_{10}$O [27-29], et al.) which also have lower GWP than SF$_6$. To a certain extent, these two ways can reduce the usage and/or emission of greenhouse gases in terms of GWP, but both have some disadvantages. The key problem of SF$_6$ mixtures lies in the fact that the buffer gases with relatively low dielectric strength weaken the insulating performance of the mixtures. For example, the reduced critical electric field strength (E/N)$_{cr}$ of SF$_6$-CO$_2$ mixtures at room temperature (300 K) drops down from 337 Td to 166 Td when

the proportion of CO_2 increases from 10% to 90% [1]. It seems that we have to make a compromise between dielectric performance and greenhouse effect. For the above fluorinated compounds, although most of them (except CF_4) have excellent dielectric strength and acceptable GWP values, the low boiling points (or liquefaction temperatures) restrict their applications in cold areas. For example, as listed in Table 1-1, GWP of c-C_4F_8 is only around 36% of SF_6, and the dielectric strength of c-C_4F_8 is about 1.35 times as large as that of SF_6, indicating that c-C_4F_8 is a good replacement of SF_6. However, the liquefaction temperature of c-C_4F_8 is about -6 °C at ambient pressure while the lowest temperature in many cities of northern countries (e.g. Iceland and Canada) reaches -30 °C or even lower. In order to increase the boiling point of these gases, it is necessary to mix them with some background gases with low boiling points (e.g. CO_2, O_2, N_2, Air, Ar, et al.) [2], but the side effect is the sacrifice of dielectric performance.

Table 1-1. Relative critical dielectric strength (E_{cr}), global warming potential (GWP) and boiling points (T_b) of SF_6 and its potential substitutes at ambient pressure.

Gas	E_{cr}	GWP	T_b (°C)	Source(s)
SF_6	1.00	23900	-63.8	[30, 31]
N_2	0.36	0	-198	[30, 31]
O_2	0.33	0	-183	[32]
Air	~0.3	0	-194	[30]
CO	0.40	2.1	-191.5	[30]
CO_2	0.30	1	-78	[30, 31]
CF_4	0.42	6300	-128	[13, 33]
CF_3I	1.21	< 5	-22.5	[31]
C_3F_8	0.96	7000	-37	[31]
c-C_4F_8	1.35	8700	-6	[30, 31]
$C_5F_{10}O$	2.07	1	27	[28]

Moreover, much more attentions were paid to the alternatives of SF_6 in dielectric applications, whereas less attentions were attracted to the substitutes of SF_6 in the arc interruption of circuit breakers. The non-ignorable fact is that a large amount of MV and HV SF_6 circuit breakers are used all over the world. The statistics show that SF_6 circuit breakers hold a 70% market share of in-service units 66 kV and above in power systems [4]. By the year 2025, a close to 100% SF_6 monopoly is expected in this range without change [4]. That is why we need to investigate the substitutes to SF_6 as an arc quenching gas in circuit breakers. It is known that the low dissociation temperature and high dissociation energy of SF_6 attribute to its excellent arc quenching performance. This implies that some gases e.g. C_3F_8 [2] are not good replacements as arc quenching medium because they decompose very quickly when gas temperature is above 300 K. It is also well known that SF_6 decomposes during the arc interruption and recombines into itself after the arc extinction. This mechanism ensures SF_6 to endure the transient recovery voltage (TRV) during the current interruption process, considering that the dielectric strength of SF_6 is much better than its dissociation products. Unfortunately, some good SF_6 replacements in terms of insulating ability and GWP, such as c-C_4F_8 and CF_3I, cannot recombine as SF_6 into the original molecules when the arc temperature goes down. This means that such gases are not ideal arc quenching medium even though they show great potential in insulating applications.

In a word, no gas or gas mixture has been proved to satisfy both sides so that it can replace SF_6 entirely. Currently we have to compromise between dielectric strength and global warming potential, and between insulating performance and interruption ability. As a result, CO_2 and N_2 have been chosen as potential alternatives of SF_6 in this work. Although CO_2, N_2 and their mixtures are not the best insulator among the potential gases, they have balanced performance both in gas insulation and in arc extinction. Meanwhile, as shown in Table 1-1, the extremely low GWP of CO_2 and N_2 also adds their advantage in preventing global warming. Actually, CO_2 and N_2 have already been applied to replace SF_6 and reduce GWP, for example, as insulating medium in gas-

insulated switchgears (GIS) [34] and as arc quenching medium in gas circuit breakers (GCB) [35]. In order to investigate CO_2-N_2 mixtures applied in circuit breakers, a complete database composed of thermophysical, radiation, and dielectric breakdown properties of gas mixtures (including the influences of copper impurities coming from the electrodes) is essential to be established. This is one of the main issues in this dissertation.

1.1.2 Copper contamination in circuit breakers

In a number of arc devices, such as circuit breakers, arc heaters, torches, and arc welding apparatus, etc., the arc at high current interacts strongly with the electrodes [36, 37]. The metallic vapour resulting from the heating of electrode surfaces in arc devices can modify the characteristics of the arc plasma. For example, in SF_6 circuit breakers, copper contamination leads to the condensation of CuF_2 at temperatures below 2000 K [37]. Chervy et al. [38], Paul et al. [39] and Wang et al. [40] all found that the electrical resistance of SF_6-Cu mixtures is strongly dependent on copper concentration. Specifically, copper vapour raises the electrical conductivity of SF_6-Cu mixtures at temperatures of 5000 – 16,000K, whereas reduces the electrical conductivity above 16,000 K [40]. Also, Zhong's et al. [41] and Cressault's et al [42] works on the combined diffusion coefficients revealed the significant effect of metallic vapour on SF_6 and Air plasmas. In addition to thermodynamic properties and transport coefficients, copper vapour also affects the dielectric breakdown properties of arc plasmas in circuit breakers. The work by Wang et al. [43] shown that the existence of copper compounds in SF_6-Cu mixtures increases the concentration of high-energy electrons significantly even in the case with very low percentage of copper (e.g. 1% Cu) at temperatures of 300 – 3500 K. The similar result was observed in Air plasma. According to the work of Tanaka [44], copper vapour remarkably increases the effective ionization coefficient of air and thus decreases its critical electric field strength significantly. In arc welding, the presence of metallic vapour was proved to have a major influence on the properties of arc and the size and shape of weld pool [45]. In the extinction process of circuit breakers,

4

the copper contamination due to electrode erosion was also proved to have a cooling effect at the arc center and broaden the arc column [36, 46, 47].

To sum up, copper contamination plays an essential role in describing arc plasmas, and therefore, the properties of plasmas contaminated by copper vapour have to be determined before setting up physical models [38]. However, little attention has been paid to the effects of metallic impurities on the CO_2-N_2 plasmas. This is another issue this dissertation focuses on.

1.2 Research review

CO_2, N_2 and their mixtures have been studied for a long time because of their wide applications both in astrophysics and industries and both through experimental and theoretical approaches. Compared with experiments, physical modelling is a more low-cost but still efficient method for the plasma investigation. Since the properties of thermal plasmas are the prerequisite of their modellings, the present work is dedicated to the thermophysical, radiation, and dielectric breakdown properties of CO_2-N_2 mixtures and the effects of copper contamination on these properties. Before that, a review of research in the thermodynamic and transport properties, radiation coefficients, and dielectric breakdown properties is presented in the following subsections 1.2.1-1.2.3 respectively.

1.2.1 Thermodynamic, transport, and combined diffusion coefficients

As the main components of many planetary atmospheres (e.g. Martian and Venusian atmospheres), the high-temperature CO_2, N_2 and CO_2-N_2 mixtures have been investigated for their thermodynamic and transport properties since 1960s. In 1963, Yos [48] published a database composed of the viscosity, thermal conductivity, electrical conductivity, binary diffusion coefficients as well as radiation power for four kinds of gases including N_2. The calculation in his work was carried out with a mixing rule of unknown accuracy. Therefore, Capitelli and Devoto [49] recalculated the transport coefficients of high-temperature N_2 plasma using the improved intermolecular

5

potentials and cross sections. Then, this work was further improved by Murphy and Arundell [50] in 1994 through the use of the more accurate collision integrals in N_2 plasma. In 1969, Lee and Bobbitt [51] published the viscosity, thermal conductivity, and Prandtl number of the gas mixtures (including pure CO_2 and the mixture of CO_2, N_2 and Ar). After that in 1970, in order to study Martian and Venusian atmospheres, Freeman and Oliver [52] determined the equilibrium compositions of CO_2-N_2 mixtures, and based on this they calculated the total specific heat, thermal conductivity, and Prandtl number of the mixtures. However, the data given in these two works are not sufficient for plasma modelling not only because some crucial data (e.g. viscosity, electrical conductivity, and diffusion coefficients) are missing but also because the upper limit of the plasma temperature (8000 K in [51] and 15,000 K in [52]) is not high enough to cover the maximal temperatures in certain applications (e.g. in circuit breakers). In 1995 Romanov et al. [53] presented the composition and thermodynamic properties of 96.5%CO_2-3.5%N_2 (Martian atmosphere) without transport coefficients. Recently Capitelli et al. [54] reported the latest collision integrals for the atomic and molecular interactions in CO_2-N_2 mixtures using a phenomenological method. Shortly, Laricchiuta et al. [55] published the latest transport cross sections for the species in Mars atmosphere including CO_2, N_2 and their mixtures. In their work, the phenomenological approach was also adopted for the derivation of the elastic collision integrals in neutral-neutral and neutral-ion interactions. At the same time, Catalfamo et al. [56] applied these data to determine the high-temperature transport properties of CO_2-N_2-Ar mixtures at temperatures up to 50,000 K.

With regard to the influences of copper contamination on the properties of CO_2-N_2 mixtures, few works could be found in literatures. Shayler and Fang [57] calculated the thermodynamic and transport properties of N_2-Cu mixtures. The results show that a small concentration of copper vapour can greatly enhance the electrical conductivity of N_2 plasma at temperatures below 8000 K [57]. The work on CO_2-Cu was published recently. Yang et al. [58] presented a calculation of equilibrium compositions,

6

thermodynamic properties, and transport coefficients (including viscosity, electrical conductivity, and thermal conductivity) for CO_2-Cu thermal plasmas. The similar result was found that a small quantity of copper vapour significantly influences the number density of charged species and thus modify the electrical conductivity of gas mixtures especially at low temperatures [58]. However, no work on CO_2-N_2-Cu mixtures has been reported so far.

Apart from the viscosity, electrical conductivity and thermal conductivity, the combine diffusion coefficients which were proposed by Murphy [59-64] and greatly simplify the treatment of diffusion, are indispensable input data in developing models of metallic vapour transfer both in arc welding [65] and in circuit breakers [66, 67]. Zhong et al. [41] and Cressault et al [42] published the combined diffusion coefficients in SF_6-Cu and Air-metal plasmas respectively. However, there are no works on the combined diffusion coefficients for CO_2-N_2-Cu mixtures.

1.2.2 Radiation properties

In the high-power arc applications (e.g. circuit breakers and arc welding), the radiation can present a predominant term in the energy balance [68]. In order to describe the radiation in a physical modelling, several radiation models were proposed [69], such as the semi-empirical model based on the net emission coefficients (NEC) [70, 71], the multi-band P1 model [72], and the method of partial characteristics [73, 74]. Among these models, the NEC-based model is mostly and widely used because of its good estimation ability and lowest computation cost [69]. The NEC-based model requires the NEC data of thermal plasmas which have been studied comprehensively since the work of Liebermann and Lowke [75] in 1976. After that, Gleizes, Cressault, and their colleagues [9, 68, 76-86] published the NEC of various gas mixtures, such as Ar, He, H_2, N_2, CO_2, CH_4, C_2F_4, SF_6, and Air which are widely used in industry. For example, Gleizes et al. [9] calculated the NEC of N_2 plasma in the temperature range of 8000 – 24,000 K. As shown in their results, the nitrogen lines are more strongly absorbed than the lines of sulphur and fluorine [9]. However, due to the selected temperature in their

work, only the atomic species were taken into account. As for CO_2 plasma, to overcome the poor ability in describing the radiation absorption in cold areas (e.g. the region near the cold wall), Cressault et al. [87] approximated the absorption of a gray body in several frequency ranges as an alternative to the NEC. The coefficient determined in this method is known as the mean absorption coefficient (MAC). For the mixture of CO_2 and N_2, the radiation emission spectrum of CO_2-N_2 plasma at atmospheric pressure was measured and calculated by Vacher et al. [88] and Lino da Silva et al. [89] respectively. Besides that, no works relating to the radiation coefficients have been reported for the CO_2-N_2 mixtures up to now.

Due to the important effects of metallic impurities, some previous works can be found on the NEC of metal-contaminated plasmas, such as Ar-Cu [68, 85], Ar-Fe [68, 85, 90], Ar-Al [85], N_2-Cu [68], CO_2-Cu [82], SF_6-Cu [68], Air-Cu/W [91]. For example, based on the calculation for N_2-Cu plasma, Gleizes et al. [68] found that the influence of copper radiation on the temperature field of arc plasma is dominant at higher currents, whereas the effect of electrical conductivity becomes important at lower currents. In regard to CO_2-Cu mixtures, Billoux et al. [82] determined the corresponding data of NEC with consideration of molecular bands. The metallic vapour was proved to strongly increase the NEC of CO_2-Cu plasma. However, for the NEC of CO_2-N_2-Cu plasmas, no results have been reported in the publications.

1.2.3 Dielectric breakdown properties

During the current interruption process in MV and HV circuit breakers, a high electric field strength caused by a transient recovery voltage (TRV) is applied to the hot working gas (e.g. Air, CO_2, SF_6, et al.) between the electrodes and between the exhaust tube and grounded tank [43, 92]. If the hot gas has a lower dielectric strength than the applied electric field strength, the gas breakdown known as 'dielectric failure' will occur, leading to the re-ignition of the arc [43, 44, 92]. In order to better understand the gas breakdown occurring in circuit breakers, it is necessary to know the dielectric breakdown properties (including ionization coefficient, electron attachment coefficient,

and critical electric field strength) of hot working gas during the dielectric recovery phase [43]. Contrary to "cold" which means the temperature is limited to room temperature (300 K), the "hot" means the temperature of working gas can reach above 300 K. Practically, the temperature of working gas in this work is set to vary from 300 K to 3500 K, representing the arc extinction process after the current zero. The works on the dielectric properties of cold gases primarily focus on their insulation applications while the works on the dielectric breakdown properties of hot gases concentrate on their usage in arc interruption.

There have been a lot of works on the dielectric properties of cold and/or hot gases in circuit breakers, and most of the publications on dielectric breakdown properties are related to SF_6 and its potential replacements. Yan et al. [93], Cliteur et al. [94] and Yousfi et al. [95] successively performed a numerical investigation to predict the dielectric breakdown properties of hot SF_6 gas. Rothhardt et al. [96, 97] and Dubinov et al. [98-100] reported the corresponding experimental results. The dielectric breakdown performance of hot SF_6 mixed with other buffer gases (e.g. N_2 [8] , CF_4 [13, 14], CO_2 [1], and He [15]) was also studied to find an alternative arc quenching medium [43].

As for CO_2, N_2 and/or their mixtures, the majority of the relating works focus on the cold gases or mixtures as insulating medium. For example, Ohmori et al. [101] studied the electron swarm behaviour of cold N_2 by a Boltzmann equation method. Qiu et al. [6] measured the breakdown voltage of CO_2 and N_2 gases when studying SF_6-CO_2 and SF_6-N_2 mixtures. Xiao et al. [102] determined the swarm parameters of CO_2 in a pulsed Townsend discharge. Xiao et al. [103] also applied the Monte Carlo method to simulate the electron transport of CO_2 gas. The result of electron swarm coefficients for CO_2-N_2 mixtures was published by Yousfi et al. [104]. However, little attention was devoted to hot CO_2-N_2 mixtures. Only the similar works conducted by Tanaka [92] for N_2-O_2 mixtures, Rong et al. [105] for CO_2-O_2 mixtures, and Zhong et al. [1] for SF_6-CO_2 mixtures could be found in literatures.

9

The significant influence of copper contamination on dielectric breakdown performance was validated by Tanaka [44] and Wang et al. [43] for Air and SF_6 respectively. However, very few works could be found for CO_2-N_2 mixtures, except for the work by Li et al. [106] who investigated the critical electric field strength of CO_2-Cu mixtures using the Boltzmann analysis. Their work also revealed the remarkable effect of copper vapour on the dielectric breakdown properties of gas mixtures.

1.3 Thesis Structure

As previously described, CO_2-N_2 mixtures are one of the potential substitutes for SF_6 as insulating and arc quenching medium mostly applied in circuit breakers. The copper contamination resulting from electrode surfaces can modify the characteristics of arc plasmas. In order to study CO_2-N_2 arc contaminated by copper vapour, it is essential to establish a complete database of CO_2-N_2-Cu mixtures at various temperatures and pressures. Therefore, a comprehensive investigation of CO_2-N_2-Cu thermal plasmas is presented in this dissertation, covering the study of their compositions, thermodynamic properties, transport coefficients, combined diffusion coefficients, radiation properties, and dielectric breakdown properties. The difference between CO_2-N_2-Cu and SF_6-Cu mixtures is compared. The rest of the thesis is organized as follows.

Chapter 2 firstly determines the equilibrium compositions of CO_2-N_2-Cu mixtures using the minimization of the Gibbs free energy. The influences arising from the mixing ratio (CO_2:N_2), copper proportion, and gas pressure are all analysed. The condensed species which are likely to exist at very low temperatures are also discussed. After that, the thermodynamic properties, including mass density, specific enthalpy, and specific heat at constant pressure, are calculated and discussed in different conditions.

Next in Chapter 3, the collision integrals between each species in CO_2-N_2-Cu mixtures are determined before the calculation of the transport coefficients. Four kinds of interactions, namely neutral-neutral, neutral-ion, neutral-electron, and charged-

charged interactions, are taken into account. Then, the electrical conductivity, viscosity, thermal conductivity, and four kinds of combined diffusion coefficients (i.e. the combined ordinary diffusion coefficient, combined electric field diffusion coefficient, combined temperature diffusion coefficient, and combined pressure diffusion coefficient) are calculated and discussed.

Chapter 4 focuses on the radiation property i.e. the net emission coefficient (NEC) of CO_2-N_2-Cu plasmas. The atomic lines and continuum as well as molecular roles are taken into account. The influences of copper contamination, plasma size, and gas pressure are discussed.

Chapter 5 is devoted to the dielectric breakdown of CO_2-N_2-Cu mixtures in circuit breakers. Based on the results of the compositions presented in Chapter 2, the dielectric breakdown properties, including the electron energy distribution function (EEDF), reduced ionization coefficient, reduced electron attachment coefficient, reduced effective ionization coefficient, and reduced critical electric field strength, are determined by a two-term approximation of the Boltzmann equation at temperatures of 300 – 3500 K. The elastic and inelastic collisions between neutral particles and electrons are taken into account. The effects of copper vapour as well as gas pressure are analysed.

Finally, in the Chapter 6, the conclusions are drawn and the possible future works are presented.

It is notable that all the mixing ratios of mixtures in the whole dissertation are given in molar proportion. The copper proportion referred in this work represents the percentage of elemental copper in the entire gas mixture. For example, 10% Cu means elemental copper accounts for 10% content by volume in the studied mixture while CO_2 and N_2 make up the rest 90% content.

CHAPTER 2 COMPOSITIONS AND THERMODYNAMIC PROPERTIES OF CO$_2$-N$_2$-CU PLASMAS

2.1 Introduction

As described in Chapter 1, CO$_2$, N$_2$ and their mixtures are widely used in industry, and show potential to replace SF$_6$ in certain applications, such as medium voltage circuit breakers (MVCB). To well understand the characteristics of CO$_2$-N$_2$ arc plasmas, their compositions and thermodynamic properties at various conditions of temperatures, pressures, and mixing ratios are necessary to be investigated. The result for compositions is also the prerequisite of the calculation of transport, diffusion, radiation, and dielectric breakdown properties which will be presented in the next Chapters 3-5. The analysis of thermodynamic properties (e.g. specific heat) also helps to understand the behavior of transport coefficients (e.g. thermal conductivity). Moreover, considering that the copper impurities resulting from electrodes in circuit breakers significantly affect the characteristics of arc plasma, the influences of copper contamination on both compositions and thermodynamic properties are investigated in this chapter.

The rest of the sections are organized as follows. In section 2.2, the compositions of CO$_2$-N$_2$-Cu mixtures is determined assuming the local thermodynamic equilibrium (LTE). Firstly, the method of the minimization of Gibbs free energy is introduced in section 2.2.1 to calculate the equilibrium compositions with and without consideration of condensed phases. The evaluation of partition functions as one of the key procedures is discussed in section 2.2.2. Next in sections 2.2.3-2.2.6, the influences of condensed species, mixing ratio (CO$_2$:N$_2$), copper contamination, and gas pressure are analyzed respectively. Based on the results of compositions, the section 2.3 describes the thermodynamic properties (including mass density, specific enthalpy, and specific heat) of CO$_2$-N$_2$-Cu thermal plasmas. After introducing the calculation method of thermodynamic functions in section 2.3.1, the discussions for mass density, specific

enthalpy, and specific heat at constant pressure are presented in sections 2.3.2-2.3.4 respectively. The comparison of the compositions and thermodynamic properties between CO_2-N_2-Cu and SF_6-Cu mixtures is presented in section 2.4. The summary of the chapter is given in the last section 2.5.

2.2 Equilibrium compositions

2.2.1 Determination of compositions

The calculation of plasma compositions is the first step to determine the thermodynamic and transport properties. The local thermodynamic equilibrium (LTE) is assumed in this work, which means that the electrons, ions and neutral particles have the same kinetic temperature. Combined with the particular conditions: electrical neutrality, state equation, and chemical equilibrium, two ways can be adopted to calculate the equilibrium compositions: using the Saha and Guldberg–Waage laws if only gaseous species are considered, or using the minimization of the Gibbs free energy if several phases (including gaseous and condensed phases) are considered [37, 107]. In the method of Gibbs free energy, it is not necessary to define the free and bound species as the method of Saha and Guldberg–Waage laws requires [108], which is more convenient to deal with the plasma composed of a large amount of species. More importantly, the copper vapour in CO_2-N_2-Cu mixtures may condense at very low temperatures. Considering this possible condensation in CO_2-N_2-Cu plasmas, the minimization of Gibbs free energy is used in this work.

Assuming that the plasma contains N species (including N_g gaseous and N_c condensed species), the Gibbs free energy G can be written as: [37, 108]

$$G = \sum_{i=1}^{N} n_i \mu_i \tag{2-1}$$

Where n_i and μ_i are the number density and the chemical potential of particle i respectively. The chemical potential of a particle depends on its state. For gaseous species,

13

$$\mu_i = \mu_i^\circ + RT \ln \left(n_i / \sum_{j=1}^{N_g} n_j \right) + RT \ln \left(P / P^\circ \right) \qquad (2\text{-}2)$$

For condensed species,

$$\mu_i = \mu_i^\circ \qquad (2\text{-}3)$$

Where R is the molar gas constant, and μ_i° is the chemical potential of particle i in the standard state at reference pressure P° which can be substituted by the standard Gibbs energy G_i° [109]. The correction to μ_i based on the Debye-Hückel theory is considered and will be presented in section 2.3.2.

As discussed above, one of the key procedures in the method of the Gibbs free energy is to calculate the standard Gibbs energy G_i° for each species in mixtures. The G_i° of a given particle can be obtained from its approximated coefficients of thermodynamic functions fitted by the least-squares method [110]. The NASA Glenn Database [111] provides such coefficients for a plenty of species including neutral and charged particles. G_i° can also been calculated directly from the partition function Q of a given particle [112]. This calculation is sometimes necessary because the maximal temperature of the fitting coefficients provided by the NASA database may be lower than the maximal temperature (i.e. 30,000 K) of the plasma mixtures we study. Due to its complexity, the calculation of partition functions will be presented in the next section 2.2.2.

Another important procedure is to find the minimum value of the Gibbs free energy for the whole mixtures with the constrained conditions of mass balance, electrical conservation, and the state equation. This is a typical problem of constrained optimization in applied mathematics. In order to simplify this problem, the Lagrange multipliers is often used to convert the constrained optimization problem to an unconstrained one [110]. And then, the so-called Newton-Raphson algorithm is applied to solve this problem numerically [109, 110, 113]. Coufal and Živný [109] introduced another solution, i.e. performing the Taylor expansion of the Gibbs free energy with the third and higher orders being neglected. Both methods can solve the problem.

In this work, totally 76 gaseous species, namely C, C_2, C_3, C_4, C_5, CO, CO_2, C_2O, C_3O_2, CN, CN_2, C_2N, C_2N_2, C_4N_2, N, N_2, N_3, NO, NO_2, NO_3, N_2O, N_2O_3, N_2O_4, NCO, O, O_2, O_3, Cu, Cu_2, CuO, C^+, C^{2+}, C^{3+}, C^{4+}, C^-, C_2^+, C_2^-, C_3^-, C_4^-, C_5^-, CO^+, CO^-, CO_2^+, CO_2^-, CN^+, CN^-, N^+, N^{2+}, N^{3+}, N_2^+, N_2^-, N_3^+, N_3^-, NO^+, NO^-, NO_2^+, NO_2^-, N_2O+, N_2O^-, O^+, O^{2+}, O^{3+}, O^-, O_2^+, O_2^-, O_3^+, O_3^-, Cu^+, Cu^{2+}, Cu^{3+}, Cu^{4+}, Cu^- as well as electrons, are taken into account in the determination of the compositions of CO_2-N_2-Cu mixtures. Considering that the copper vapour resulting from electrode surfaces of circuit breakers is likely to exist in the form of nongaseous species at low temperatures, three possible condensed particles (including graphite (C(c)), copper (Cu(c)), and copper oxide (CuO(c))) are also considered. The letter c in the brackets denotes the condensed state i.e. liquid and/or solid state.

2.2.2 Evaluation of partition functions

Partition functions describe the statistical properties of a system in thermodynamic equilibrium. As described above, partition functions play an essential role in determining the compositions and thermodynamic properties of gas mixtures. Generally, the partition function of a particle can be expressed as:

$$Q = Q_{tr} \cdot Q_{int} = Q_{tr} \cdot Q_{elec} \cdot Q_{vib} \cdot Q_{rot} \qquad (2\text{-}4)$$

Where Q_{tr}, Q_{elec}, Q_{vib}, and Q_{rot} denote the contribution of translation, electronic motion, vibrational motion, and rotational motion respectively to the total partition function. Q_{int} is the internal partition function which is equal to the product of Q_{elec}, Q_{vib} and Q_{rot}, and is usually used to express the thermodynamic functions since the translational partition function Q_{tr} has a simple form and explicit contribution to the thermodynamic functions.

For monatomic species, their internal partition function only have the contribution from the electronic motion, and is computed as: [114, 115]

$$Q_{int} = Q_{elec} = \sum_{i}^{\varepsilon_{ei} < E_{ieff}} g_{ei} e^{-\frac{\varepsilon_{ei}}{kT}} \qquad (2\text{-}5)$$

15

Where g_{ei} is the degeneracy, ε_{ei} the energy of the ith electronic level, k the Boltzmann constant, and E_{ieff} is the effective ionization energy of particle i considering the lowering of the ionization energy. The ionization potential lowering is the function of the Debye length of the plasma, and the Debye length depends on the plasma compositions. Consequently, an iterative procedure should be applied until the convergence of the calculation of compositions.

For diatomic species, their internal partition functions are the product of Q_{elec}, Q_{vib} and Q_{rot}, and can be determined by Morse potential minimization method [114, 116].

$$
\begin{aligned}
Q_{\mathrm{int}} &= Q_{elec} \cdot Q_{vib} \cdot Q_{rot} \\
&= \frac{1}{\sigma_c} \sum_{i}^{\varepsilon_{ei} < E_{ieff}} g_{ei} e^{-\frac{\varepsilon_{ei}}{kT}} \cdot \sum_{v}^{v_{\max}} e^{-\frac{\varepsilon_{vib}}{kT}} \cdot \sum_{J}^{J_{\max}} (2J+1) e^{-\frac{\varepsilon_{rot}}{kT}}
\end{aligned}
\tag{2-6}
$$

Where σ_c is the symmetry factor that is the number of different ways the molecule can be rotated into a configuration indistinguishable from the original [117]. ε_{vib} and ε_{rot} are the vibrational and rotational energy respectively, v and J are their corresponding quantum numbers, v_{max} and J_{max} are the maximal value of v and J. v_{max} is determined with rotationless ($J = 0$) molecular state. J_{max} is determined when the potential curve no longer displays a minimum. ε_{vib} and ε_{rot} of a diatomic particle can be approximated using the spectroscopic constants [114, 116].

$$
\frac{\varepsilon_{vib}}{hc} = \omega_e \left(v + \frac{1}{2} \right) - \omega_e x_e \left(v + \frac{1}{2} \right)^2 + \omega_e y_e \left(v + \frac{1}{2} \right)^3 + \omega_e z_e \left(v + \frac{1}{2} \right)^4
\tag{2-7}
$$

$$
\frac{\varepsilon_{rot}}{hc} = B_v J (J+1) - D_v J^2 (J+1)^2
\tag{2-8}
$$

Where h and c are respectively the Planck constant and the speed of light, ω_e, $\omega_e x_e$, $\omega_e y_e$, $\omega_e z_e$, B_v, and D_v are all spectroscopically determined constants for each electronic state of a diatomic molecule [116].

For polyatomic species, their internal partition functions are also the product of Q_{elec}, Q_{vib} and Q_{rot}. However, due to the lack of accurate spectroscopic data, Q_{int} of a polyatomic particle is usually approximated using the following expression [114, 118].

16

$$Q_{\text{int}} = Q_{elec} \cdot Q_{vib} \cdot Q_{rot}$$

$$= \sum_{i}^{\varepsilon_{ei} < E_{ieff}} g_{ei} e^{-\frac{\varepsilon_{ei}}{kT}} \cdot \prod_{j} \left[e^{-\frac{\omega_j}{2kT}} \middle/ \left(1 - e^{-\frac{\omega_j}{kT}} \right) \right]^{g_j} \cdot \left(\frac{T}{\theta_{rot}} \right)^{3/2} \qquad (2\text{-}9)$$

Where g_j and ω_j are the statistical weight and frequency of vibrational energy level respectively, θ_{rot} is the rotational constant.

In this work, the basic data for the calculation of internal partition functions were compiled from the NIST database [119] and the NIST-JANAF Thermochemical Tables [120].

2.2.3 Influence of condensed species

In order to investigate the influence of condensed species on the compositions of CO_2-N_2-Cu plasmas, Figure 2-1, Figure 2-2 and Figure 2-3 show respectively the equilibrium compositions of CO_2-N_2 mixtures (mixing ratio 7:3) contaminated by three different proportion of copper (10%, 50% and 90%) at ambient pressure. The parts (a) and (b) in each figure describe the results without and with consideration of condensed phases respectively.

It is obvious that copper condenses at temperatures below 3000 K. Graphite and solid CuO are not observed even though they are considered in the calculation. When the condensed species are not taken into account in the calculation, elemental copper exists in the form of copper dimer (Cu_2) at low temperatures, and then Cu_2 decomposes shortly into Cu with the increase of temperature.

As seen in Figure 2-1 for the case of 10% Cu, the condensed copper evaporates at around 2200 K, whereas for the cases of 50% Cu and 90% in Figure 2-2 and Figure 2-3 the phase transition occurs at 2500 K and 2700 K respectively. This indicates that the phase transition of copper from condensed state (liquid and/or solid) to gaseous state is affected by the working gases, considering that the boiling point of copper is 2840 K. This observation agrees with the result reported by Rong et al. [37] for the phase transition of condensed CuF_2 in SF_6-Cu mixtures.
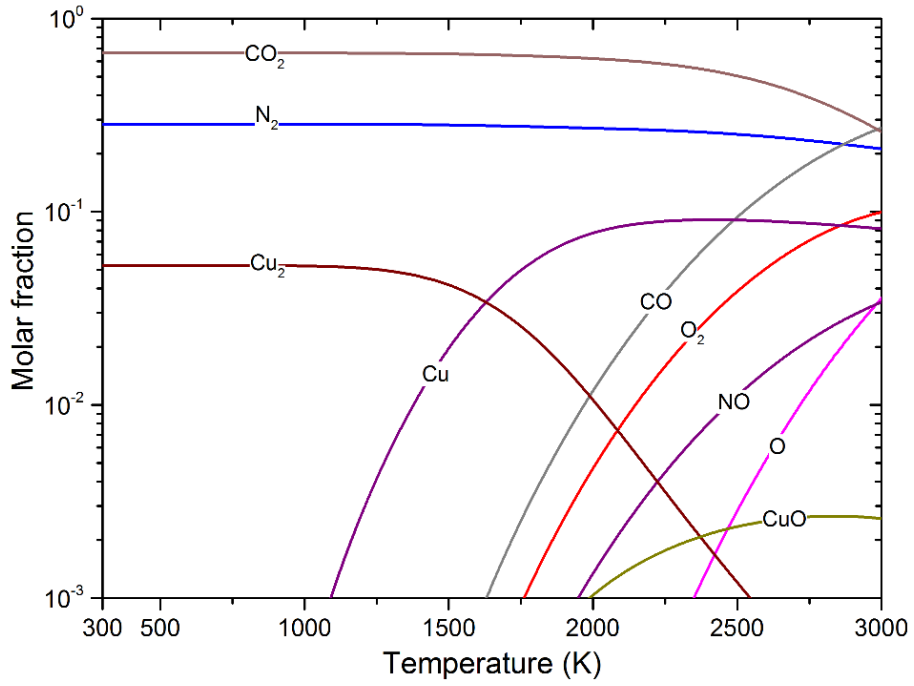
(a) Without condensed species
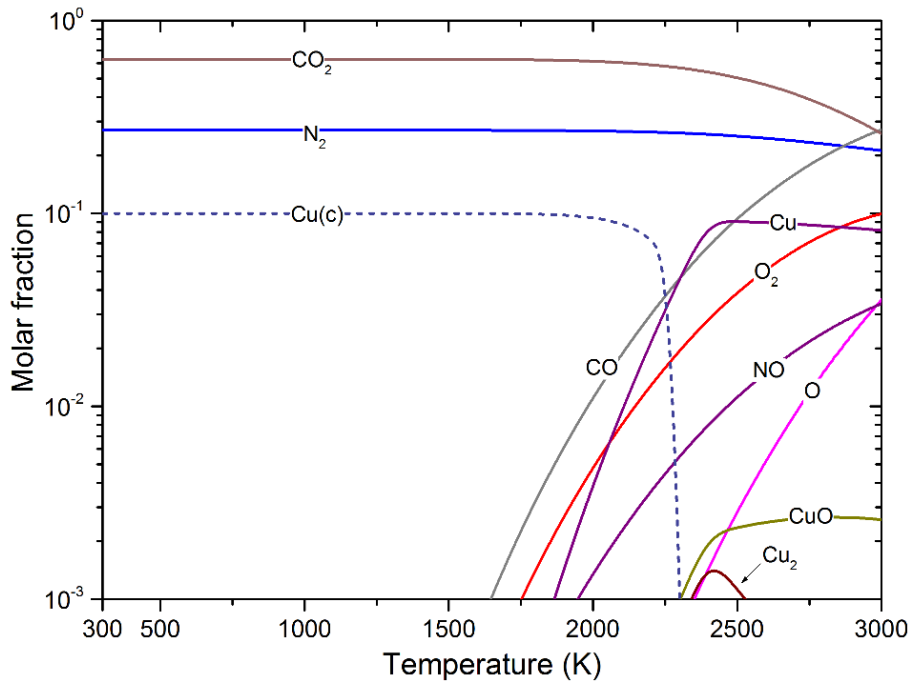
(b) With condensed species

Figure 2-1. Equilibrium compositions of CO_2-N_2 (mixing ratio 7:3) mixtures

contaminated by 10% Cu at temperatures of $300 - 3000$ K and at 1 bar

(a) Without condensed species

(b) With condensed species

Figure 2-2. Equilibrium compositions of CO_2-N_2 (mixing ratio 7:3) mixtures

contaminated by 50% Cu at temperatures of $300 - 3000$ K and at 1 bar
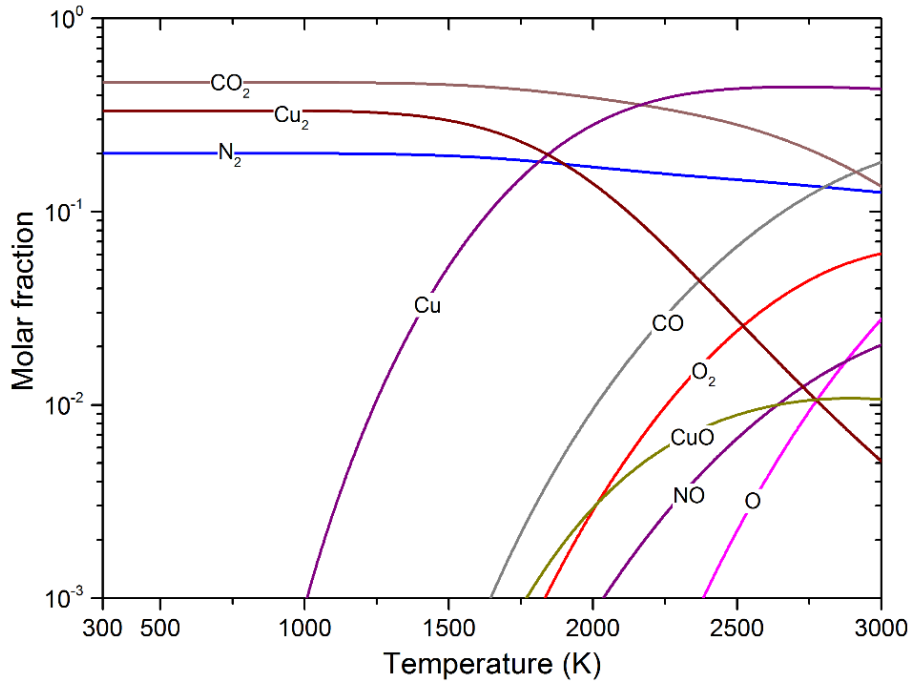
(a) Without condensed species
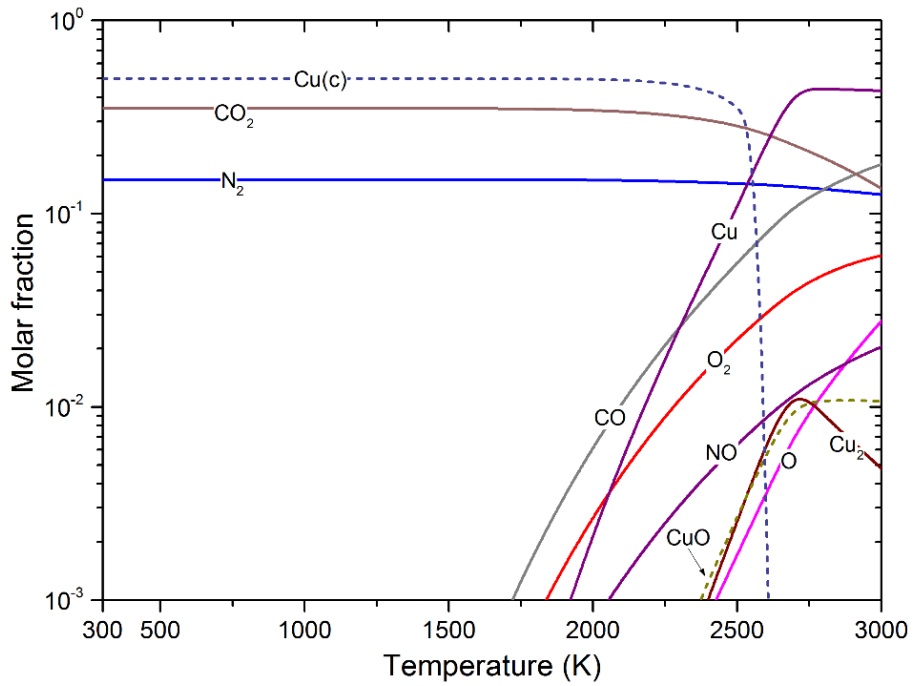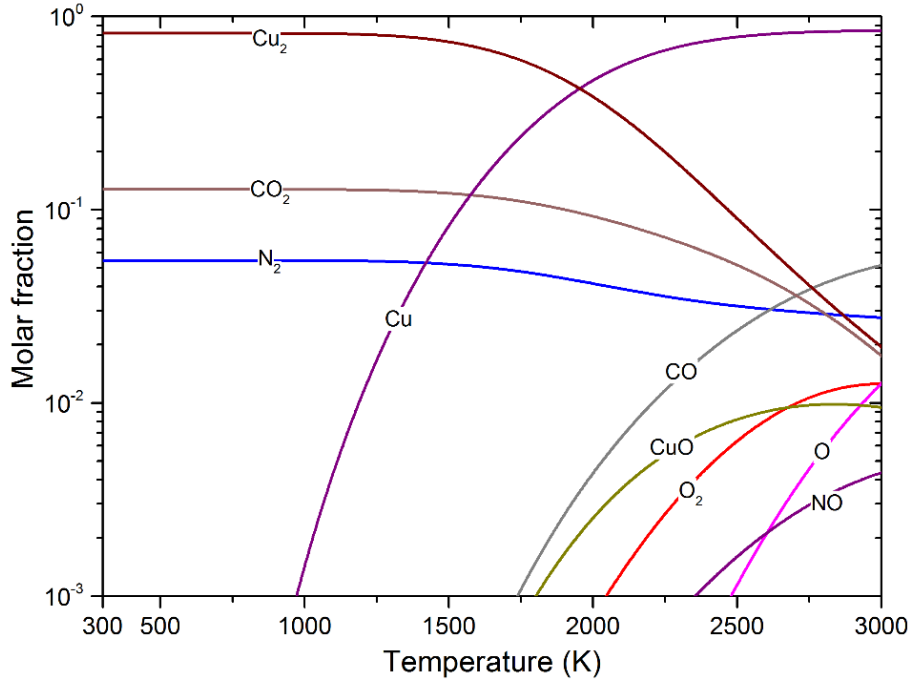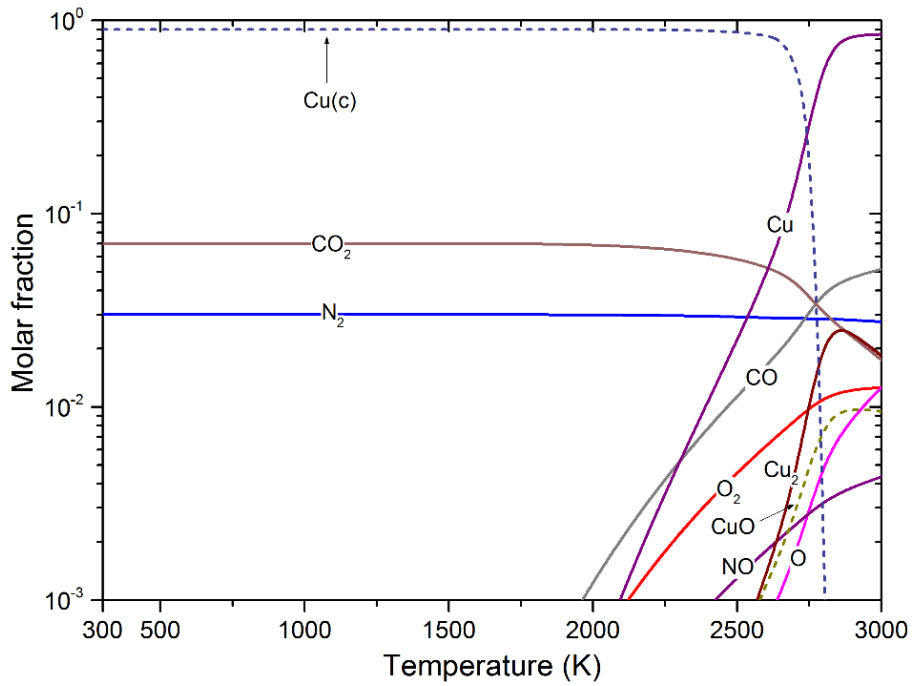

(b) With condensed species

Figure 2-3. Equilibrium compositions of CO_2-N_2 (mixing ratio 7:3) mixtures

contaminated by 90% Cu at temperatures of $300 - 3000$ K and at 1 bar

2.2.4 Influence of mixing ratios (CO₂:N₂)

The mixing ratio between CO_2 and N_2 is fixed to 7:3 in the previous section 2.2.3. In this section, this mixing ratio is set to be changeable to show its effect on the plasma compositions.

Figure 2-4 and Figure 2-5 describe the equilibrium compositions of pure N_2 and pure CO_2 plasmas contaminated by 10% Cu respectively in the temperature range of 300 – 10,000 K at ambient pressure. The condensed phases are considered in the calculation. Contaminated by the same percentage (10%) of Cu, CO_2 and N_2 are mixed with each other, and the corresponding results of their compositions are shown in Figure 2-6, Figure 2-7 and Figure 2-8. The mixing ratios (CO_2:N_2) of these mixtures are 7:3, 5:5 and 3:7 respectively.

The condensed copper evaporates at around 2200 K and 2300 K in the CO_2-Cu and N_2-Cu plasmas respectively. As a result, the phase transition in CO_2-N_2-Cu mixtures occurs between these two temperature points. After the evaporation, the gaseous copper starts to ionize ahead of atomic carbon, oxygen and nitrogen because the ionization energy of copper is the lowest among them (Cu 7.73 eV < C 11.26 eV < O 13.62 eV < N 14.53 eV [119]).

Considering that the strong ionization reactions in plasma mixtures result in the peaks of their specific heat and thermal conductivity, the addition of N_2 to CO_2 gas can raise the peak values of specific heat and thermal conductivity of CO_2-N_2-Cu plasmas because the ionization energy of nitrogen is larger than that of carbon and oxygen.

Besides, we notice that the triple-bond (N≡N) energy of N_2 (942 kJ/mol) is larger than the double-bond (C=O) energy of CO_2 (799 kJ/mol) [121], which means that N_2 has the more stable chemical structure and thus is more difficult to dissociate than CO_2. This also can affect the peak values of specific heat and thermal conductivity because these peaks are usually attributed to the strong dissociation reactions (e.g. the decomposition of CO_2 and N_2).
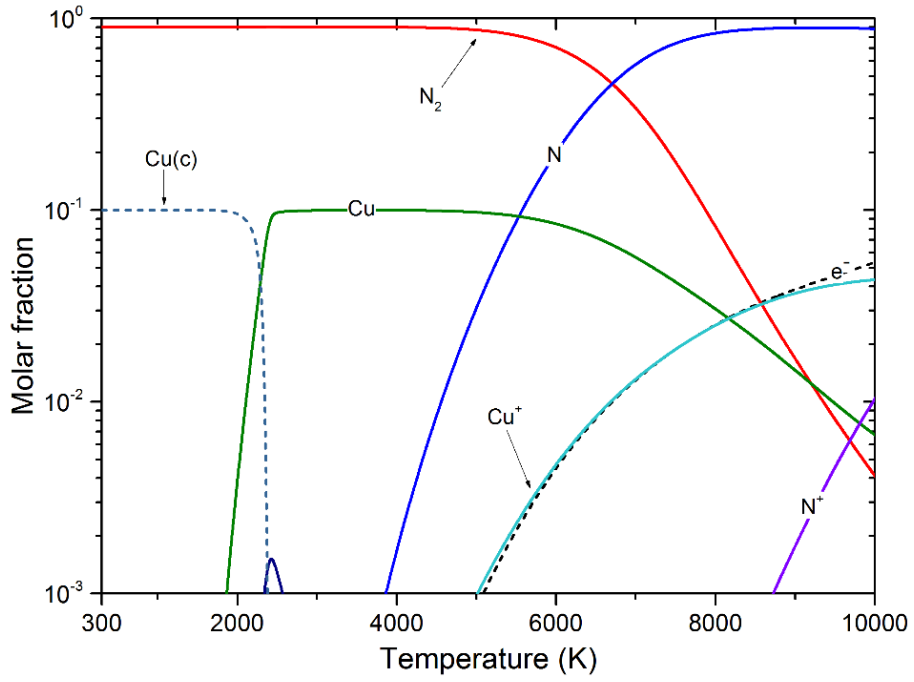
Figure 2-4. Equilibrium compositions of pure N_2 plasma contaminated by 10% Cu at temperatures of 300 – 10,000 K and at 1 bar
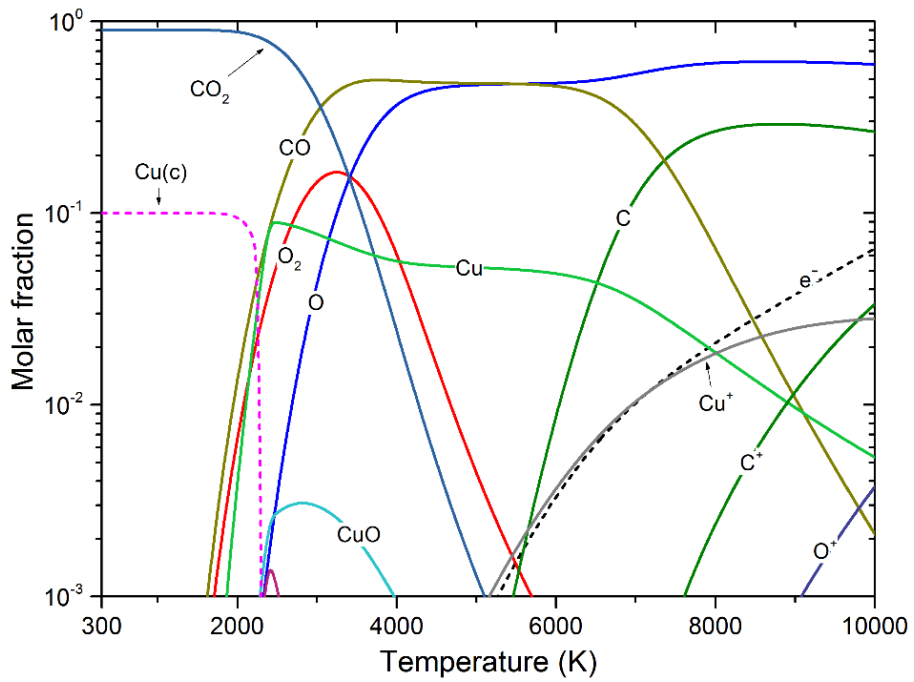
Figure 2-5. Equilibrium compositions of pure CO_2 plasma contaminated by 10% Cu at temperatures of 300 – 10,000 K and at 1 bar

Figure 2-6. Equilibrium compositions of CO_2-N_2 (mixing ratio 7:3) mixtures contaminated by 10% Cu at temperatures of 300 – 10,000 K and at 1 bar

Figure 2-7. Equilibrium compositions of CO_2-N_2 (mixing ratio 5:5) mixtures contaminated by 10% Cu at temperatures of 300 – 10,000 K and at 1 bar

Figure 2-8. Equilibrium compositions of CO_2-N_2 (mixing ratio 3:7) mixtures contaminated by 10% Cu at temperatures of 300 – 10,000 K and at 1 bar

2.2.5 Influence of pressures

In this section, the equilibrium compositions of CO_2-N_2 mixtures contaminated by 10% Cu are calculated at various pressures in the temperature range of 3000 – 30,000 K. The mixing ratio is set to be 7:3. The results for the pressures of 0.1 bar, 1 bar, 6 bar and 16 bar are illustrated in Figure 2-9, Figure 2-10, Figure 2-11 and Figure 2-12 respectively.

As can be seen from these figures, the higher pressures suppress the dissociation of molecules (i.e. $CO_2 \rightarrow CO + O$, $CO \rightarrow C + O$, $O_2 \rightarrow O + O$, $N_2 \rightarrow N + N$, $NO \rightarrow N + O$, $CN \rightarrow C + N$, $CuO \rightarrow Cu + O$ and $Cu_2 \rightarrow Cu + Cu$), leading to more molecules and less atoms at temperatures below 10,000 K. At temperatures above 10,000 K, the higher pressures also suppress the ionization reactions (i.e. $C \rightarrow C^+ + e^-$, $C \rightarrow C^{2+} + e^-$, $O \rightarrow O^+ + e^-$, $O \rightarrow O^{2+} + e^-$, $N \rightarrow N^+ + e^-$, $N \rightarrow N^{2+} + e^-$, $Cu \rightarrow Cu^+ + e^-$, $Cu \rightarrow Cu^{2+} + e^-$, and $Cu \rightarrow Cu^{3+} + e^-$), resulting in less atomic ions.

24

Due to the suppression of pressures described above, the curves of the compositions from Figure 2-9 to Figure 2-12 look like to shift towards higher temperatures with the increasing pressure from 0.1 bar to 16 bar. For example, the particle Cu^{2+} starts to occur at around 14,500 K at 0.1 bar. When the pressure is increased to be 1 bar, 6 bar and 16 bar, this ionization temperature is shifted to be 16,000 K, 18,000 K and 19,000 K respectively.

All the above observation can be explained by Le Chatelier's principle. This principle states that a system in equilibrium adjusts so as to minimize the effect of an applied alteration in conditions. Specifically, the pressure decrease is minimized if the total number of moles of species in the system is increased [37]. This is achieved by a shift in the position of equilibrium to favour the decompositions of molecules and the multiple ionization of atoms and hence the yield of atoms (from the decompositions) and high-valence ions (from the ionization) [37].
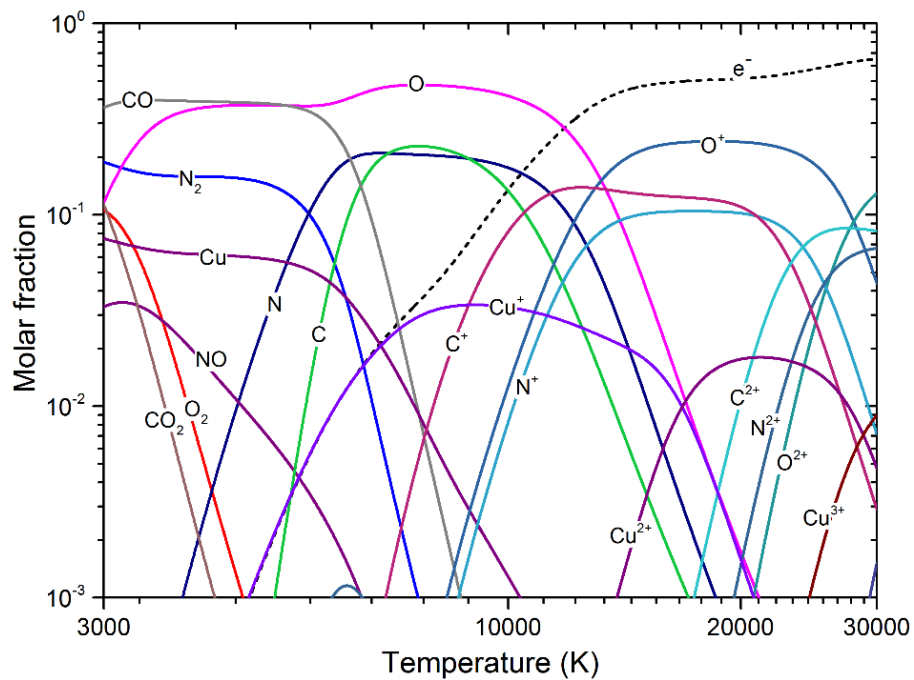
Figure 2-9. Equilibrium compositions of CO_2-N_2 (mixing ratio 3:7) mixtures contaminated by 10% Cu at temperatures of 3000 – 30,000 K and at 0.1 bar

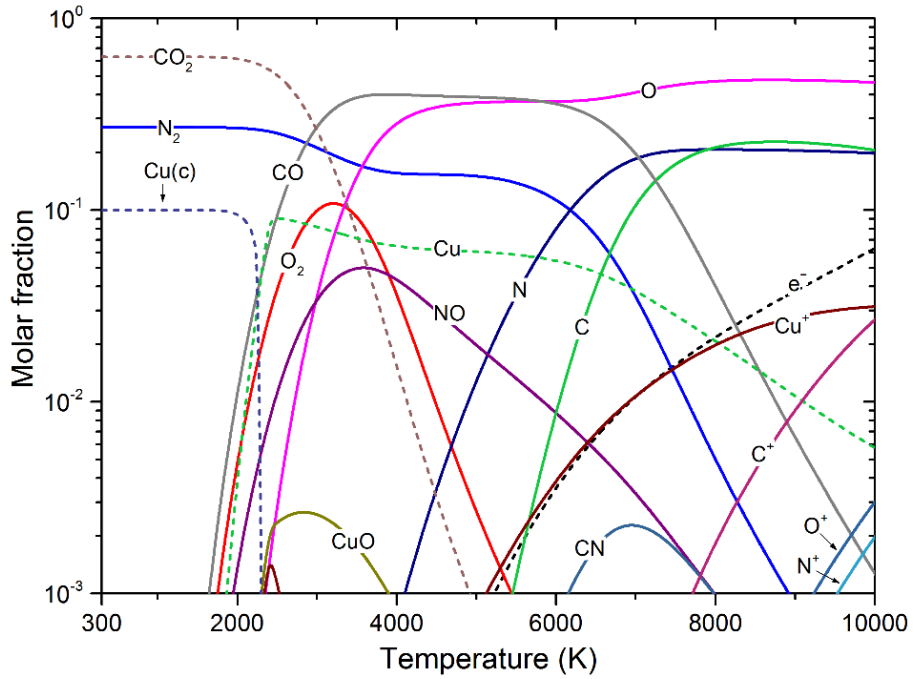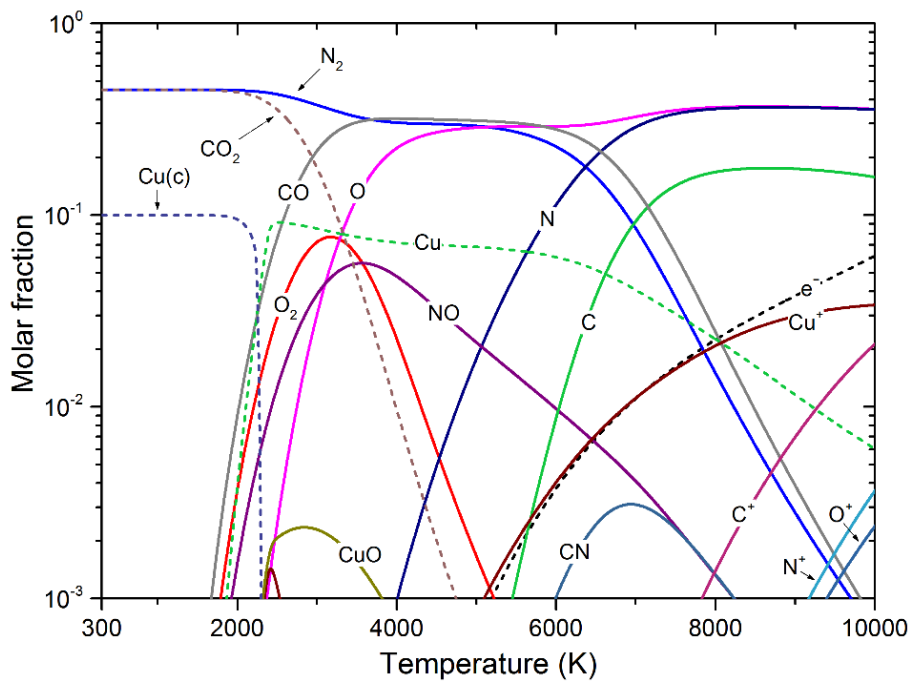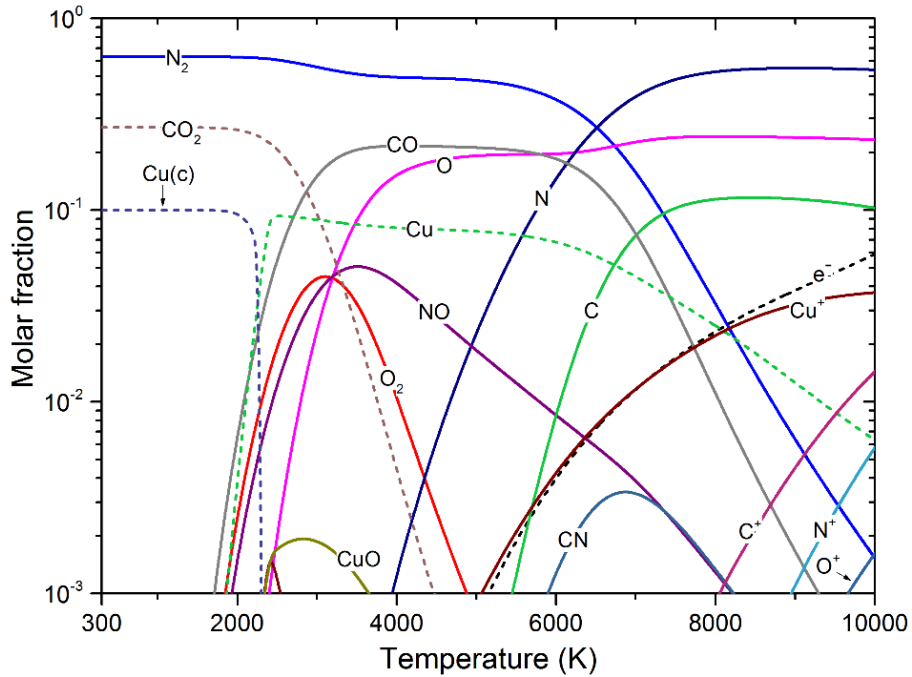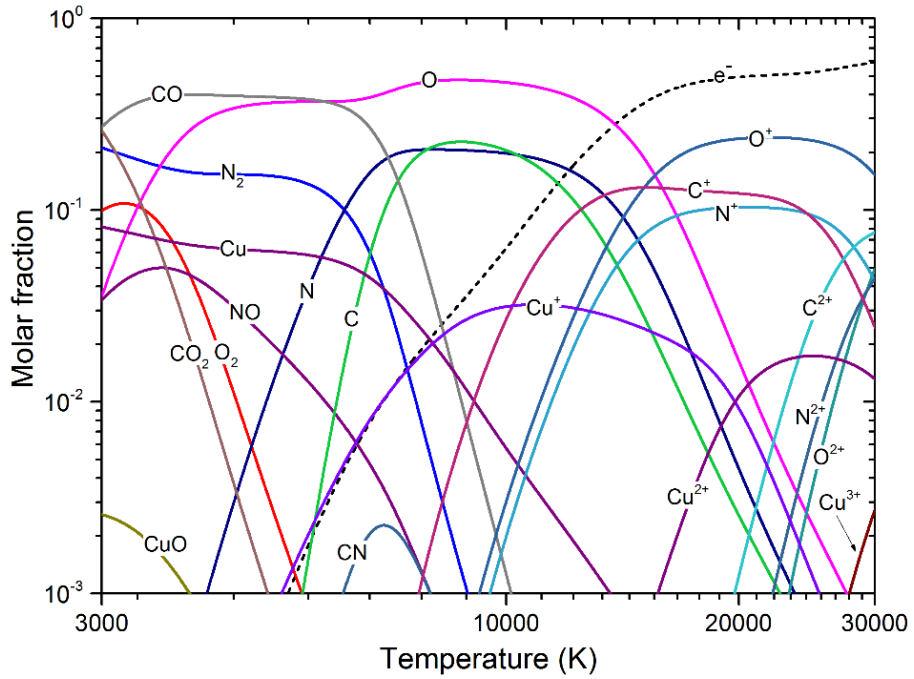Figure 2-10. Equilibrium compositions of CO_2-N_2 (mixing ratio 3:7) mixtures contaminated by 10% Cu at temperatures of 3000 – 30,000 K and at 1 bar
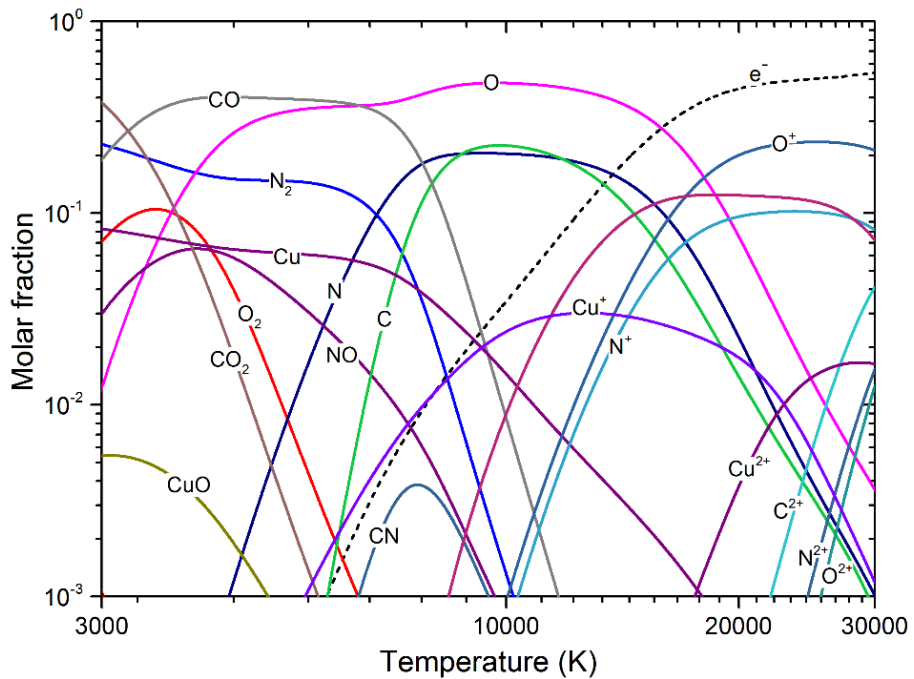
Figure 2-11. Equilibrium compositions of CO_2-N_2 (mixing ratio 3:7) mixtures contaminated by 10% Cu at temperatures of 3000 – 30,000 K and at 6 bar
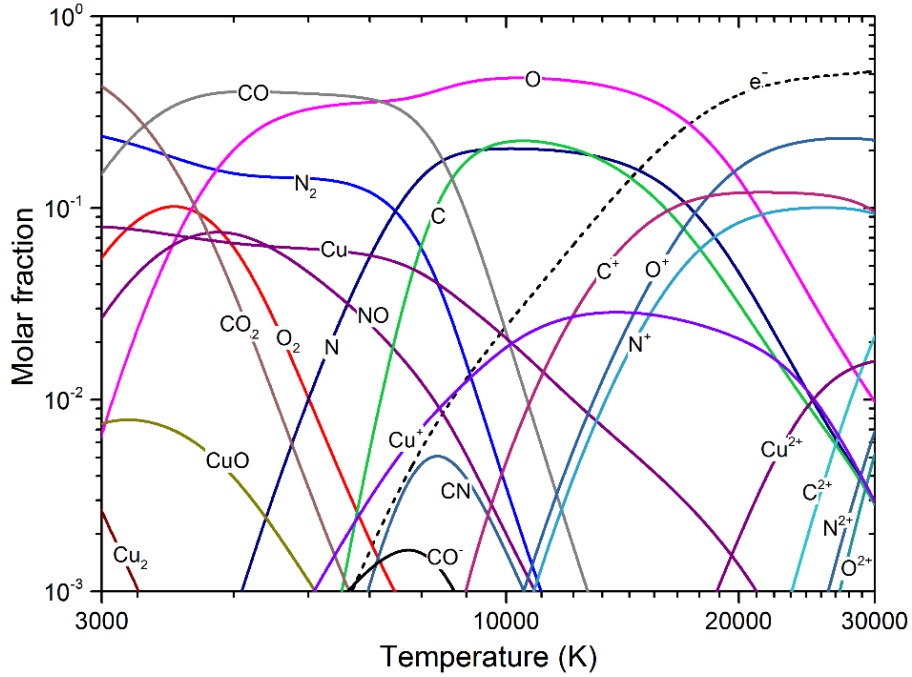
Figure 2-12. Equilibrium compositions of CO_2-N_2 (mixing ratio 3:7) mixtures contaminated by 10% Cu at temperatures of 3000 – 30,000 K and at 16 bar

2.3 Thermodynamic properties

2.3.1 Determination of thermodynamic properties

The thermodynamic properties in this work include mass density, specific enthalpy, and specific heat at constant pressure, all of which are the prerequisites of thermal plasma modelling. Once obtaining the compositions, the thermodynamic properties can be determined easily according to their definitions.

For mass density ρ, [37, 110, 122]

$$\rho = \frac{\sum_{i=1}^{N} m_i c_i}{V_g} \tag{2-10}$$

Where m_i and c_i are the mass and amount of particle i respectively, V_g is the total volume of gaseous phase. V_g can be determined using the ideal gas law with considering the Debye-Hückel correction which will be discussed in the next section 2.3.2.

For specific enthalpy h, [37, 110, 122]

27

$$h = \sum_{i=1}^{N} x_i H_i^{\circ} / M \tag{2-11}$$

Where x_i and H_i° are the molar fraction and the standard-state molar enthalpy of particle i respectively. M refers to the molar mass of the mixtures and is calculated using the follow expression.

$$M = \sum_{i=1}^{N} x_i M_i \tag{2-12}$$

Where M_i is the molar mass of particle i.

For specific heat at constant pressure C_p, [37, 110, 122]

$$C_p = \left(\frac{\partial h}{\partial T} \right)_p \tag{2-13}$$

Similar to the calculation of G_i° described in section 2.2.1, the standard molar enthalpy H_i° can also be determined by two ways. One is to use the following formula (2-14) with the fitting coefficients of enthalpy [110], the other is to calculate it from the internal partition function of particle i using the expression (2-15) [123].

$$\frac{H_i^{\circ}(T)}{RT} = -a_1 T^{-2} + a_2 T^{-1} \ln T + a_3 + a_4 \frac{T}{2} + a_5 \frac{T^2}{3} + a_6 \frac{T^3}{4} + a_7 \frac{T^4}{5} + \frac{a_8}{T} \tag{2-14}$$

$$\frac{H_i^{\circ}(T) - H_i^{\circ}(0)}{RT} = T \frac{d(\ln Q_{\text{int}})}{dT} + \frac{5}{2} \tag{2-15}$$

Where a_i (i = 1-9) is the fitted coefficients, and R is the ideal gas constant.

2.3.2 Debye-Hückel correction

The thermodynamic functions are usually calculated under the assumption of ideal gases formed by dimensionless particles colliding with each other as hard spheres [37, 112]. However, plasmas are also composed of charged particles interacting through electrostatic forces which are effective even at a long distance [37, 112]. In this work, the corrections to the ideal plasmas are determined in the framework of the Debye-Hückel theory [37, 112]. Another correction called Virial correction is not taken into account as its effect is expected to be negligible for the pressures considered in this

work [37]. The Debye-Hückel corrections to the pressure ΔP, chemical potential $\Delta \mu_i$, enthalpy ΔH_i, frozen heat capacity at constant pressure ΔC_{pfi} can be calculated using the following formulas (2-16), (2-17), (2-18), and (2-19) respectively: [37, 112]

$$\Delta P = -kT / \left(24\pi \lambda_D^3 \right) \tag{2-16}$$

$$\Delta \mu_i = -N_a e^2 Z_i^2 / \left(8\pi \varepsilon_0 \lambda_D \right) \tag{2-17}$$

$$\Delta H_i = -kTV / \left(6\pi \lambda_D^3 \right) \tag{2-18}$$

$$\Delta C_{pfi} = kV / \left(6\pi \lambda_D^3 \right) \tag{2-19}$$

Where N_a, e and ε_0 are the Avogadro number, the elementary charge and the vacuum electric permittivity respectively. Z_i is the charge number of particle i. λ_D is the Debye length which is defined with or without considering the contributions from ions.

There is a debate about whether ions should be considered in the determination of the Debye length. For example, Devoto [124] calculated the Debye length without ions when he determined the electrical and thermal conductivities of argon plasma, because he achieved better agreement if ions were not considered. Murphy [125] followed Devoto's [124] preference when he calculated the transport coefficients of hydrogen and argon-hydrogen plasmas. However, Capitelli et al. [112] took ions into account when calculating the Debye-Hückel corrections. In this work, following our previous publications [37, 40, 41], the ions in CO_2-N_2-Cu mixtures are not considered in the calculation of the Debye length. Actually, although the different definitions of the Debye length give different Debye-Hückel corrections. This difference does not affect the thermodynamic properties significantly because the Debye-Hückel corrections to these properties are small [37].

2.3.3 Mass density

The influence of copper contamination on the mass density of CO_2-N_2 mixtures (mixing ratio 7:3) is described in Figure 2-13 in the temperature range of 300 – 30,000 K at ambient pressure.

29

Obviously, with the increase of copper content, the values of mass density go up in the whole temperature range. This is because copper has larger molar mass (63.5 g·mol^{-1}) than CO_2 (44.0 g·mol^{-1}) and N_2 (28.0 g·mol^{-1}). In addition to the difference of molar mass, more atoms (i.e. Cu) and hence less molecules (i.e. CO_2 and N_2) result in the smaller volume of CO_2-N_2-Cu plasmas, which also increases the mass density. This is because the dissociation products of the molecules lead to the expansion of the plasma mixtures. Less molecules mean the less expansion of the mixtures.

Due to the phase transition of the condensed copper, the mass density of the mixtures is observed to drop sharply below 3000 K. The corresponding temperature of the phase transition is shifted to a higher value with a higher copper proportion. This also agrees with the observation in Figure 2-1, Figure 2-2 and Figure 2-3 for the compositions.

Figure 2-13. Mass density of CO_2-N_2 (mixing ratio 7:3) mixtures contaminated by different proportions of Cu at temperatures of 300 – 30,000 K and at 1 bar

Figure 2-14 shows the mass density of pure CO_2, pure N_2 and their mixtures with

mixing ratios of 7:3, 5:5 and 3:7 contaminated by 10% copper in the temperature range of 300 – 30,000 K at ambient pressure.

It can be seen that the addition of N_2 into CO_2 has a negligible effect on the mass density of CO_2-N_2-Cu mixtures, especially at temperatures above 7000 K. According to the results of the compositions as shown in Figure 2-4, Figure 2-5, Figure 2-6, Figure 2-7 and Figure 2-8, the atoms start to dominate the mixtures above 7000 K. Accordingly, in this temperature range, the mass density of the mixtures depends on the average mass of a single atom. This value for CO_2 ($44.0/3 = 14.67$ g·mol^{-1}) is very close to that for N_2 ($28.0/2 = 14.0$ g·mol^{-1}), resulting the very little influence of N_2 on the mass density of CO_2-N_2-Cu mixtures.

Figure 2-14. Mass density of CO_2, N_2, and their different mixtures contaminated by 10% Cu at temperatures of 300 – 30,000 K and at 1 bar

Figure 2-15 illustrates the influence of pressure on the mass density of CO_2-N_2-Cu plasma mixtures at temperature up to 30,000 K. The mixing ratio of CO_2 and N_2 is set to be 7:3, and the content of the copper contamination is 10%. The four curves on the

graph correspond to the mass density calculated at 0.1 bar, 1 bar, 6 bar and 16 bar respectively. It is clear that the mass density of CO_2-N_2-Cu mixtures increases with the pressure because the gas mixtures are compressed.

Figure 2-15. Mass density of CO_2-N_2 (mixing ratio 7:3) mixtures contaminated by 10% Cu at temperatures of 300 – 30,000 K and at different pressures

2.3.4 Specific enthalpy

The influence of copper contamination on specific enthalpy of CO_2-N_2 mixtures (mixing ratio 7:3) is described in Figure 2-16 in the temperature range of 300 – 30,000 K at ambient pressure.

Due to the increase of mass density as shown in Figure 2-13, the specific enthalpy of CO_2-N_2-Cu mixtures decreases with copper contamination at temperatures above 4500 K. However, when the temperature is below 4500 K. the contrary influence is observed. This can be attributed to the balance between molar enthalpy and mass density, considering that the molar enthalpies of the species composed of Cu are different from those composed of C, N and O.
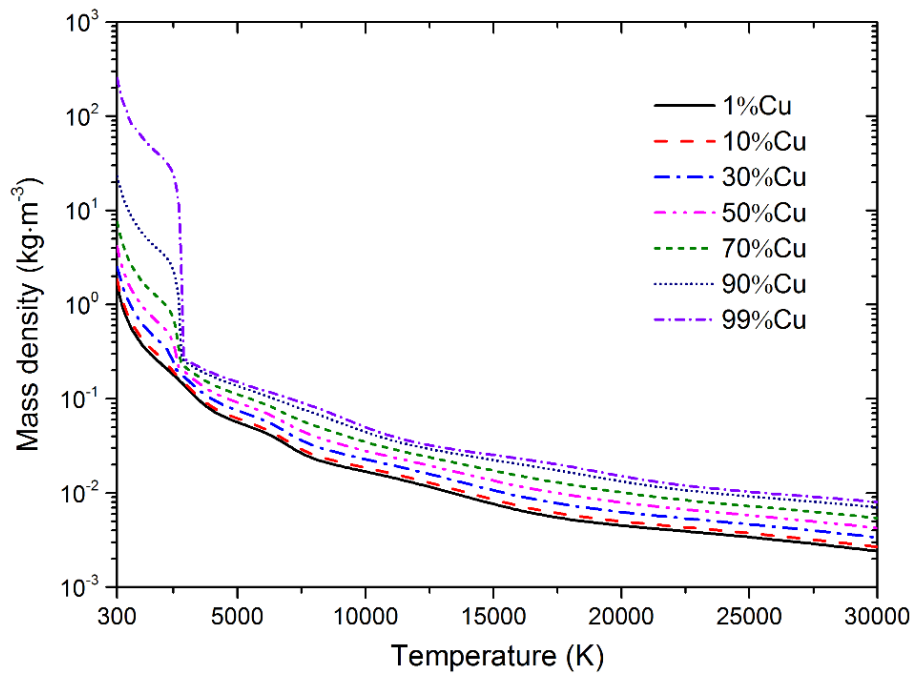
32

Figure 2-16. Specific enthalpy of CO_2-N_2 (mixing ratio 7:3) mixtures contaminated by different proportions of Cu at temperatures of 300 – 30,000 K and at 1 bar

Figure 2-17 presents the specific enthalpy of pure CO_2, pure N_2 and their mixtures with mixing ratios of 7:3, 5:5 and 3:7 in the temperature range of 300 – 30,000 K at ambient pressure. The volume proportion of copper contamination is fixed to be 10% for all the mixtures in this figure.

It is obvious that N_2 shows very slight effect on the specific enthalpy of CO_2-N_2-Cu mixtures. According to the definitions of thermodynamic functions presented in the section 2.3.1, the specific enthalpy of a gas mixture is inversely proportional to its mass density. And we notice that the mass density of CO_2-N_2-Cu mixtures is almost independent of N_2 content as shown in Figure 2-14. As a result, the addition of N_2 into CO_2-N_2-Cu mixtures does not change their specific enthalpy significantly.

However, due to the different enthalpy values of carbon, oxygen and nitrogen, the mixing of N_2 leads to a slight increase in the specific enthalpy of CO_2-N_2-Cu plasma mixtures, especially at high temperatures.
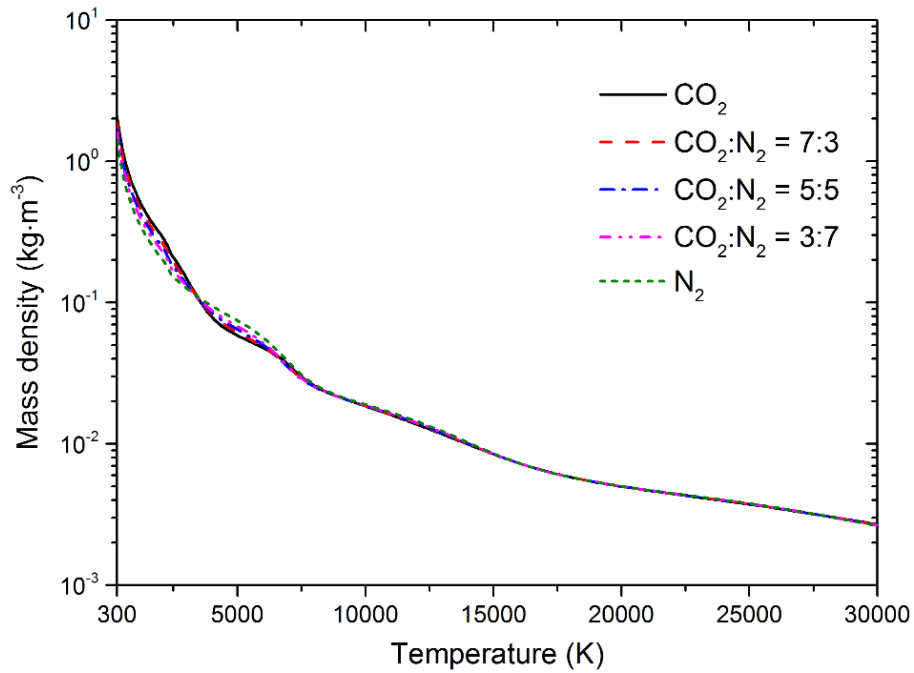
33

Figure 2-17. Specific enthalpy of CO_2, N_2, and their different mixtures contaminated by 10% Cu at temperatures of 300 – 30,000 K and at 1 bar
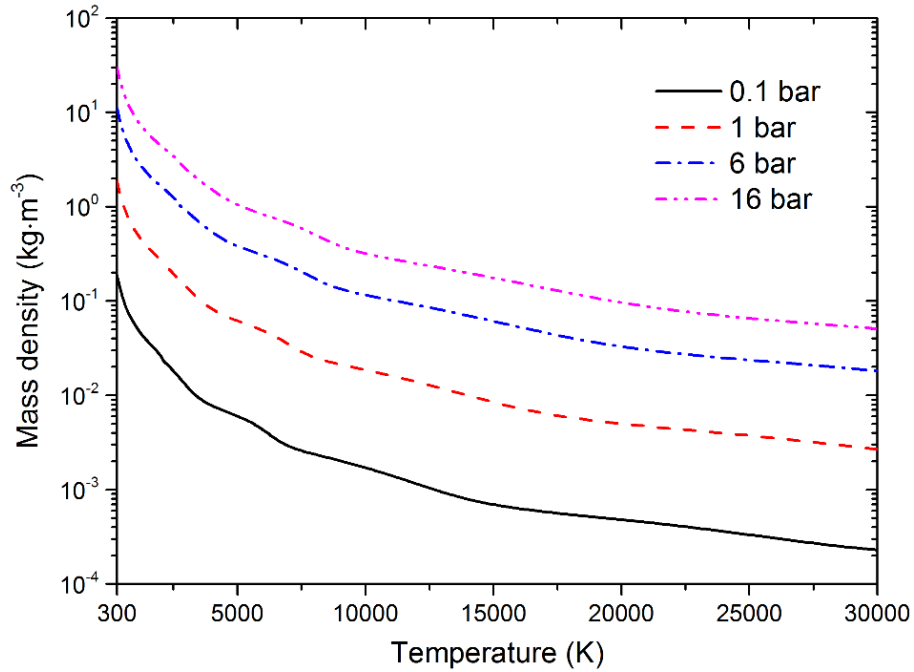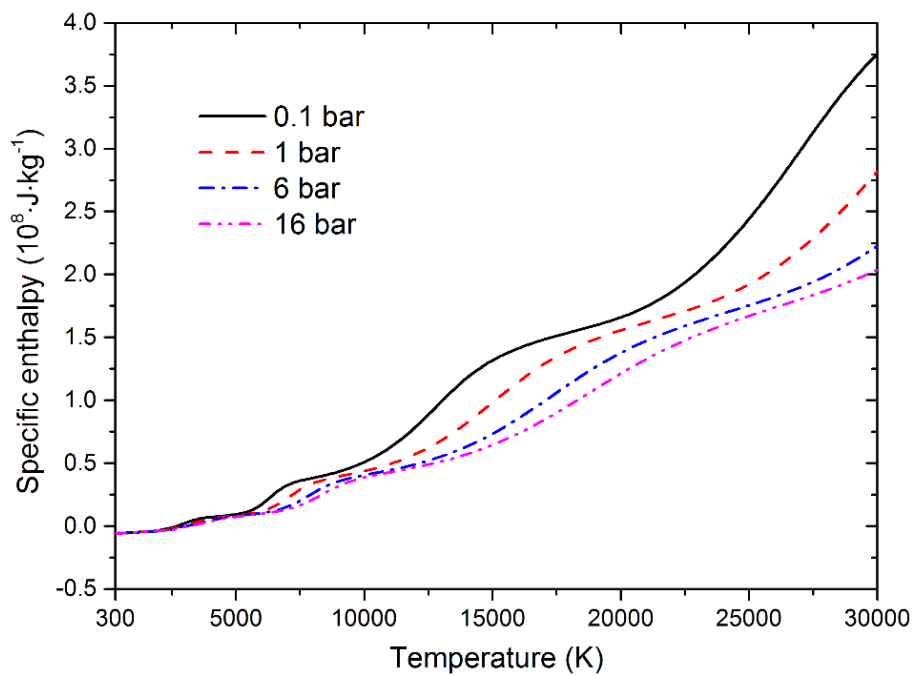

Figure 2-18. Specific enthalpy of CO_2-N_2 (mixing ratio 7:3) mixtures contaminated by 10% Cu at temperatures of 300 – 30,000 K and at different pressures

Figure 2-18 shows the influence of pressure on the specific enthalpy of CO_2-N_2 mixtures contaminated by 10% copper at temperatures of 300 – 30,000 K. The mixing ratio of CO_2 and N_2 is fixed to be 7:3. The four curves in the figure represent the mass density determined at 0.1 bar, 1 bar, 6 bar and 16 bar respectively.

It is clear that increasing the pressure decreases the specific enthalpy and also shifts the peaks of the specific enthalpy to higher temperatures. This is the consequence of the increase of mass density with pressure as explain in the previous section 2.3.3, considering the inverse relation between specific enthalpy and mass density.

2.3.5 Specific heat at constant pressure

The influence of condensed phases on the specific heat at constant pressure (hereinafter referred to as specific heat) is investigated and described in Figure 2-19 in the temperature range of 300 – 3000 K at ambient pressure.
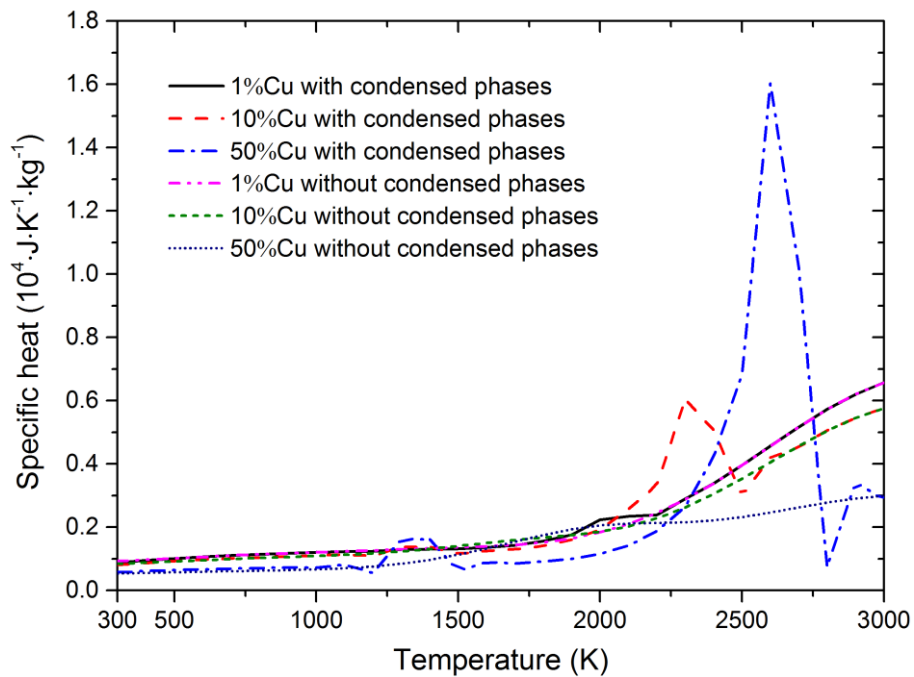
Figure 2-19. Specific heat of CO_2-N_2 (mixing ratio 7:3) mixtures contaminated by different proportions of Cu at temperatures of 300 – 3000 K and at 1 bar with and without condensed phases

As can been observed in Figure 2-19, the phase transition (i.e. the copper evaporation) affects the specific heat significantly, which leads to the sharp increase and steep drop in the specific heat. And also because of this, the influence of condensed species is strongly enhanced when the copper percentage is raised. Figure 2-19 also gives the conclusion that the temperature point of phase transition is shifted towards a higher value with the increase of copper contamination, which agrees with the observation in the compositions as shown in Figure 2-1, Figure 2-2 and Figure 2-3.

After the phase transition, the specific heat of CO_2-N_2-Cu mixtures becomes smoother. Figure 2-20 presents the specific heat of CO_2-N_2 mixtures (mixing ratio 7:3) contaminated by various proportions of copper in the temperature range of 3000 – 30,000 K at 1 bar with consideration of condensed phases.
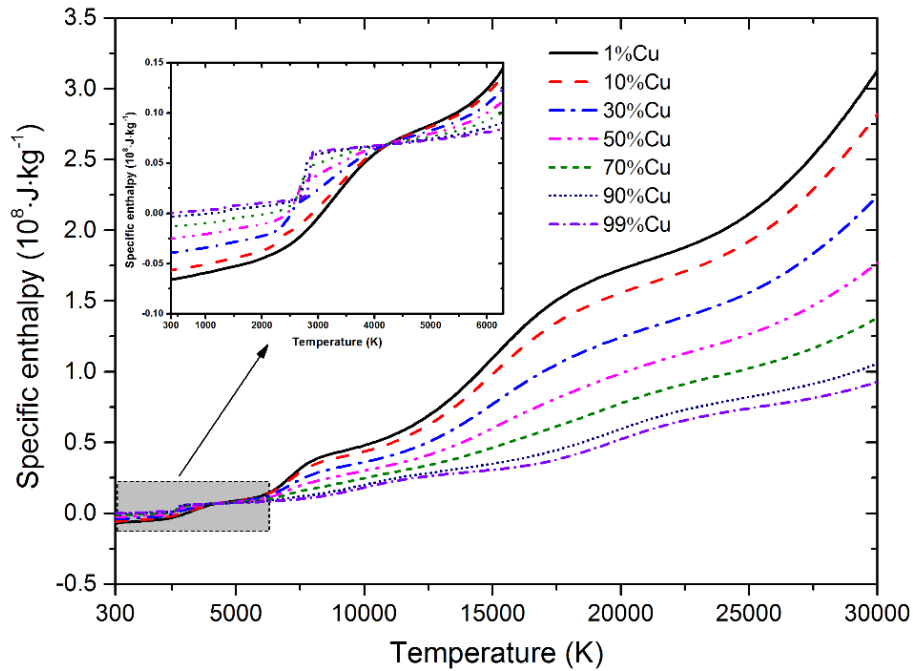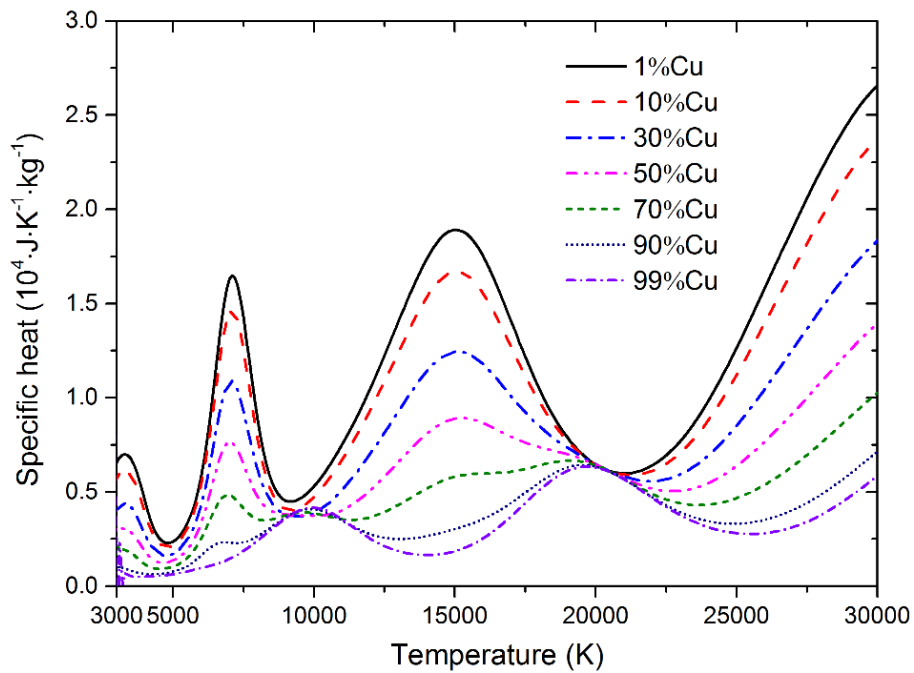

Figure 2-20. Specific heat of CO_2-N_2 (mixing ratio 7:3) mixtures contaminated by different proportions of Cu at temperatures of 3000 – 30,000 K and at 1 bar

As can been in Figure 2-20, the CO_2-N_2-Cu mixtures with a low or medium copper concentration ($\leq 50\%$) have three peaks in the specific heat at around 3200 K, 7000 K

and 14,900 K, which correspond to the decomposition of O_2, dissociation of CO and N_2, and ionization of O and N respectively. When more copper is added in the mixtures, the above three peaks will disappear gradually, and instead, two new peaks at round 9600 K and 19,500 K will be observed, which correspond to the first and second ionizations of copper.

In general, copper contamination reduces the specific heat of CO_2-N_2-Cu mixtures in the whole temperature range because of the increase of mass density (as explained in section 2.3.3) as well as because of its smaller heat capacity than that of CO_2 and N_2.

Figure 2-21 describes the specific heat of pure CO_2, pure N_2 and their mixtures with mixing ratios of 7:3, 5:5 and 3:7 in the temperature range of 3000 – 30,000 K at ambient pressure. The proportion of the copper contamination is set be 10%.
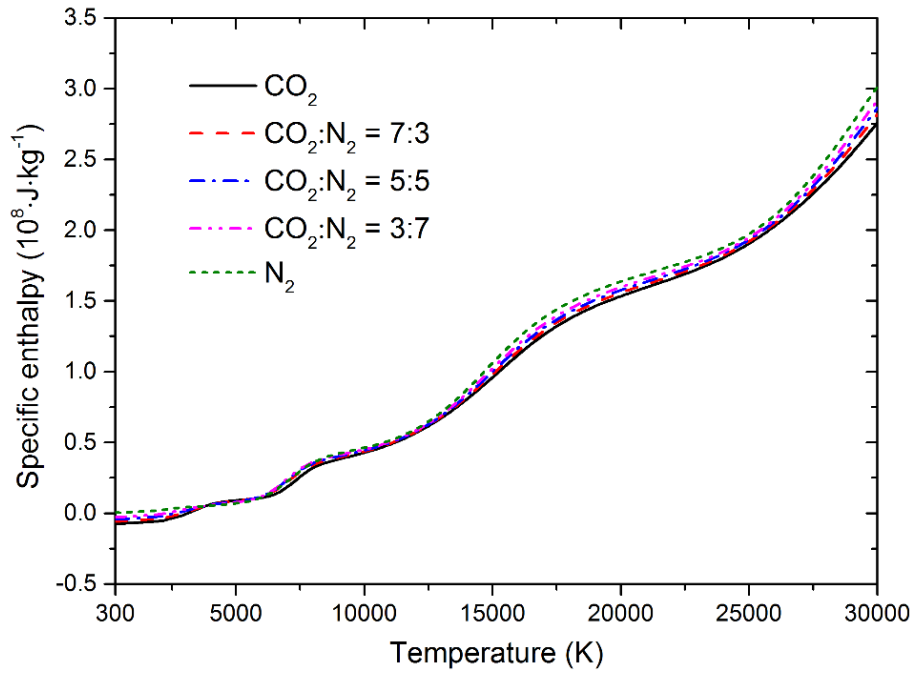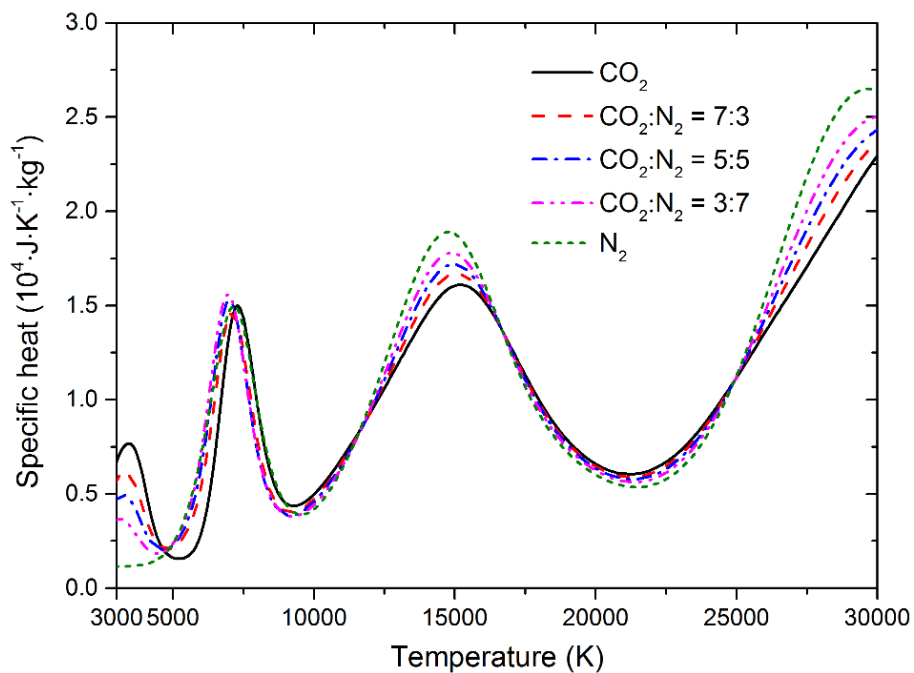

Figure 2-21. Specific heat of CO_2, N_2, and their different mixtures contaminated by 10% Cu at temperatures of 3000 – 30,000 K and at 1 bar

As observed in Figure 2-21, with the addition of N_2, the peak values of specific heat are affected by the dissociation of N_2 or ionization of N. For example, the peak

observed at around 3200 K in CO_2-N_2-Cu mixtures gradually diminishes when N_2 is mixed as CO_2 dissociates at around this temperature. Moreover, considering that the ionization potential of N (14.53 eV) is higher than that of O (13.62 eV) [119], the peak due to the ionization of N and O at around 14,900 K is inevitably reduced with the increase of N_2. Another interesting observation is that the peak at around 7000 K is shifted lightly to the left (the low temperature) with the increasing addition of N_2. This can be attributed to the dissociation of N_2 and CO, considering that the bond enthalpy of N_2 (942 kJ·mol^{-1}) is slightly lower than that of CO (1072 kJ·mol^{-1}).

The influence of pressures on the specific heat of CO_2-N_2 mixtures (mixing ratio 7:3) contaminated by 10% copper is also studied and presented in Figure 2-22 as a function of temperature from 3000 K to 30,000 K.
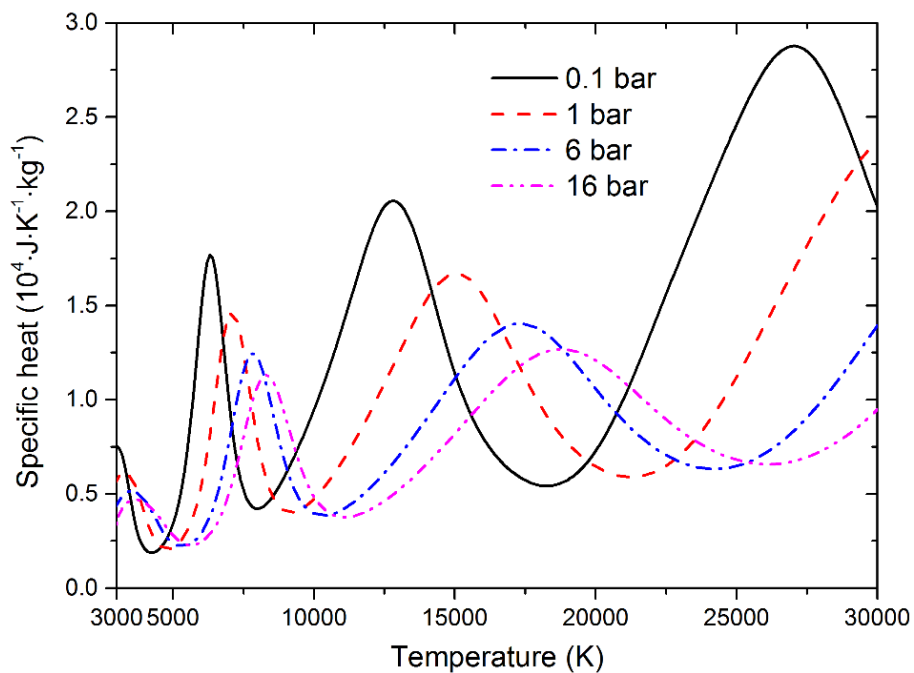
Figure 2-22. Specific heat of CO_2-N_2 (mixing ratio 7:3) mixtures contaminated by 10% Cu at temperatures of 3000 – 30,000 K and at different pressures

Differently from the mass density and specific enthalpy, the specific heat of CO_2-N_2-Cu mixtures does not vary monotonically with pressure. The multiple peaks of the

specific heat are observed to shift to higher temperatures at higher pressures. This can be explained by Le Chatelier's principle [37]: the increase of pressure in gas mixtures tends to suppress the dissociation and ionization reactions. As a result, the shift of the peaks in specific heat is the consequence of the shift of temperature points at which the dissociation and ionization reactions occur [37]. The suppression of dissociation and ionization are also responsible for the decrease of peak values.

2.4 Comparison with SF$_6$-Cu mixtures

In order to highlight the difference between SF$_6$ and CO$_2$-N$_2$ mixtures, we performed a calculation of equilibrium compositions and thermodynamic properties of SF$_6$-Cu mixtures. As discussed in our published work [37], 56 species (including 5 condensed particles S(c), Cu(c), CuS(c), CuF(s), and CuF$_2$(c)) as well as electrons were taken into account. Figure 2-23 shows the composition of 90%SF$_6$-10%Cu mixtures as a function of temperature at ambient pressure.
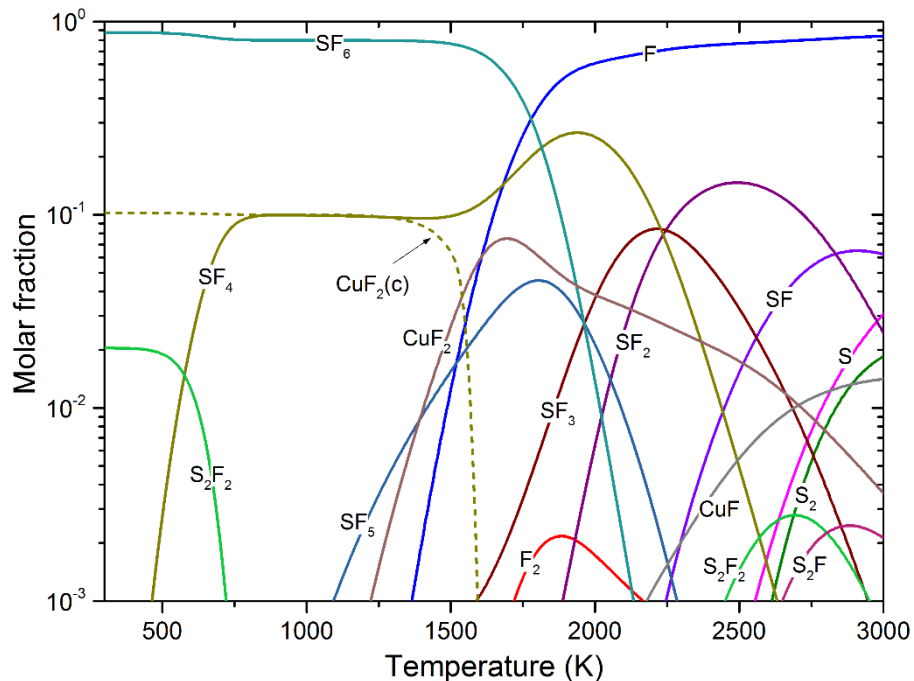
Figure 2-23. Equilibrium compositions of SF$_6$ contaminated by 10% Cu at temperatures of 300 – 3000 K and at 1 bar

39

It can be found that elemental copper in SF_6-Cu mixtures exists in the form of condensed CuF_2 instead of condensed copper as observed in CO_2-N_2-Cu mixtures at low temperatures. This is because fluorine atoms are more active than carbon, oxygen and nitrogen, and hence easier to combine with the copper atoms [37]. Furthermore, fluorine atoms are so electronegative that they will always oxidize copper to +2 oxidation state and cause the generation of CuF_2 rather than CuF [37].

The turbulent convection which is characterized by the product of mass density and specific heat (denoted as $\rho \cdot C_p$) [126] plays an important role in cooling arc plasmas. Figure 2-24 describes the values of $\rho \cdot C_p$ for the CO_2-N_2 mixture (mixing ratio 7:3) and SF_6 gas, both of which are contaminated by 1% copper.
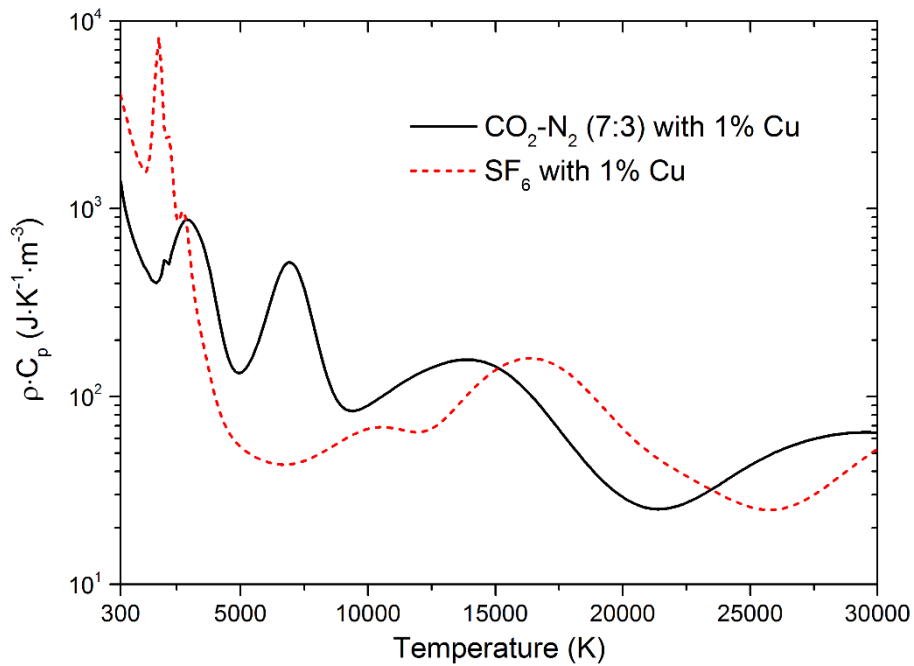
Figure 2-24. Comparison of $\rho \cdot C_p$ of CO_2-N_2 (mixing ratio 7:3) mixture and SF_6 gas contaminated by 1% copper at temperatures of 300 – 3000 K and at 1 bar

The peaks of $\rho \cdot C_p$ correspond to the dissociation of molecules. For example, the peak observed at around 1800 K in SF_6-Cu mixtures is the consequence of the decomposition of SF_6. On one hand, to cool the arc quickly during the current zero period, the gas mixtures should have high values of $\rho \cdot C_p$ at low temperatures. From this

point, SF_6 is far superior to CO_2-N_2 mixtures as the $\rho \cdot C_p$ of SF_6-Cu mixtures is much higher than that of CO_2-N_2-Cu mixtures when the temperature is below 2800 K. On the other hand, from 2800 K to 15,200 K, CO_2-N_2-Cu mixtures present much larger $\rho \cdot C_p$ than SF_6-Cu mixtures, which is also beneficial to remove energy from arc and cool arc down.

2.5 Summary

In this chapter, we calculate the equilibrium compositions and thermodynamic properties of CO_2-N_2-Cu mixtures at various temperatures and pressures. The condensed species are taken into account to investigate the influences of their phase transition on the compositions and thermodynamic properties. Additionally, the effect of mixing ratios between CO_2 and N_2 and the influence of gas pressures are also discussed.

The condensed copper is found to exist at temperatures below 3000 K although the other condensed species e.g. graphite and solid CuO are also considered in the calculation. The temperature point relating to the phase transition of condensed copper does not keep constant but increase with copper proportion until the temperature reaches the boiling point of copper. This phase transition inevitably affects the thermodynamic properties. For example, the copper evaporation causes the value of specific heat of CO_2-N_2-Cu mixtures to increase sharply and drop steeply.

Cu has larger molar mass than CO_2 and N_2, which leads to the remarkable increase in the mass density of CO_2-N_2-Cu mixtures. And mainly because of this, the mixing of copper results in the decrease in the specific enthalpy of the mixtures, considering that specific enthalpy is inversely proportional to mass density. For specific heat, the addition of copper makes the three peaks in the specific heat diminish gradually. These three peaks correspond to the decomposition of O_2, dissociation of CO and N_2, and ionization of O and N respectively. Instead, the peaks due to the first and second ionizations of copper are observed more and more clearly when the copper percentage

41

is raised.

The mixing ratio between CO_2 and N_2 shows a slight or even negligible effect on the mass density and specific enthalpy of the mixtures. For specific heat, the peak values are affected by the mixing of N_2. This can be attributed to the dissociation of N_2 and ionization of N.

The influences arising from gas pressure on the compositions and thermodynamic properties of CO_2-N_2-Cu mixtures are more understandable. Due to the compression of gas mixtures with pressures, the mass density and specific enthalpy increases and decreases respectively. Also with the increase of pressure, the dissociation and ionization reactions in CO_2-N_2-Cu mixtures are suppressed. Consequently, the multiple peaks of specific heat are shifted to higher temperatures.

In SF_6-Cu mixtures copper exists in the form of condensed CuF_2 instead of condensed copper as observed in CO_2-N_2-Cu mixtures at low temperatures. Compared with SF_6-Cu mixtures, CO_2-N_2-Cu mixtures present lower $\rho \cdot C_p$ at low temperatures but higher $\rho \cdot C_p$ at medium temperatures. As an arc quenching medium, the gas mixtures with higher $\rho \cdot C_p$ is easier to remove energy from the arc and thus the arc is easier to be interrupted successfully.

CHAPTER 3 TRANSPORT AND COMBINED DIFFUSION COEFFICIENTS OF CO₂-N₂-CU PLASMAS

3.1 Introduction

The transport coefficients in this dissertation include electrical conductivity, viscosity, and thermal conductivity. Electrical conductivity is the transport of electrons and ions in plasmas because of their gradients in concentration, pressure, and temperature [40]. Viscosity represents the transport of momentum due to the gradient in the velocity [40]. Thermal conductivity is the transfer of thermal energy resulting from the thermal gradients, chemical reactions and internal degrees of freedom [40, 127]. The combined diffusion coefficients in this work includes four kinds of coefficients, namely the combined ordinary diffusion coefficient, combined electric field diffusion coefficient, combined temperature diffusion coefficient, and combined pressure diffusion coefficient, which describe the diffusion due to the composition gradients, applied electric fields, temperature gradients, and pressure gradients respectively [41].

The transport and diffusion coefficients of a thermal plasma are necessary in determining whether it can be applied in a certain industrial application. For example, in circuit breakers, a successful interruption requires that the arc quenching gas must have high thermal conductivity to remove energy quickly from itself [30]. Also in circuit breakers, the diffusion coefficients are needed to model the mixing of the electrode vapour with the filling gas [41]. Therefore, this chapter is devoted to the calculation and discussion of the transport coefficients and combined diffusion coefficients of CO_2-N_2-Cu mixtures.

The following sections are organized as follows. In section 3.2, the calculation methods of the transport coefficients and collision integrals are presented firstly in subsections 3.2.1 and 3.2.2 respectively. Then in sections 3.2.3 – 3.2.5, the results for the electrical conductivity, viscosity, and thermal conductivity of CO_2-N_2-Cu mixtures

are discussed respectively. Next, the section 3.3 focuses on the combined diffusion coefficients. The calculation procedure is introduced in section 3.3.1, and the results for the combined ordinary diffusion coefficient, combined electric field diffusion coefficient, combined temperature diffusion coefficient, and combined pressure diffusion coefficient of CO_2-N_2-Cu plasmas are presented and discussed in sections 3.3.2 – 3.3.5 respectively. A comparison between CO_2-N_2-Cu and SF_6-Cu mixtures is discussed in section 3.4. Finally, the section 3.5 summarizes this chapter.

3.2 Transport coefficients

3.2.1 Determination of transport coefficients

In a gas mixture, species interact with each other through collisions [108]. The statistical behaviour of gas mixtures is described by the Boltzmann equation, and the calculation of the transport coefficients is based on the solution of this equation. However, even in a quite simple case of an ideal gas, the solving of the Boltzmann equation is rather complicated because it is a nonlinear integral-differential equation. To simplify the calculation, the well-known Chapman-Enskog method was developed and has been widely used to calculate the transport coefficients of gas mixtures. The Chapman-Enskog method is founded on the assumption that the distribution function of species changes as a result of particle collisions and the macroscopic flow variables or macro-parameters (i.e. temperature, pressure, hydrodynamic velocity, and composition) are the first moments of the distribution function [40, 56]. The Maxwellian distribution function with a first-order perturbation is used in the Chapman-Enskog method [40, 128], and the solution of the Boltzmann equation is generally expressed as Sonine polynomial expansions, yielding a system of linear equations. The solutions of these linear equations to a selected order allow the transport coefficients to be determined [40, 128]. Chervy et al [38], Capitelli et al. [129], Cressault et al. [130], and André et al. [131] gave the expressions of these solutions as functions of temperature, pressure, and number density to a certain order approximation.

These expressions are adopted in this work and summarized as follows.

The electrical conductivity σ of plasma mixtures is calculated to a third-order approximation, neglecting the contribution of ions due to their high mobility [38, 40, 130, 131].

$$
\sigma = \frac{3e^2}{2} n_e^2 \sqrt{\frac{2\pi}{m_e kT}} \frac{\begin{vmatrix} q^{11} & q^{12} \\ q^{12} & q^{22} \end{vmatrix}}{\begin{vmatrix} q^{00} & q^{01} & q^{02} \\ q^{01} & q^{11} & q^{12} \\ q^{02} & q^{12} & q^{22} \end{vmatrix}}
\tag{3-1}
$$

Where e is the elementary charge, n_e the number density of electrons, k the Boltzmann constant, and m_e is the mass of an electron. The parameters q^{ij} were given by Devoto [132] as functions of number densities of species and collision integrals between each species. The collision integrals will be introduced in the next section 3.2.2.

The viscosity η of plasma mixtures is calculated to a first-order approximation which neglects the electrons because of their extremely low mass [38, 40, 130, 131].

$$
\eta = -\frac{\begin{vmatrix} H_{11} & \cdots & H_{1v} & x_1 \\ \vdots & & \vdots & \vdots \\ H_{v1} & \cdots & H_{vv} & x_v \\ x_1 & \cdots & x_v & 0 \end{vmatrix}}{\begin{vmatrix} H_{11} & \cdots & H_{1v} \\ \vdots & & \vdots \\ H_{v1} & \cdots & H_{vv} \end{vmatrix}}
\tag{3-2}
$$

With

$$
H_{ii} = \frac{x_i^2}{\eta_i} + \sum_{k=1, k \neq i}^{v} \frac{2 x_i x_k}{\eta_{ik}} \frac{M_i M_k}{\left(M_i + M_k\right)^2} \left(\frac{5}{3 A_{ik}^*} + \frac{M_k}{M_i} \right)
\tag{3-3}
$$

$$
H_{ij} = -\frac{2 x_i x_j}{\eta_{ij}} \frac{M_i M_j}{\left(M_i + M_j\right)^2} \left(\frac{5}{3 A_{ij}^*} - 1 \right) \quad (i \neq j)
\tag{3-4}
$$

$$
A_{ij}^* = \frac{\overline{\Omega}_{ij}^{(2,2)}}{\overline{\Omega}_{ij}^{(1,1)}}
\tag{3-5}
$$

45

$$\eta_i = \frac{5}{16} \frac{1}{\overline{\Omega}_{ii}^{(2,2)}} \sqrt{\frac{kT}{\pi N_a}} \sqrt{M_i} \tag{3-6}$$

$$\eta_{ij} = \frac{5}{16} \frac{1}{\overline{\Omega}_{ij}^{(2,2)}} \sqrt{\frac{kT}{\pi N_a}} \sqrt{\frac{2M_i M_j}{M_i + M_j}} \tag{3-7}$$

$$\tag{3-8}$$

Where x_i and M_i are the molar fraction and molar mass of particle i, N_a the Avogadro number, v the number of heavy particles, and $\overline{\Omega}_{ij}^{(l,s)}$ are the collision integrals which will be presented in section 3.2.2.

The calculation of the thermal conductivity in plasma mixtures is quite complicated as it can be represented as the sum of three components, respectively the translational thermal conductivity κ_{tr}, internal thermal conductivity κ_{int}, and reaction thermal conductivity κ_{reac} [38, 40, 50]. The translational thermal conductivity κ_{tr}, can be further broken down into the contributions denoted as κ_{tr}^h and κ_{tr}^e for heavy particles and electrons respectively [38, 40, 130, 131].

$$\kappa_{tr} = \kappa_{tr}^h + \kappa_{tr}^e \tag{3-9}$$

$$\kappa_{tr}^e = \frac{75}{8} n_e^2 k \sqrt{\frac{2\pi kT}{m_e}} \frac{q^{22}}{q^{11} q^{22} - \left(q^{12}\right)^2} \tag{3-10}$$

$$\kappa_{tr}^h = 4 \frac{\begin{vmatrix} L_{11} & \cdots & L_{1v} & x_1 \\ \vdots & & \vdots & \vdots \\ L_{v1} & \cdots & L_{vv} & x_v \\ x_1 & \cdots & x_v & 0 \end{vmatrix}}{\begin{vmatrix} L_{11} & \cdots & L_{1v} \\ \vdots & & \vdots \\ L_{v1} & \cdots & L_{vv} \end{vmatrix}} \tag{3-11}$$

With

$$L_{ii} = -4 \frac{x_i^2}{k_{ii}} - \sum_{k=1,k\neq i}^{v} \frac{2x_i x_k \left(\frac{15}{2} M_i^2 + \frac{25}{4} M_k^2 - 3B_{ik}^* M_k^2 + 4A_{ik}^* M_i M_k\right)}{k_{ik} A_{ik}^* \left(M_i + M_k\right)^2} \tag{3-12}$$

46

$$L_{ij} = \frac{2x_i x_j M_i M_j}{k_{ij} A_{ij}^* \left(M_i + M_j \right)^2} \left(\frac{55}{4} - 3B_{ij}^* - 4A_{ij}^* \right) \quad (i \neq j) \tag{3-13}$$

$$B_{ij}^* = \frac{5\overline{\Omega}_{ij}^{(1,2)} - 4\overline{\Omega}_{ij}^{(1,3)}}{\overline{\Omega}_{ij}^{(1,1)}} \tag{3-14}$$

$$k_{ij} = \frac{75}{64} \frac{k}{\overline{\Omega}_{ij}^{(2,2)}} \sqrt{\frac{N_a kT}{\pi}} \sqrt{\frac{M_i + M_j}{2M_i M_j}} \tag{3-15}$$

Where A_{ij}^* is expressed as formula (3-5).

The internal thermal conductivity κ_{int} is calculated considering the effect of internal degrees of freedom [38, 40, 130, 131].

$$\kappa_{int} = \sum_{i=1}^{N} \frac{\kappa_{int}^i}{1 + \sum_{j=1, j\neq i}^{N} \frac{x_j D_{ii}}{x_i D_{ij}}} \tag{3-16}$$

$$\kappa_{int}^i = \frac{PD_{ii}}{T} \left(\frac{C_{pi}}{R} - \frac{5}{2} \right) \tag{3-17}$$

$$D_{ij} = \frac{3}{8} \frac{kT}{P\overline{\Omega}_{ij}^{(1,1)}} \sqrt{\frac{N_a kT}{\pi}} \sqrt{\frac{M_i + M_j}{2M_i M_j}} \tag{3-18}$$

Where P is the pressure and C_{pi} is the specific heat at constant pressure of particle i.

The calculation of reaction thermal conductivity κ_{reac} was developed by Butler and Brokaw [133]. For a gas mixture composed N species and in which μ linearly-independent chemical reactions can occur, κ_{reac} can be calculated as [38, 40, 130, 131]

$$\kappa_{reac} = -\frac{1}{RT^2} \frac{\begin{vmatrix} A_{11} & \cdots & A_{1\mu} & \Delta H_1 \\ \vdots & & \vdots & \vdots \\ A_{\mu 1} & \cdots & A_{\mu\mu} & \Delta H_\mu \\ \Delta H_1 & \cdots & \Delta H_\mu & 0 \end{vmatrix}}{\begin{vmatrix} A_{11} & \cdots & A_{1\mu} \\ \vdots & & \vdots \\ A_{\mu 1} & \cdots & A_{\mu\mu} \end{vmatrix}} \tag{3-19}$$

$$A_{ij} = \sum_{k=1}^{N-1} \sum_{l=k+1}^{N} \frac{RT}{PD_{kl}} x_l x_k \left(\frac{a_{ik}}{x_k} - \frac{a_{il}}{x_l} \right) \left(\frac{a_{jk}}{x_k} - \frac{a_{jl}}{x_l} \right) \tag{3-20}$$

47

Where ΔH_i is the reaction enthalpy of reaction i and a_{ij} are the stoichiometric coefficients.

Additionally, according to the results for the compositions presented in Chapter 2, 40 species in CO_2-N_2-Cu mixtures, including C, C_2, C_3, CN, CO, CO_2, N, N_2, NO, NO_2, O, O_2, Cu, Cu_2, CuO, C^+, C^{2+}, C^{3+}, C^-, C_2^+, CN^+, CO^+, CO^-, N^+, N^{2+}, N^{3+}, N_2^+, N_2^-, NO^+, O^+, O^{2+}, O^{3+}, O^-, O_2^+, Cu^+, Cu^{2+}, Cu^{3+}, Cu^{4+}, Cu^-, and e^-, the molar fractions of all of which are more than 10^{-5}, are considered in the calculation of transport coefficients. The condensed species are not taken into account because there has not been a proper theory so far to describe the interaction of condensed species [40].

3.2.2 Collision integrals

As described above, the calculation of transport coefficients is based on the Chapman-Enskog theory. In this theory, the collision dynamics enter the transport equations through the so-called collision integrals $\Omega_{ij}^{(l,s)}$, associated to the (i,j) interaction pair, characterized by the order (l,s) and depending on the temperature [40, 134]. The collision integrals $\Omega_{ij}^{(l,s)}$ is written as [40, 135]:

$$\Omega_{ij}^{(l,s)} = \sqrt{\frac{kT}{2\pi\mu_{ij}}} \int_0^\infty e^{-\gamma_{ij}^2} \gamma_{ij}^{2s+3} Q_{ij}^{(l)}(\varepsilon) d\gamma_{ij} \qquad (3\text{-}21)$$

Where $\gamma_{ij} = (\varepsilon/kT)^{1/2}$, ε being the kinetic energy, k the Boltzmann constant, μ_{ij} the reduced mass of species i and j. $Q_{ij}^{(l)}(\varepsilon)$ represents the transport cross section corresponding to the lth moment and is defined by the following expression [19, 40]:

$$Q_{ij}^{(l)}(\varepsilon) = 2\pi \int_0^\pi \sigma_{ij}(\chi,\varepsilon) \cdot (1-\cos^l \chi) \sin \chi d\chi \qquad (3\text{-}22)$$

Where $\sigma_{ij}(\chi,\varepsilon)$ is the differential cross section corresponding to the collision between species i and j, χ is the deflection angle after the collision. In practical computation, the reduced collision integrals are used as defined by the expression [38, 40, 136]:

$$\overline{\Omega}_{ij}^{(l,s)} = \frac{4(l+1)}{\pi(s+1)!\left[2l+1-(-1)^l\right]} \int_0^\infty e^{-\gamma_{ij}^2} \gamma_{ij}^{2s+3} Q_{ij}^{(l)}(\gamma_{ij}) d\gamma_{ij} \tag{3-23}$$

In order to determine the collision integrals, four kinds of interactions, namely neutral-neutral, neutral-ion, neutral-electron and charged-charged interactions, need be considered. In the following subsections, these four interactions are discussed in details. The similar work for SF₆-Cu mixtures was published in [40] during my Ph.D. study.

A. Neutral-Neutral interactions

To describe the interaction between two neutral particles, several potentials, such as the Morse potential [137], the Lennard-Jones potential [138], the exponential repulsive potential [139], and the Hulburt-Hirschfelder potential [140], have been used. Each of these potentials is a good description of neutral-neutral interactions and is commonly used. However, some potentials have their limitations and are not valid for all interactions. For example, the Morse potential does not become infinite at zero separation, which disobeys the law of physics [141]; The Lennard-Jones potential has a sixth-power term which models dipole-dipole interactions due to electron dispersion, but it does not represent other kinds of bonding well [138]. Recently, Laricchiuta, Capitelli and their co-workers [54, 142] proposed a Lennard-Jones like phenomenological model potential which can be considered as an improvement of the Lennard-Jones potential. Compared with other potentials, this phenomenological potential is valid in the whole interaction range [142] and has been applied to produce many reliable collision integrals and corresponding transport coefficients [12, 16, 40, 56, 128, 143, 144]. Therefore, in this work, the Lennard-Jones like phenomenological potential is adopted to calculate neutral-neutral collision integrals.

The Lennard-Jones like phenomenological potential is written as [142]

$$\varphi(x) = \varepsilon_b \left[\frac{m}{n(x)-m}\left(\frac{1}{x}\right)^{n(x)} - \frac{n(x)}{n(x)-m}\left(\frac{1}{x}\right)^m \right] \tag{3-24}$$

Where $x = r/r_e$, $n(x) = \beta + 4x^2$, r_e is the equilibrium distance, ε_b is the binding

energy, and *m* has the value of 6 for neutral-neutral interactions. The parameter β can be estimated by a simple empirical formula [142]

$$\beta = 6 + \frac{5}{s_i + s_j} \tag{3-25}$$

Where s_i and s_j are defined as the cubic root of the polarizability of the colliding particles *i* and *j*. Laricchiuta et al. [142] and Capitelli et al. [54] pointed out that, for open-shell atoms, a multiplicative factor which is the ground state spin multiplicity should be considered in the determination of s_i and s_j.

Table 3-1 lists the polarizability of neutral species considered in the calculation of transport coefficients. All the data were compiled from NIST Computational Chemistry Comparison and Benchmark Database [145] and the previous work [40].

Table 3-1. Polarizability of neutral species (Å^3)

Species	Polarizability	Species	Polarizability
C	1.760	N	1.100
C_2	7.815	N_2	1.710
C_3	5.179	NO	1.698
CN	3.161	NO_2	2.910
CO	1.953	Cu	6.200
CO_2	2.507	Cu_2	11.554
O	0.802	CuO	4.658
O_2	1.562		

Figure 3-1 and Figure 3-2 present the collision integrals $\overline{\Omega}(1,1)$ and $\overline{\Omega}(2,2)$ respectively for C-C, N-N, O-O and Cu-Cu interactions. The results show the much larger collision integrals of Cu-Cu than the others, which predictably affect the transport coefficients of CO_2-N_2 plasmas contaminated by copper. In the sections 3.2.3 – 3.2.5, these collision integrals will help to explain the behaviours of transport coefficients.

Figure 3-1. Collision integrals $\overline{\Omega}(1,1)$ for C-C, N-N, O-O, and Cu-Cu interactions
using the Lennard-Jones like phenomenological potential at 300 – 30,000 K
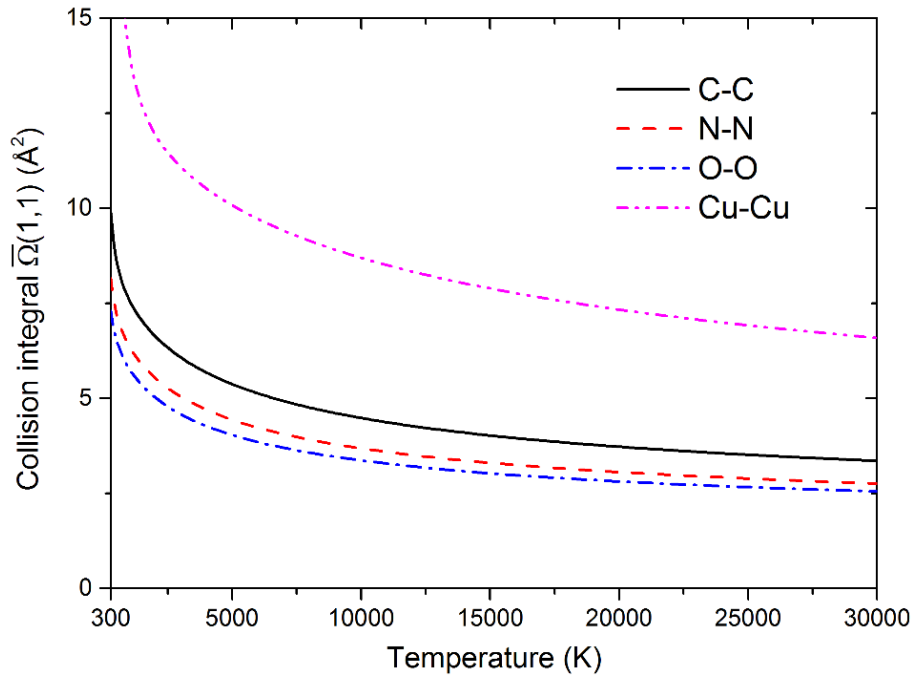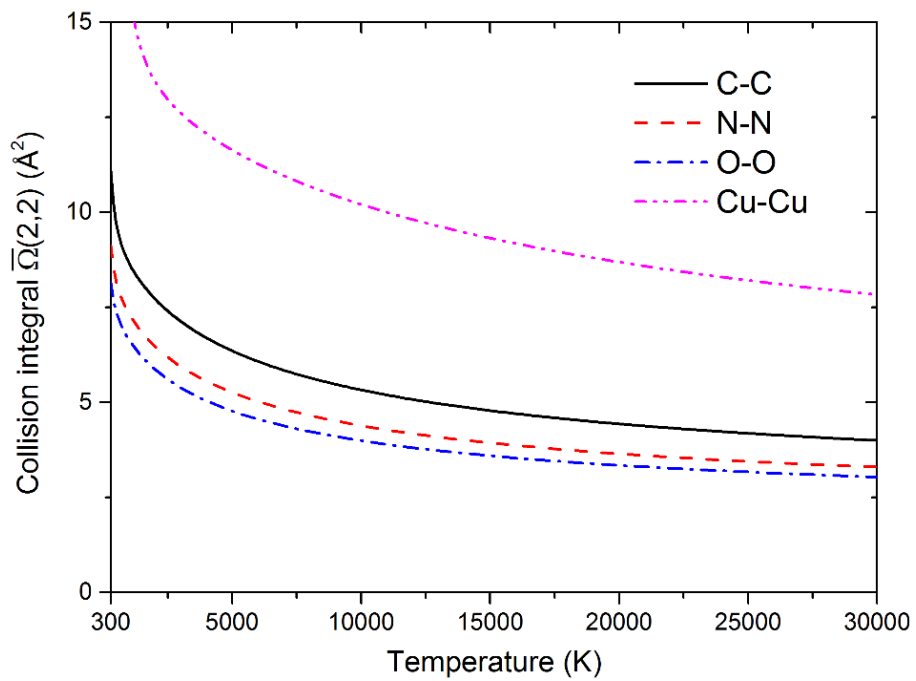

Figure 3-2. Collision integrals $\overline{\Omega}(2,2)$ for C-C, N-N, O-O, and Cu-Cu interactions
using the Lennard-Jones like phenomenological potential at 300 – 30,000 K

B. Neutral-Ion interactions

To describe the neutral-ion interactions, two types of processes need to be taken into account: purely elastic collisions and resonant charge-exchange inelastic process [38, 128]. For the interaction between the neutral particle (X) and the ionized particle (Y^{z+} or Y^{z-}) which are of the different chemical species, elastic collisions dominate the process in determining collision integrals [38, 50, 84, 128], whereas for the interaction between the neutral particle (X) and its ion (X^{z+} or X^{z-}), two different cases should be considered: if the order l is even (i.e. $l = 2$), the collision integrals are wholly determined by the elastic interaction while for the order l is odd (i.e. $l = 1$ or 3), the resonant charge-exchange plays an important role in determining collision integrals [38, 50, 84, 128]. For the cases in which resonant charge-exchange process cannot be ignored, we use an empirical mixing rule proposed by Murphy [50, 125, 146, 147] to calculate the total collision integrals:

$$\Omega^{(l,s)} = \sqrt{\left(\Omega_{el}^{(l,s)}\right)^2 + \left(\Omega_{in}^{(l,s)}\right)^2} \tag{3-26}$$

Where the subscripts 'el' and 'in' denote the collision integrals derived from the elastic and inelastic interactions respectively.

For the calculation of elastic collision integrals $\Omega_{el}^{(l,s)}$, some researchers used the polarization potential [19, 38, 50, 80, 84, 130, 131, 148-150]. Recently, a more sophisticated potential which is an extension of the Lennard-Jones like phenomenological potential used for neutral-neutral interactions is proposed to calculate neutral-ion collision integrals [142]. In this work, we prefer to use this phenomenological potential to describe the elastic collisions between ions and neutral particles. The polarizability data of the ions considered in the calculation are given in Table 3-2. Most of the data (except for multiply charged ions of nitrogen and copper) were compiled from NIST Computational Chemistry Comparison and Benchmark Database [145] and the previous work [40, 58]. The rest data (N^{2+}, N^{3+}, Cu^{2+}, Cu^{3+}, and Cu^{4+}) are determined by a quantum chemical calculation using B3LYP density

52

functional and the aug-cc-PVQZ basic set [40].

Table 3-2. Polarizability of ions (Å^3)

Species	Polarizability	Species	Polarizability
C^+	0.829	Cu^-	0.252
C^{2+}	0.578	N^+	0.568
C^{3+}	0.289	N^{2+}	0.384
C^-	7.280	N^{3+}	0.319
C_2^+	3.200	N^{2+}	2.146
CN^+	3.360	N_2^-	8.311
CO^+	1.341	NO^+	1.031
CO^-	14.153	O^+	0.376
Cu^+	0.938	O^{2+}	0.228
Cu^{2+}	0.422	O^{3+}	0.182
Cu^{3+}	0.237	O^-	3.200
Cu^{4+}	0.148	O_2^+	0.958

For the calculation of inelastic collision integrals $\Omega_{in}^{(l,s)}$, we follow the works of Chervy et al. [38], Murphy and Arundelli [50], and Wang et al. [113], using the charge-exchange cross section Q_{ex} to evaluate $\Omega_{in}^{(l,s)}$ numerically through the cross section $Q_{ij}^{(l)}(\varepsilon)$ [38, 50, 113]:

$$Q_{ij}^{(l)}(\varepsilon) = 2Q_{ex} \qquad (3\text{-}27)$$

Where Q_{ex} can be obtained as a function of impact velocity g through experimental or theoretical approaches, and is usually fitted in two parameters A and B.

$$Q_{ex} = \frac{1}{2}\left[A - B\ln(g)\right]^2 \qquad (3\text{-}28)$$

Table 3-3 lists the fitting parameters A and B for the charge-exchange cross sections

considered in this work. The data were compiled from the works by Copeland and Crothers [151], Capitelli et al. [129], Aubreton et al. [152] and Yang et al. [153]. It should be noted that these parameters were determined with the impact velocity g in unit of cm·s^{-1}. Many publications did not point this out explicitly and some of them probably used g in unit of m·s^{-1}.

Table 3-3. Fitting parameters A and B for the charge-exchange cross sections (Å)

Interaction	A	B
C-C$^+$	28.7289	1.2888
O-O$^+$	19.5	0.832
O-O$^-$	36.22	1.744
N-N$^+$	26.61	1.27
Cu-Cu$^+$	24.54	1.091
CO-CO$^+$	25.3650	1.0629
NO-NO$^+$	23.61	1.095
N$_2$-N$_2^+$	24.5	1.032
O$_2$-O$_2^+$	24.05	1.132
O$_2$-O$_2^-$	14.05	0.572

C. Electron-Neutral interactions

To obtain collision integrals corresponding to electron-neutral interactions, an integration of transport cross sections must be performed. If the differential cross section $\sigma_{ij}(\chi, \varepsilon)$ is available, we can use formula (3-22) to determine an arbitrary order cross section. However, the differential cross sections for some particles are usually hard to obtain. Some approximations are therefore needed. Chervy et al. [38] assumed that the differential cross section is independent of deflection angle and thus derived the relation $Q_{ij}^{(2)}(\varepsilon) = 2/3 \cdot Q_{ij}^{(1)}(\varepsilon)$. Similarly, Murphy [50, 125] assumed that

$\Omega_{ij}^{(1,1)} = \Omega_{ij}^{(2,2)}$. Recently, Capitelli [127], Laricchiuta [55] and their co-workers proposed a more accurate approximation method. In their method, when the total elastic cross section $Q_{ij}^{(0)}(\varepsilon)$ is available, the ratio $Q_{ij}^{(2)}(\varepsilon)/Q_{ij}^{(1)}(\varepsilon)$ can be determined from the known $Q_{ij}^{(1)}(\varepsilon)/Q_{ij}^{(0)}(\varepsilon)$ assuming a model angular dependence of the differential cross section [55].

$$\sigma_{ij}(\chi,\varepsilon) \propto \frac{1}{\left(1 - h(\varepsilon)\cos\theta\right)^2} \tag{3-29}$$

Where $h(\varepsilon)$ is an adjustable parameter, which depends on the electron energy, obtained from the ratio $Q_{ij}^{(1)}(\varepsilon)/Q_{ij}^{(0)}(\varepsilon)$. When $Q_{ij}^{(0)}(\varepsilon)$ is unavailable, the parameter h can be fixed according to Born scattering for a Coulomb screened potential [55].

$$\frac{1}{\left(1 + 2\eta\right)^2} \quad \text{with} \quad \eta = 10.9 \, Z^{2/3}/\varepsilon \tag{3-30}$$

When the momentum transfer cross section $Q_{ij}^{(1)}(\varepsilon)$ is also unavailable, we determine the collision integrals using the polarizability potential [131, 149].

$$\overline{\Omega}_{ij}^{(l,s)} = \frac{4(l+1)}{(s+1)!\left[2l+1-(-1)^l\right]} \sqrt{\frac{4}{kT}} \sqrt{\frac{\alpha Z e^2}{4\pi\varepsilon_0}} \Gamma\left(s + \frac{3}{2}\right) A_4^{(l)} \tag{3-31}$$

Where $\Gamma()$ is the Euler gamma function, α the polarizability of neutral species, ε_0 the vacuum electric permittivity, Z the charge number of ions, and e is the elementary charge. The parameters $A_4^{(l)}$ were given by Kihara et al. [154].

In this work, the collision integrals relating to e⁻-Cu₂, e⁻-CuO, e⁻-CN and e⁻-NO₂ are calculated using the polarizability potential, the others are determined through differential cross sections or momentum transfer cross sections which were compiled from the literatures [40, 149, 153].

D. Charged-Charged interactions

The interactions between two charged particles are described by a shielded

Coulomb potential [131].

$$V(r) = \frac{1}{4\pi\varepsilon_0} \frac{Z_i Z_j e^2}{r} \exp(-r/\lambda_d) \qquad (3\text{-}32)$$

Where Z_i and Z_j are the charge numbers of particle i and j respectively, and λ_d is the Debye length without consideration of ions, which is consistent with the definition in Chapter 2.

3.2.3 Electrical conductivity

The influence of copper contamination on the electrical conductivity of CO_2-N_2-Cu mixtures are investigated, and part of the results is shown in Figure 3-3 for CO_2-N_2 mixtures with a mixing ratio 7:3 in temperature range of 300 – 30,000 K at 1 bar. To help understand the behavior of electrical conductivity, the electron number density of CO_2-N_2-Cu mixtures in the same condition is illustrated in Figure 3-4.

As can be seen in Figure 3-3, the temperature range can be fragmented into three parts for electrical conductivity: 300 – 4500 K, 4500 – 15,800 K and 15,800 – 30,000 K. Below 4500 K, due to the very weak ionization as shown in Figure 3-4 for electron number density, the electrical conductivity of the mixtures is almost zero and therefore independent of copper content. From 4500 to 15,800 K, with the increase of copper and gradual enhancement of ionization, the electrical conductivity is raised because copper is easier to ionize than the other species in the mixtures. However, at temperatures above 15,800 K, the electrical conductivity drops dramatically despite the increase of copper.

The drop of electrical conductivity can be explained by the charged-charged interactions in this temperature range. According to the work of Deveto et al. [132], the electrical conductivity of plasma mixtures is inversely proportional to the collision integrals in a first approximation. Although the copper contamination results in more electrons, more ions due to the ionization of copper are generated simultaneously. As a result, the large collision integrals between charged particles cause the decrease of electrical conductivity when the copper proportion increases [40].
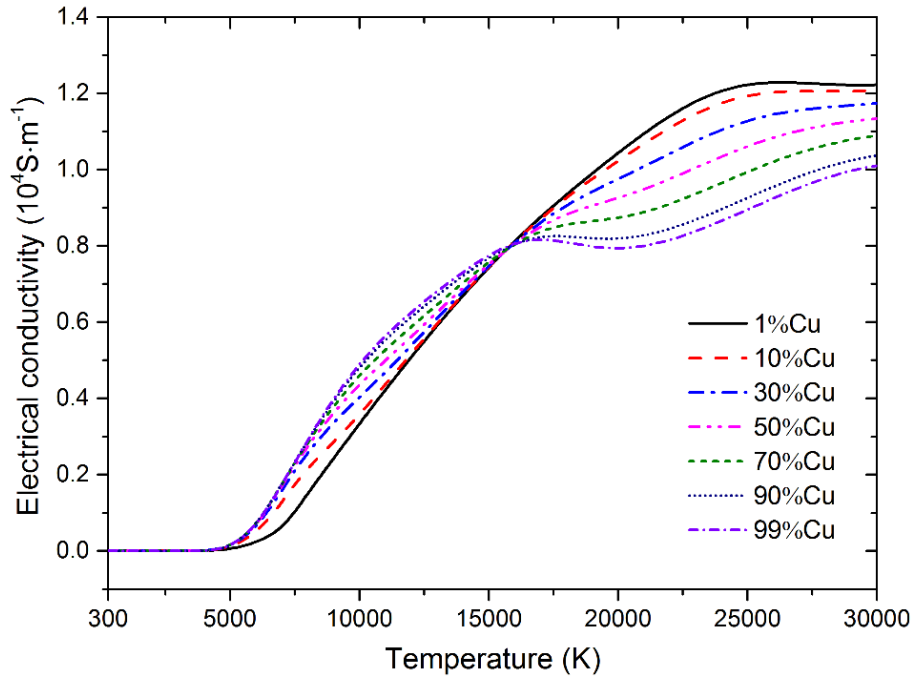
Figure 3-3. Electrical conductivity of CO_2-N_2 (mixing ratio 7:3) mixtures contaminated by different proportions of Cu at 300 – 30,000 K and at 1 bar
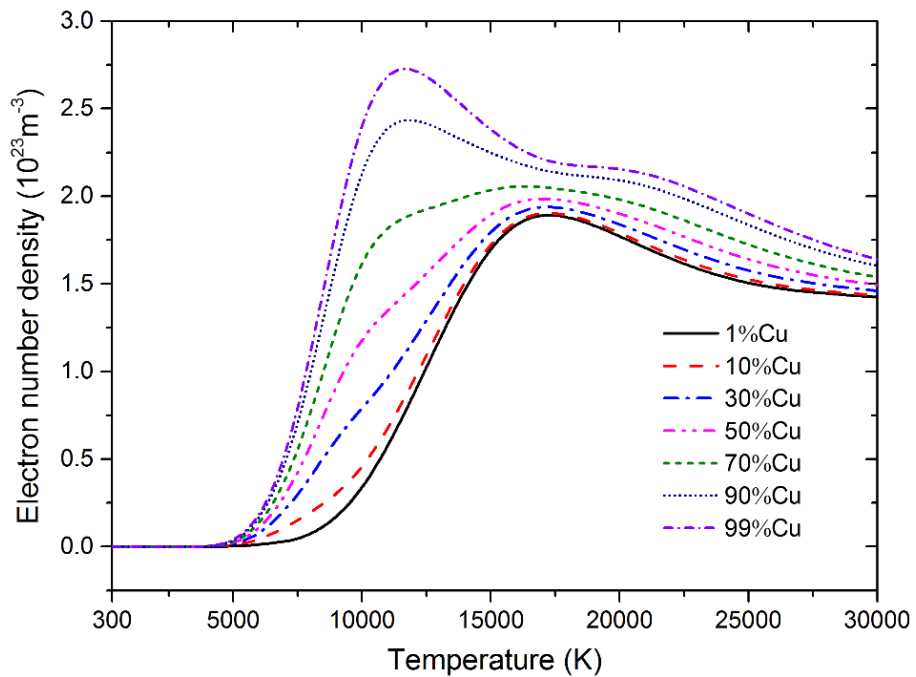
Figure 3-4. Electron number density of CO_2-N_2 (mixing ratio 7:3) mixtures contaminated by different proportions of Cu at 300 – 30,000 K and at 1 bar

Figure 3-5 shows the electrical conductivity of pure CO_2, pure N_2 and their mixtures with mixing ratios of 7:3, 5:5 and 3:7 in the temperature range of 300 – 30,000 K at ambient pressure. The proportion of copper contamination is fixed to be 10%. Generally, the ionization ability of carbon, oxygen and nitrogen is close to each other. Therefore, the addition of N_2 into CO_2 does not affect the electrical conductivity of CO_2-N_2-Cu mixtures.
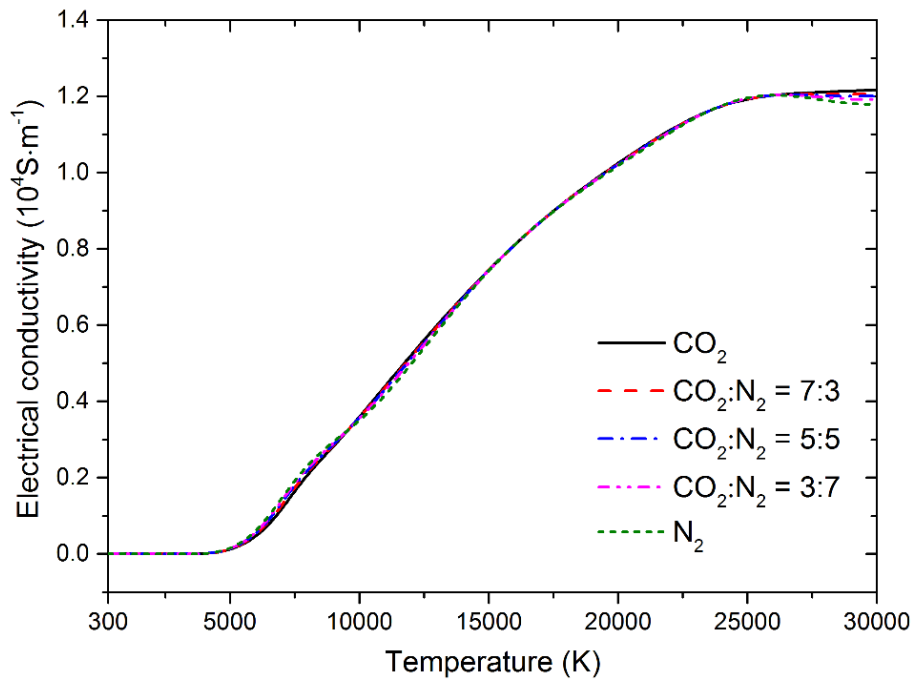
Figure 3-5. Electrical conductivity of CO_2, N_2, and their different mixtures contaminated by 10% Cu at temperatures of 300 – 30,000 K and at 1 bar

The effect of gas pressure on the electrical conductivity is investigated as presented in Figure 3-6. On this graph, the electrical conductivity of CO_2-N_2 mixtures (mixing ratio 7:3) contaminated by 10% copper is calculated at different pressures (0.1 bar, 1 bar, 6 bar and 16 bar) as a function of temperature up to 30,000 K.

Below 4500 K, the electrical conductivity is almost zero. From 4500 K to 9500 K, the increase of pressure results in the decrease of electrical conductivity, whereas the opposite effect is observed at high temperatures above 9500 K. According to our

58

previous work for SF$_6$-Cu mixtures [40], the evolution of the main elastic collisions involving electrons are responsible for this observation. At temperatures below 9500K, the electron-neutral interactions (i.e. e$^-$-C, e$^-$-O, e$^-$-N and e$^-$-Cu) are the main collisions. Due to the formula given by Devoto [132], the electrical conductivity has a first approximation: $\sigma \propto n_e /(\sum_{j\neq e} n_j \overline{\Omega}_{ej})$. As the pressure increases, all particle densities increase. However, the ionization is delayed, consequently, the electron density n_e does not increase as rapidly with pressure as do the densities of other particles (n_j for $j\neq e$). At high temperatures, electron-ions collisions become predominant. The increase of pressure delays the ionization of atoms and thus reduces the concentration of high-valence ions which have large Coulomb potential interacting with electrons. Therefore, the parameters q^{nk} are reduced, resulting in the increase of electrical conductivity.

Figure 3-6. Electrical conductivity of CO$_2$-N$_2$ (mixing ratio 7:3) mixtures contaminated by 10% Cu at temperatures of 300 – 30,000 K and at different pressures

3.2.4 Viscosity

Figure 3-7 presents the viscosity of CO$_2$-N$_2$ mixtures (mixing ratio 7:3)

59

contaminated by different percentage of copper in the temperature range of 300 – 30,000 K at ambient pressure.
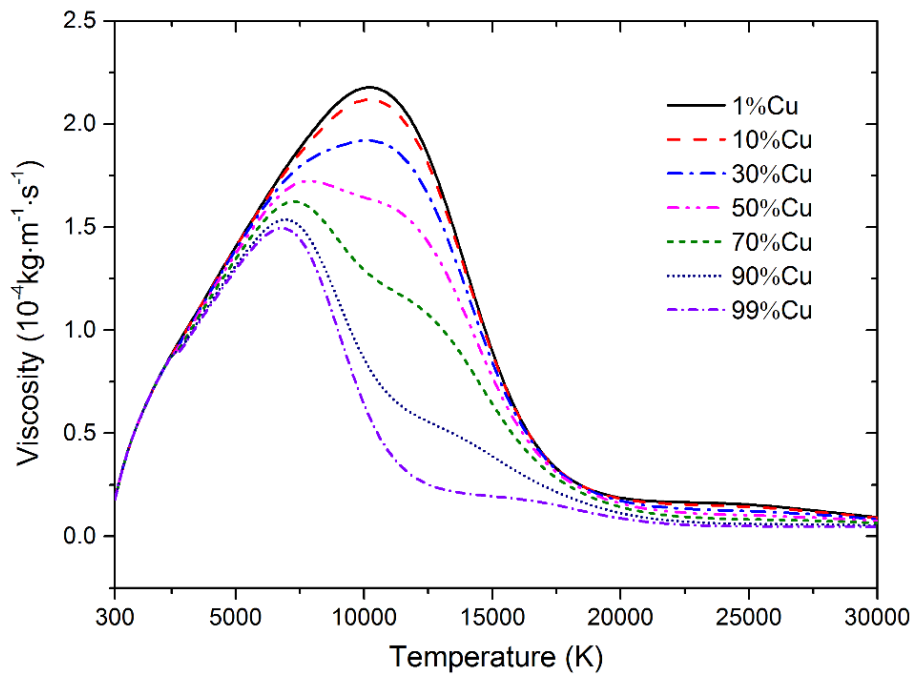
Figure 3-7. Viscosity of CO_2-N_2 (mixing ratio 7:3) mixtures contaminated by different proportions of Cu at temperatures of 300 – 30,000 K and at 1 bar

As shown in Figure 3-7, elemental copper mainly exists in the form of condensed species at temperatures below 2500 K, showing negligible effect on the viscosity of CO_2-N_2-Cu mixtures. However, at around 2500 K, the condensed copper evaporates into gaseous species, leading to the significant drop of viscosity at temperatures over 2500 K, especially between 7000 K and 16,000 K. At the beginning of this temperature range (before the viscosity peaks the value), the atoms instead of molecules play an important role in the mixtures. Considering that viscosity is in inverse proportion to collision integrals [38], the large collision integrals of Cu-Cu interaction (as shown in Figure 3-1 and Figure 3-2) are responsible for such significant decrease of viscosity. After viscosity reaches the maximum, the charged particles start to dominate the mixtures, and the large collision integrals due to ion-ion interactions reduces the

60

viscosity. More copper leads to more ions and hence lower viscosity. Besides, as discussed before, copper has larger molar mass than CO_2 and N_2, which also contributes to the decrease of viscosity.

The influence of mixing ratio (CO_2:N_2) on the viscosity of CO_2-N_2-Cu mixtures is presented in Figure 3-8. The percentage of copper contamination is set to be 10%.
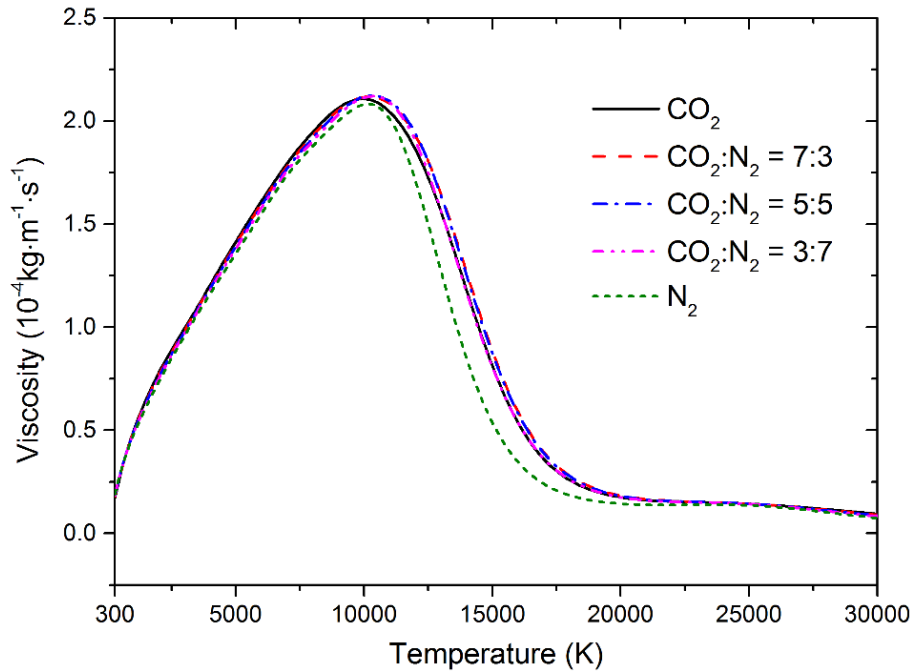
Figure 3-8. Viscosity of CO_2, N_2, and their different mixtures contaminated by 10% Cu at temperatures of 300 − 30,000 K and at 1 bar

Generally, N_2 shows almost no effect on the viscosity of CO_2-N_2-Cu mixtures before the viscosity reaches the maximal value at around 10,400 K. When the temperature is over 10,400 K, the influence of N_2 is still slight if its content is less than 70%, whereas for pure N_2 plasma, the viscosity is much smaller than those of CO_2-N_2 mixtures at temperatures of 11,500 − 20,000 K. This can be attributed to the larger ionization potential of N than that of C, O and Cu. Actually, in this temperature range, the ions due to the first ionization of atoms rule the mixtures, and nitrogen is harder to generate atomic ions, causing the viscosity to shift towards a lower temperature.

Figure 3-9 illustrates the viscosity of CO_2-N_2 mixtures with a mixing ratio 7:3 contaminated by 10% copper at temperatures up to 30,000 K at different pressures (0.1 bar, 1 bar, 6 bar, and 16 bar).

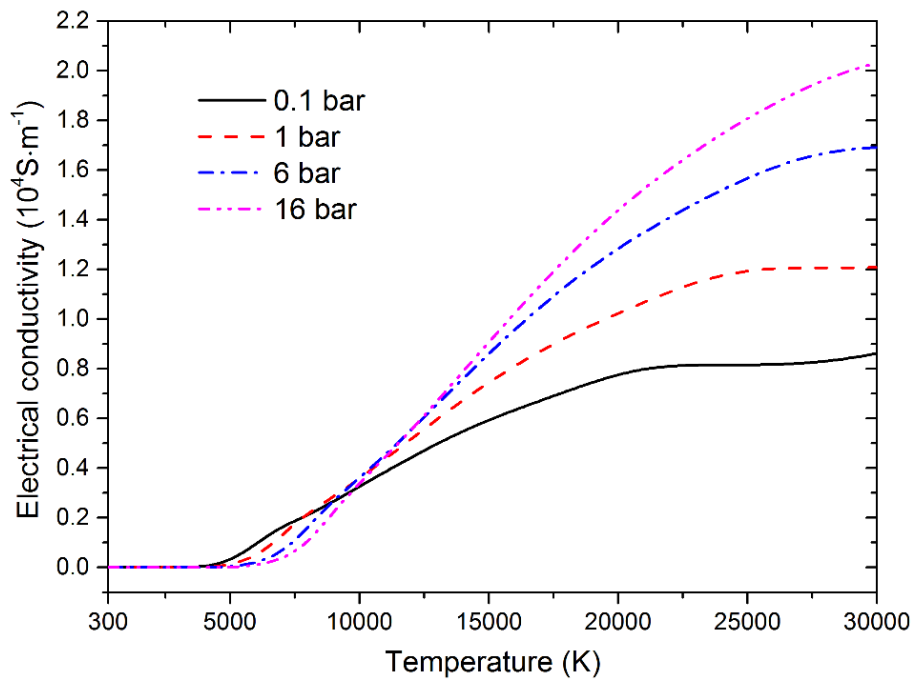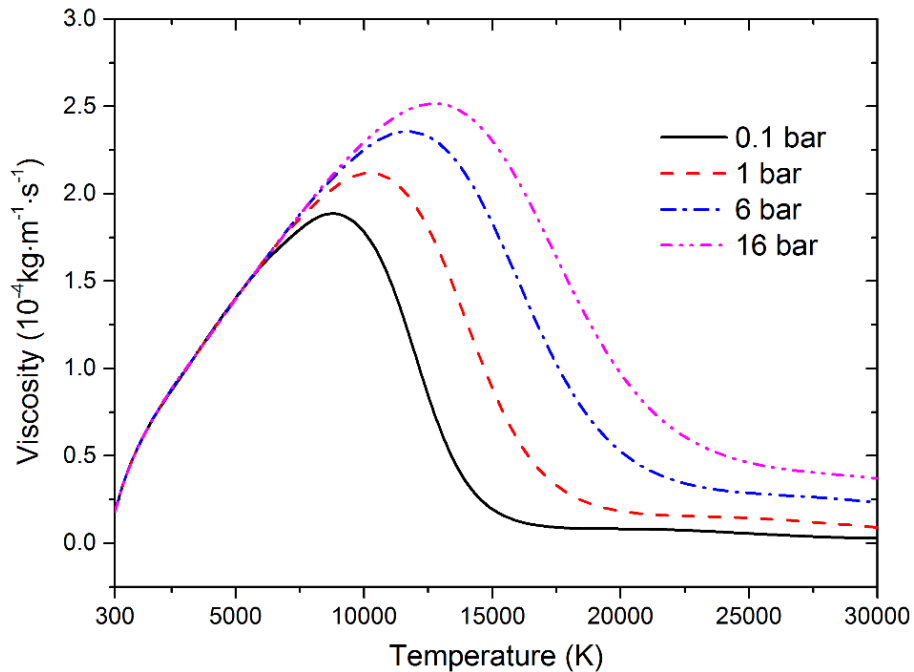
Figure 3-9. Viscosity of CO_2-N_2 (mixing ratio 7:3) mixtures contaminated by 10% Cu at temperatures of 300 – 30,000 K and at different pressures

As can be seen from Figure 3-9, the independence of pressure on the viscosity can be observed at temperatures below 6500 K mainly because the viscosity is more sensitive to temperature than other parameters (e.g. pressure) in this temperature range. However, when the temperature is above 6500 K, the viscosity is raised to a higher value at a larger pressure. This is due to the suppressing of ionization reactions and thus the reduced fractions of ions, leading to a decreased contribution to total collision integrals from Coulomb potentials and thus an increase of viscosity [40].

Another interesting observation is that the temperature at which the viscosity peaks its value is shifted to a higher point at a larger pressure. This also can be explained by the suppression of ionization due to the increase of pressure. At this circumstance, the

strong Coulomb interactions do not dominate until the temperature reaches a higher value [40].

3.2.5 Thermal conductivity

The condensed copper also shows an effect on the thermal conductivity as it does on specific heat discussed in section 2.3.5. Figure 3-10 describes the thermal conductivity of CO_2-N_2 (mixing ratio 7:3) contaminated by 10% Cu with and without considering condensed phases at temperatures of 300 – 3000 K.

It is seen that the copper evaporation dramatically affects the thermal conductivity, leading to a hump in the thermal conductivity when the phase transition occurs. Similar to the observation in the specific heat, the hump in thermal conductivity is also shifted to higher temperatures when the copper proportion increases.

Figure 3-10. Thermal Conductivity of CO_2-N_2 (mixing ratio 7:3) mixtures contaminated by different proportions of Cu at temperatures of 300 – 3000 K and at 1 bar with and without condensed phases

At temperatures above 3000 K, all the condensed species diminish through phase

63

transitions. Consequently, the influence arising from the copper contamination becomes clearer. Figure 3-11 presents the thermal conductivity of CO_2-N_2 mixtures (mixing ratio 7:3) contaminated by various proportions of copper in the temperature range of 3000 – 30,000 K at 1 bar.

Obviously, the copper contamination reduces the thermal conductivity significantly both in the low and high temperature ranges. At low temperatures, the reaction component dominates the total thermal conductivity. The increase of copper and thus decrease of CO_2 and N_2 lead to the drop of reaction thermal conductivity because the decomposition of molecules is weakened. At high temperatures, the translation of electrons plays the leading role in the total thermal conductivity. However, although more electrons are generated through ionization when more copper is mixed, the stronger interactions and thus larger collision integrals between charged particles result in the decrease of thermal conductivity.
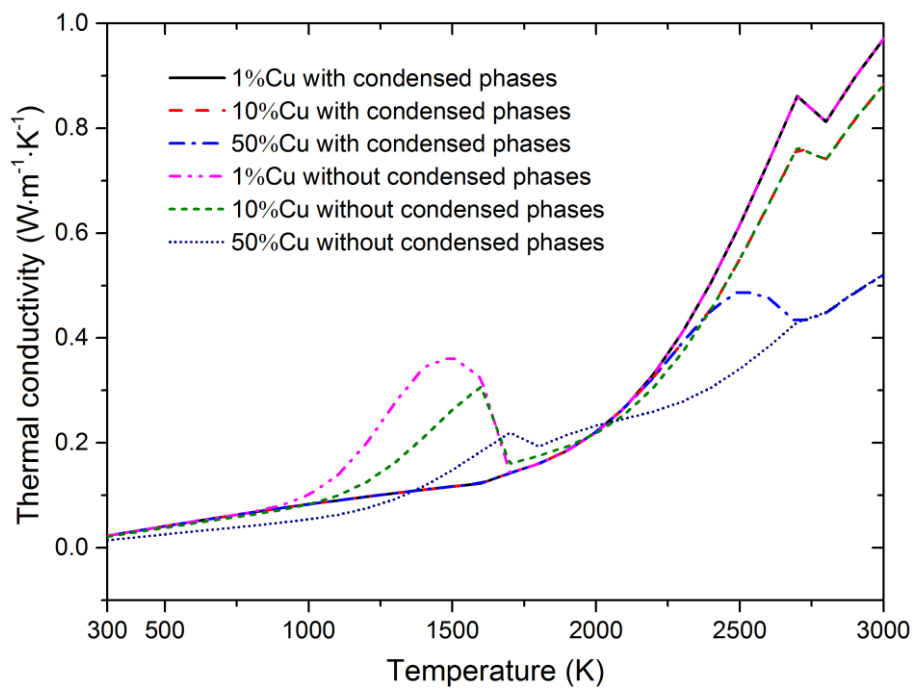

Figure 3-11. Thermal Conductivity of CO_2-N_2 (mixing ratio 7:3) mixtures contaminated by different proportions of Cu at temperatures of 3000 – 30,000 K and at 1 bar

64

Furthermore, similar to the specific heat as shown in Figure 2-20, three peaks can be observed at 3300 K, 7000 K and 15,000 K respectively in Figure 3-11 for the thermal conductivity of CO_2-N_2 mixtures contaminated by small fraction of copper. These three peaks can also be attributed to the decomposition of O_2, dissociation of CO and N_2, and ionization of O and N respectively. When increasing copper proportion, due to the gradual reduction of O_2, CO and N, the peaks of thermal conductivity will gradually diminish and vanish eventually.

Compared with the electrical conductivity and viscosity, the thermal conductivity of CO_2-N_2-Cu mixtures is affected more significantly by the mixing ratio of CO_2 and N_2. Figure 3-12 gives the thermal conductivity of pure CO_2, pure N_2 and their mixtures with mixing ratios of 7:3, 5:5 and 3:7 contaminated by 10% copper in the temperature range of 3000 – 30,000 K at ambient pressure.
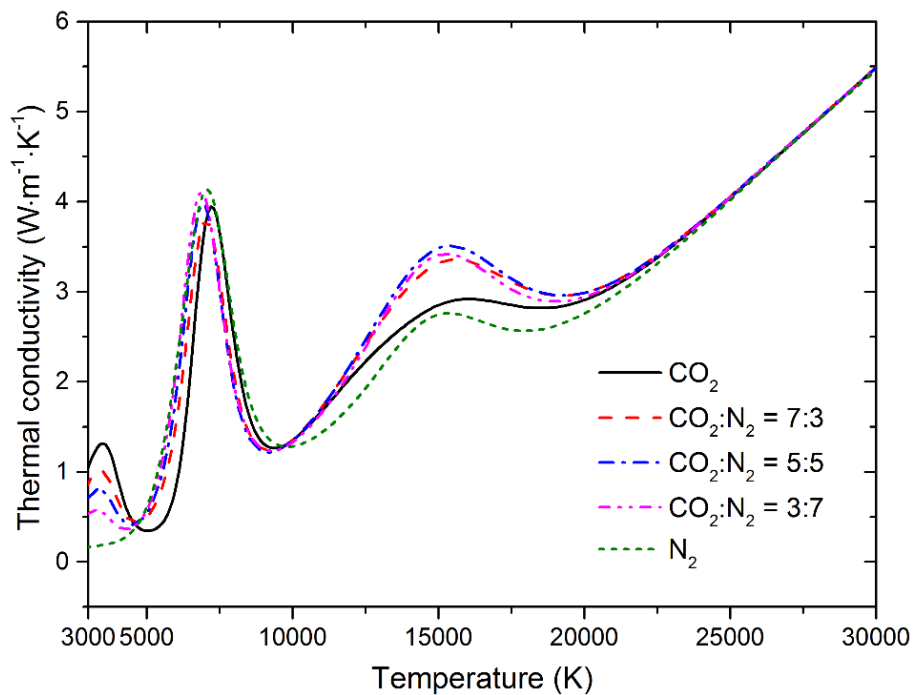
Figure 3-12. Thermal Conductivity of CO_2, N_2, and their different mixtures contaminated by 10% Cu at temperatures of 3000 – 30,000 K and at 1 bar

As observed in Figure 3-12, three peaks of thermal conductivity can be observed

at around 3500 K, 6800 – 7200 K and 15,000 K. With the addition of N_2, the first peak diminishes gradually; the value of the second peak changes slightly but the position is shifted to a slightly lower temperature; and the third peak is reduced considerably. All of these can be explained by the different dissociation and/or ionization reactions in the corresponding temperature range as discussed in section 2.3.5.

Figure 3-13 describes the influence of pressure on the thermal conductivity of CO_2-N_2 mixtures (mixing ratio 7:3) contaminated by 10% copper as a function of temperature up to 30,000 K. The gas pressure ranges from 0.1 bar to 16 bar.

Due to the suppression of dissociation and ionization reactions with pressure, the values of the first and second peaks in thermal conductivity associated with dissociation of molecules are reduced, whereas the third peak corresponding to ionization of atoms is raised. Moreover, increasing pressure results in the shift of peaks to a high temperature. This is also attributed to the suppression of the corresponding reactions.
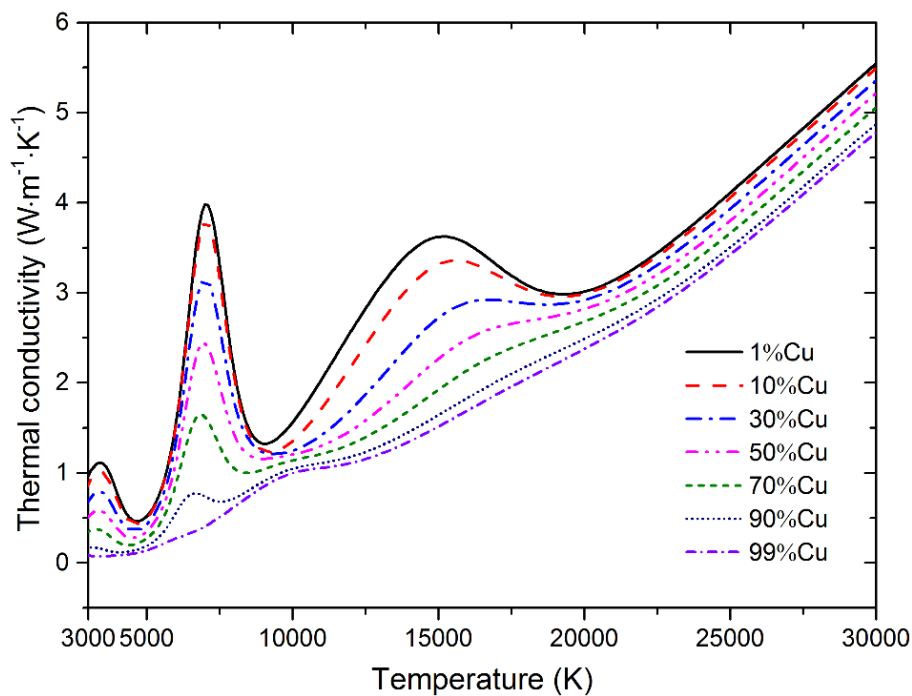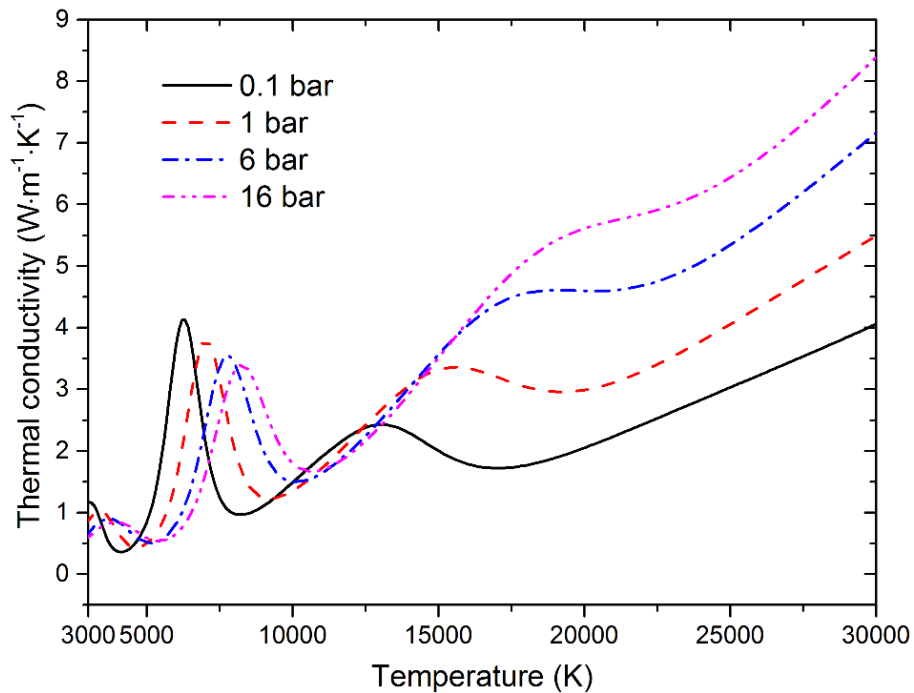

Figure 3-13. Thermal Conductivity of CO_2-N_2 (mixing ratio 7:3) mixtures contaminated by 10% Cu at temperatures of 3000 – 30,000 K and at different pressures

66

3.3 Combined diffusion coefficients

3.3.1 Determination of combined diffusion coefficients

In Murphy's theory, the multicomponent diffusion coefficients for each pair of species are combined into just four combined diffusion coefficients, termed the combined ordinary diffusion coefficient $\overline{D_{AB}^x}$, combined electric field diffusion coefficient $\overline{D_{AB}^E}$, combined temperature diffusion coefficient $\overline{D_{AB}^T}$ and combined pressure diffusion coefficient $\overline{D_{AB}^P}$. These four coefficients describe the diffusion due to composition gradients, applied electric field, temperature gradients, and pressure gradients respectively [64]. For a mixture of two homonuclear and non-reacting gases in local thermal equilibrium, denoted as gas A and gas B, the diffusion mass flux of gas A can be written as [64]:

$$\overline{\mathbf{J}_A} = \frac{n^2}{\rho} \overline{m_A}\,\overline{m_B} \left(\overline{D_{AB}^x} \nabla \overline{x_B} + \overline{D_{AB}^P} \nabla \ln P + \overline{D_{AB}^E} \mathbf{E} \right) - \overline{D_{AB}^T} \nabla \ln T \qquad (3\text{-}33)$$

Where n and ρ are respectively the total number density and total mass density, $\overline{m_A}$ and $\overline{m_B}$ are the average masses of heavy species in gas A and gas B, and $\overline{x_B}$ is the total mole fractions of species in gas B. With the individual species denoted by the subscript i, where $i = 1$ denotes the electrons, $i = 2, \ldots, p$ denote the species derived from gas A, and $i = p+1, \ldots, q$ the species derived from gas B, $\overline{m_A}$, $\overline{m_B}$ and $\overline{x_B}$ can be calculated using the following formulas [60, 64]:

$$\overline{m_A} = \sum_{k=2}^{p} m_k x_k \Big/ \sum_{k=2}^{p} x_k \qquad (3\text{-}34)$$

$$\overline{m_B} = \sum_{k=p+1}^{q} m_k x_k \Big/ \sum_{k=p+1}^{q} x_k \qquad (3\text{-}35)$$

$$\overline{x_B} = \sum_{k=p+1}^{q} \left(1 + Z_k \right) x_k \qquad (3\text{-}36)$$

Where m_k, x_k and Z_k are respectively the mass, mole fraction and charge number of

particle *k*.

The four diffusion coefficients $\overline{D_{AB}^x}$, $\overline{D_{AB}^E}$, $\overline{D_{AB}^T}$, and $\overline{D_{AB}^P}$ in equation (3-33) can be calculated as follows [60, 64]:

$$\overline{D_{AB}^x} = \frac{1}{\overline{m_A}\,\overline{m_B}} \sum_{i=1}^{p} k_i m_i \sum_{j=1}^{q} m_j D_{ij}^a \frac{\partial x_i}{\partial \overline{x_B}} \tag{3-37}$$

$$\overline{D_{AB}^E} = -\frac{e}{kT} \frac{1}{\overline{m_A}\,\overline{m_B}} \sum_{i=1}^{p} k_i m_i \sum_{j=1}^{q} m_j x_j Z_j D_{ij} \tag{3-38}$$

$$\overline{D_{AB}^T} = \sum_{i=1}^{p} k_i \left(D_i^{Ta} - \frac{n^2}{\rho} m_i \sum_{j=1}^{q} m_j D_{ij}^a T \frac{\partial x_j}{\partial T} \right) \tag{3-39}$$

$$\overline{D_{AB}^P} = \frac{1}{\overline{m_A}\,\overline{m_B}} \sum_{i=1}^{p} k_i m_i \sum_{j=1}^{q} m_j D_{ij}^a \left(x_j - \frac{\rho_j}{\rho} + P \frac{\partial x_j}{\partial P} \right) \tag{3-40}$$

where *e* is the elementary charge, *k* the Boltzmann constant, ρ_j the mass density of species *j*. D_{ij} is the ordinary diffusion coefficient, and D_{ij}^a and D_i^{Ta} are the ordinary and thermal diffusion coefficients with a correction taking into account the ambipolar diffusion [60, 150]. The stoichiometric coefficients k_i are defined by [64]

$$k_1 = \sum_{k=2}^{p} \frac{Z_k x_k}{x_1} \tag{3-41}$$

$$k_i = 1, \quad i \neq 1 \tag{3-42}$$

The ordinary diffusion coefficient D_{ij} and the thermal diffusion coefficient D_i^T used in equations (3-37), (3-38), (3-39) and (3-40), and the determination of D_{ij}^a and D_i^{Ta}, are calculated based on the Chapman-Enskog theory, which is widely used to determine transport coefficients to a selected order as described in the previous section 3.2.1. To ensure the adequate accuracy, the third order of approximation is adopted in this work.

It is important to note that the combined diffusion coefficients are only completely equivalent to the full multi-component diffusion coefficients for a mixture of two homonuclear and non-reacting gases in local thermal equilibrium. For the CO_2-N_2-Cu mixtures considered here, we choose gas A to consist of the species derived from CO_2

68

and N_2, and gas B the species derived from Cu. However, CuO which exists in the low-temperature range, cannot be dealt with strictly in the combined diffusion coefficient approach, which requires that the gases do not react with each other. Cressault et al. [42] addressed an analogous problem by ignoring metal oxides in calculating the combined diffusion coefficients of air-metal mixtures. They showed that the metal oxides exist at very low temperatures and had almost no impact on the results. Rong et al. [67] and Yang et al. [66] also used the combined diffusion coefficients without consideration of metal oxides and applied these coefficients to yield a successful simulation of electrode and splitter-plate erosions in low-voltage circuit breakers. In our published work [41], the combined ordinary diffusion coefficient of SF_6-Cu mixtures without consideration of CuF_2, CuF and CuS is compared with the results calculated with these species assigned to gas B. The result indicates that the influence arising from copper fluorides and sulfides can be neglected since only a very slight difference is observed, and only at very low temperatures. Similarly, CuO is therefore assigned to gas B in this work.

Before presenting the results, it is desirable to point out that the lower temperature limit for the combined diffusion coefficients is set to be 3000 K because copper exists mainly in the form of condensed species at temperatures below 3000 K.

3.3.2 Combined ordinary diffusion coefficient

Figure 3-14 shows the combined ordinary diffusion coefficient $\overline{D_{AB}^x}$ of CO_2-N_2 (mixing ratio 7:3) mixtures contaminated by different percentage of copper at ambient pressure. At low temperatures, the mean free path of neutral particles play a major role in $\overline{D_{AB}^x}$ [42, 60, 149]. The contamination of copper changes the mean free path so weakly that $\overline{D_{AB}^x}$ is almost independent of copper concentration. However, at high temperatures, copper contamination raises $\overline{D_{AB}^x}$ dramatically. The turning points are found to be at the round of the peaks of $\overline{D_{AB}^x}$, and furthermore, the temperatures corresponding to the peaks are shifted to higher values when more copper is mixed. As

69

discussed in the previous work [41], $\overline{D_{AB}^x}$ is mainly affected by the Coulomb interactions between charged particles at high temperatures. According to standard chemical equilibrium considerations, copper with higher concentration ionizes at higher temperature, which means that the Coulomb interaction becomes important at higher temperature, causing the shift of the peak in $\overline{D_{AB}^x}$.

Figure 3-14. Combined ordinary diffusion coefficient $\overline{D_{AB}^x}$ of CO_2-N_2 (mixing ratio 7:3) mixtures contaminated by different proportions of Cu at temperatures of 3000 – 30,000 K and at 1 bar

The influence of gas pressure on $\overline{D_{AB}^x}$ is described in Figure 3-15 for CO_2-N_2 (mixing ratio 7:3) mixtures contaminated by 10% Cu. Due to the compression of gas mixtures and thus the decrease of the mean free path, the coefficient $\overline{D_{AB}^x}$ is reduced with pressure [41]. In addition, the position of the peak in $\overline{D_{AB}^x}$ moves towards a higher temperature as the pressure increases because the ionization of mixtures is

70

shifted to higher temperatures according to Le Chatelier's principle [41].
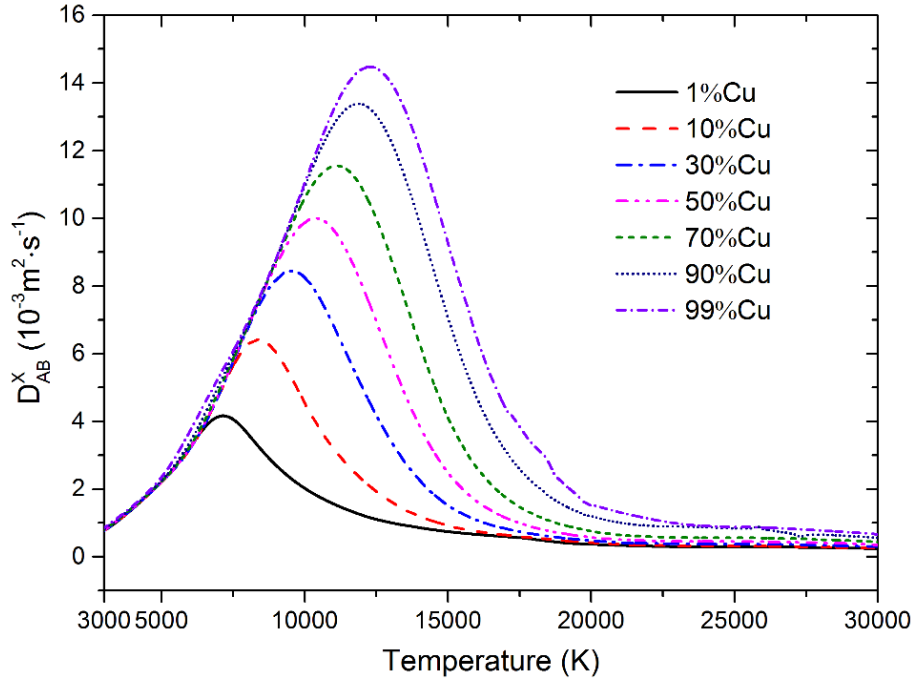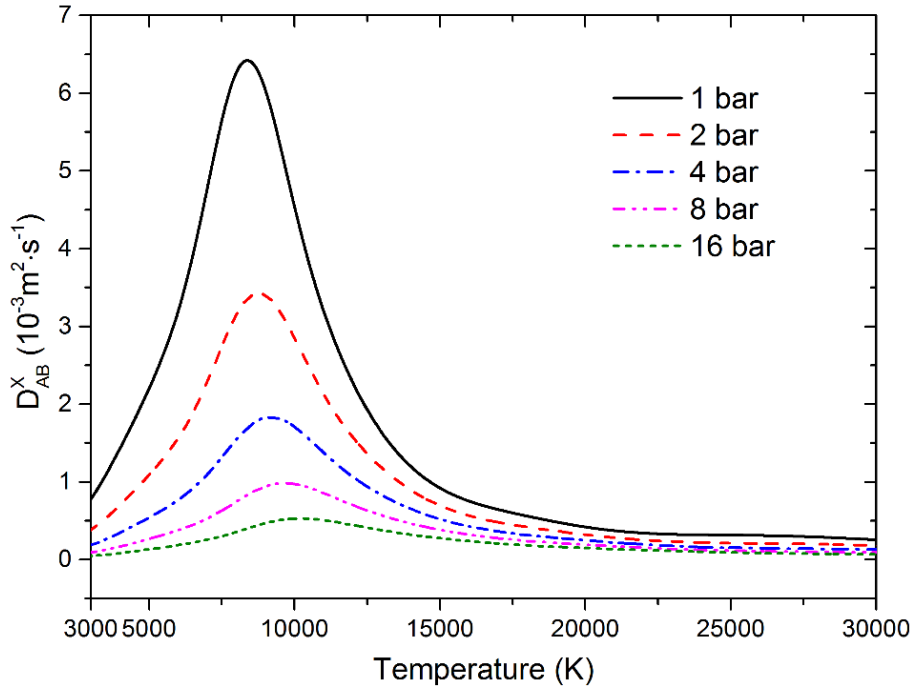

Figure 3-15. Combined ordinary diffusion coefficient $\overline{D_{AB}^{x}}$ of CO_2-N_2 (mixing ratio 7:3) mixtures contaminated by 10% Cu at temperatures of 3000 – 30,000 K and at different pressures

3.3.3 Combined electric field diffusion coefficient

Figure 3-16 illustrates the combined electric field diffusion coefficient $\overline{D_{AB}^{E}}$ of CO_2-N_2 (mixing ratio 7:3) mixtures contaminated by different percentage of copper at ambient pressure.

Similar to the discussion for the electrical conductivity in section 3.2.3, the temperatures in Figure 3-16 for $\overline{D_{AB}^{E}}$ also can be divided into three ranges: 3000 – 4000 K, 4000 – 16,500 K and 16,500 – 30,000 K. Below 4000 K, due to the negligible effect of ionization, $\overline{D_{AB}^{E}}$ is approximately zero, whatever the proportion of copper. Above 4000 K, because of the electric field acting on the ionized mixtures, the sign of $\overline{D_{AB}^{E}}$ reverses at nearby 16,500 K. In these temperature ranges, the influence of copper

is not monotonous but changes with copper concentration. This can be explained by the balance of dependences of $\overline{D_{AB}^{E}}$ on the mass and the ionization degree of mixtures, because the values of $\overline{D_{AB}^{E}}$ decrease with the mass but increases with the ionization degree [41].

Figure 3-16. Combined electric field diffusion coefficient $\overline{D_{AB}^{E}}$ of CO_2-N_2 (mixing ratio 7:3) mixtures contaminated by different proportions of Cu at temperatures of 3000 – 30,000 K and at 1 bar

The influence of gas pressure on $\overline{D_{AB}^{E}}$ is shown in Figure 3-17 for CO_2-N_2 mixtures contaminated by 10% Cu. The mixing ratio of CO_2 and N_2 is set to be 7:3 in the calculation. Obviously, increasing pressure shortens the mean free path, reducing the absolute value of $\overline{D_{AB}^{E}}$ [41]. In addition, due to the shift of ionization reactions to higher temperatures, increasing pressure raises the temperature at which $\overline{D_{AB}^{E}}$ reaches its negative peak value [41].

Figure 3-17. Combined electric field diffusion coefficient $\overline{D_{AB}^{E}}$ of CO_2-N_2 (mixing

ratio 7:3) mixtures contaminated by 10% Cu at temperatures of 3000 – 30,000 K and

at different pressures

3.3.4 Combined temperature diffusion coefficient

Figure 3-18 shows the combined temperature diffusion coefficient $\overline{D_{AB}^{T}}$ of CO_2-N_2 mixtures contaminated by different percentage of copper at ambient pressure. The mixing ratio of CO_2 and N_2 is fixed to be 7:3.

Generally, if the proportion of copper is not extremely high (i.e. < 90%), the values of $\overline{D_{AB}^{T}}$ are raised by the copper contamination due to the impact of large mass of copper. However, the further increase of copper (i.e. > 90%) starts to reduce the values of $\overline{D_{AB}^{T}}$. This is because the very high percentage of copper leads to the increase of mass density of CO_2-N_2-Cu mixtures as shown in Figure 2-13, and thus decreases the values of $\overline{D_{AB}^{T}}$, considering that $\overline{D_{AB}^{T}}$ is approximately in inverse to the mass density of mixtures [41].
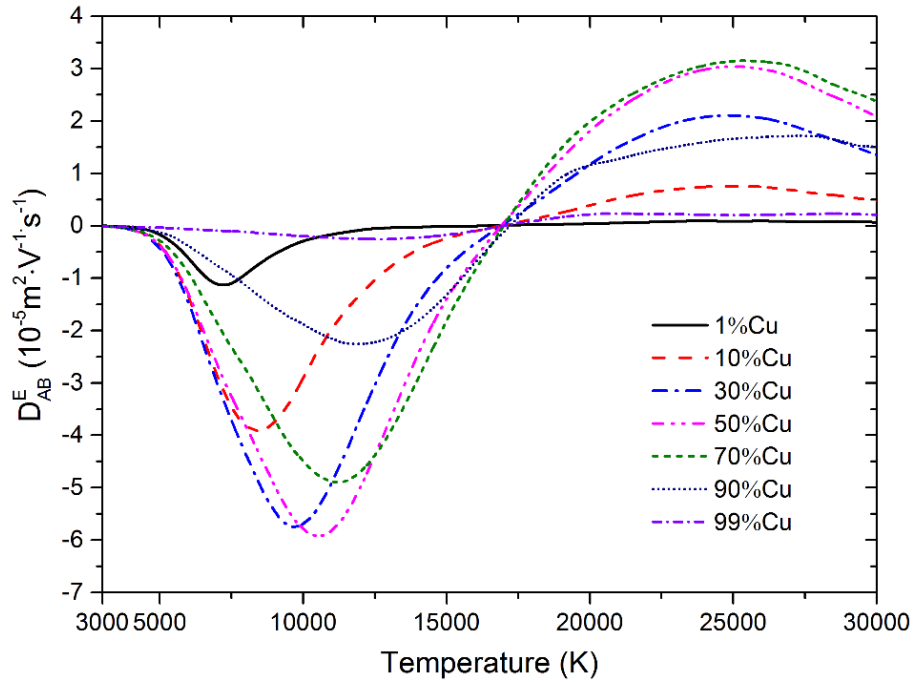
73

Figure 3-18. Combined temperature diffusion coefficient $\overline{D_{AB}^{T}}$ of CO_2-N_2 (mixing ratio 7:3) mixtures contaminated by different proportions of Cu at 1 bar
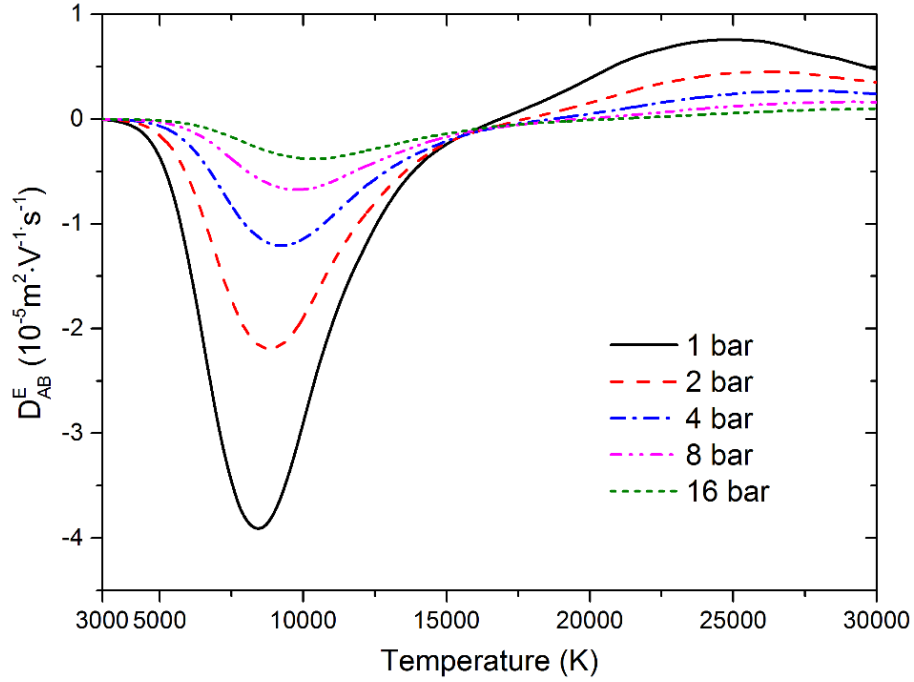

Figure 3-19. Combined temperature diffusion coefficient $\overline{D_{AB}^{T}}$ of CO_2-N_2 (mixing ratio 7:3) mixtures contaminated by 10% Cu at different pressures

The influence of gas pressure on $\overline{D_{AB}^T}$ is shown in Figure 3-19 for the CO_2-N_2 (mixing ratio 7:3) mixtures contaminated by 10% Cu. It is observed that the features of $\overline{D_{AB}^T}$ are shifted towards higher temperatures as the pressure increases. This behaviour can, as was the case for $\overline{D_{AB}^x}$ and $\overline{D_{AB}^E}$, be explained by the shift of dissociation and ionization reactions to higher temperatures as pressure increases, which occurs according to Le Chatelier's principle [41].

3.3.5 Combined pressure diffusion coefficient

Figure 3-20 shows the combined pressure diffusion coefficient $\overline{D_{AB}^P}$ of CO_2-N_2 (mixing ratio 7:3) mixtures contaminated by different proportions of copper at ambient pressure.

The behavior of $\overline{D_{AB}^P}$ is very close to that of $\overline{D_{AB}^T}$. When the proportion is below 90%, the copper contamination increases the values of $\overline{D_{AB}^P}$ while the further increase of copper (i.e. > 90%) starts to reduce the values of $\overline{D_{AB}^P}$. This also can be explained by the increase of mass density of CO_2-N_2-Cu mixtures due to the mixing of copper, considering that $\overline{D_{AB}^P}$ is also approximately in inverse to the mass density of mixtures as $\overline{D_{AB}^T}$ [41].

The influence of gas pressure on $\overline{D_{AB}^P}$ is shown in Figure 3-21 for CO_2-N_2 (mixing ratio 7:3) mixtures contaminated by 10% Cu. The five curves on the graph are calculated at pressures of 1, 2, 4, 8 and 16 bar respectively.

As can be seen in Figure 3-21, due to the reduction of the mean free path, increasing the pressure reduces the values of $\overline{D_{AB}^P}$. The peak in $\overline{D_{AB}^P}$ is also shifted to higher temperatures as the pressure increases, as was found for the other combined diffusion coefficients [41].
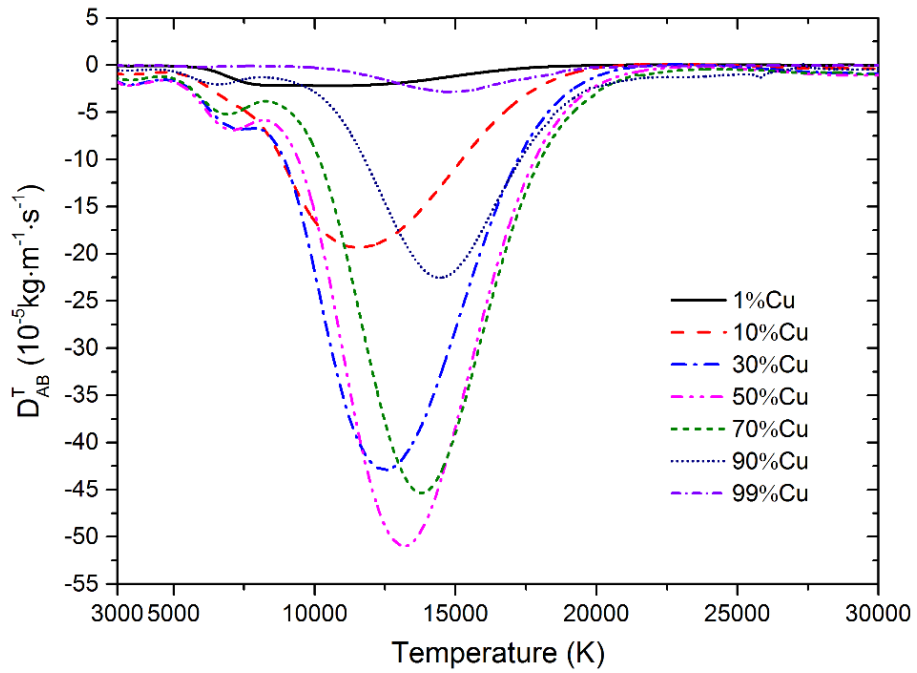
Figure 3-20. Combined pressure diffusion coefficient $\overline{D_{AB}^P}$ of CO_2-N_2 (mixing ratio

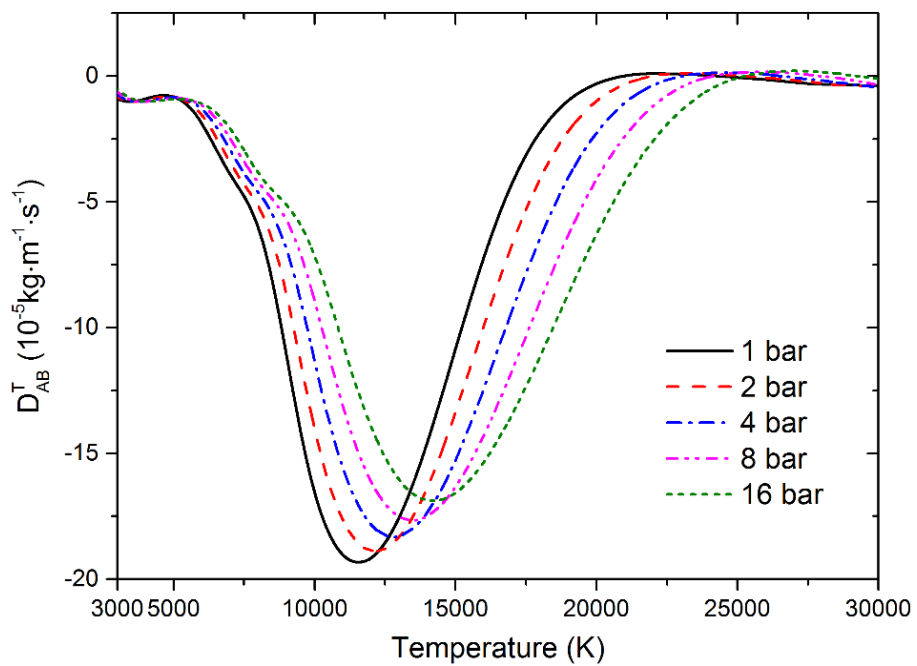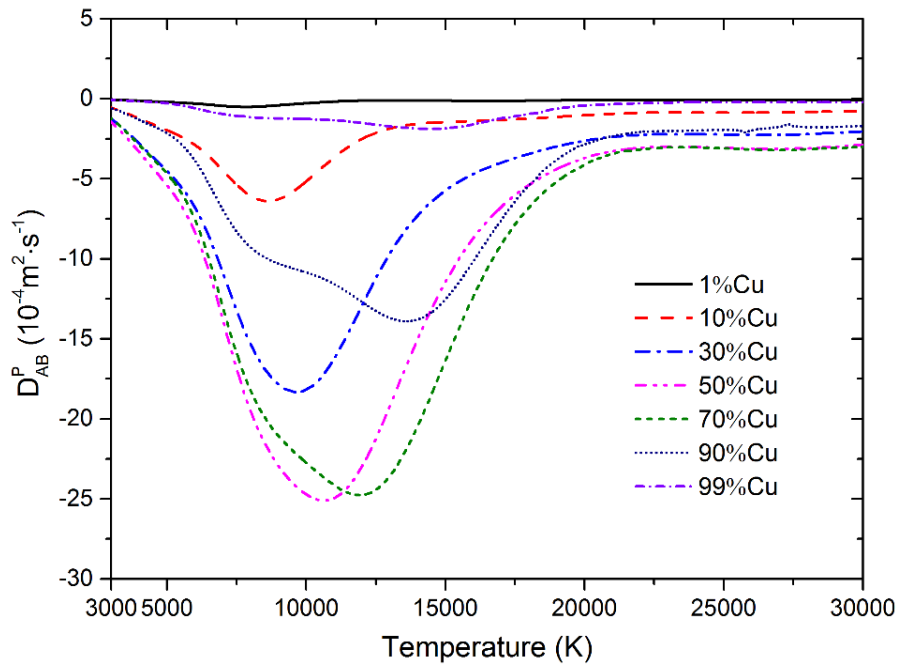7:3) mixtures contaminated by different proportions of Cu at 1 bar
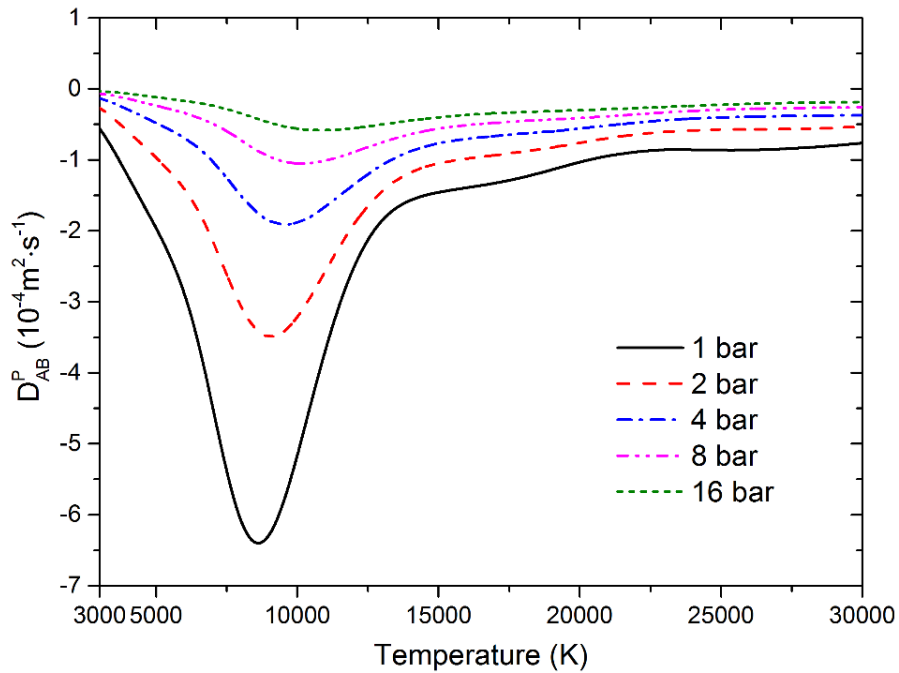
Figure 3-21. Combined pressure diffusion coefficient $\overline{D_{AB}^P}$ of CO_2-N_2 (mixing ratio

7:3) mixtures contaminated by 10% Cu at different pressures

3.4 Comparison with SF$_6$-Cu mixtures

In order to highlight the differences of transport and diffusion properties between SF$_6$ and CO$_2$-N$_2$ mixtures, the transport coefficients and combined diffusion coefficients of SF$_6$-Cu mixtures are calculated according to our previous publication [40].

The four parts (a) – (d) of Figure 3-22 show the electrical conductivity, viscosity, thermal conductivity, and combined ordinary diffusion coefficient respectively for the CO$_2$-N$_2$ mixtures and SF$_6$ gas contaminated by 1% copper at ambient pressure. The mixing ratio of CO$_2$ and N$_2$ is set to be 7:3.

A. Electrical conductivity

As we can see, at low temperatures below 7000 K, the electrical conductivity of CO$_2$-N$_2$-Cu mixtures is higher than that of SF$_6$-Cu mixtures, whereas above 7000 K the difference between the two mixtures is not significant.

B. Viscosity

In general, the viscosity of CO$_2$-N$_2$-Cu mixtures is lower than that of SF$_6$-Cu mixtures, especially at medium temperatures (3000 – 20,000 K) around the peak of viscosity. Besides, compared with SF$_6$-Cu mixtures, CO$_2$-N$_2$-Cu mixtures reach their peaks at lower temperatures.

C. Thermal conductivity

For the thermal conductivity, the observation is similar to that for $\rho \cdot C_p$ in Figure 2-24, i.e. CO$_2$-N$_2$-Cu mixtures present lower and higher thermal conductivity in the low (below 2800 K) and medium (2800 – 17,000 K) temperature range respectively. Considering that the peaks at low temperatures correspond to the dissociation of molecules, the result indicates that the dissociation temperatures of CO$_2$-N$_2$ mixtures are higher than those of SF$_6$ mixtures.

77

D. Combined ordinary diffusion coefficient

In the combined ordinary diffusion coefficient, CO_2-N_2-Cu mixtures reach their peaks at higher temperatures than SF_6-Cu mixtures, and have higher peak values as well.
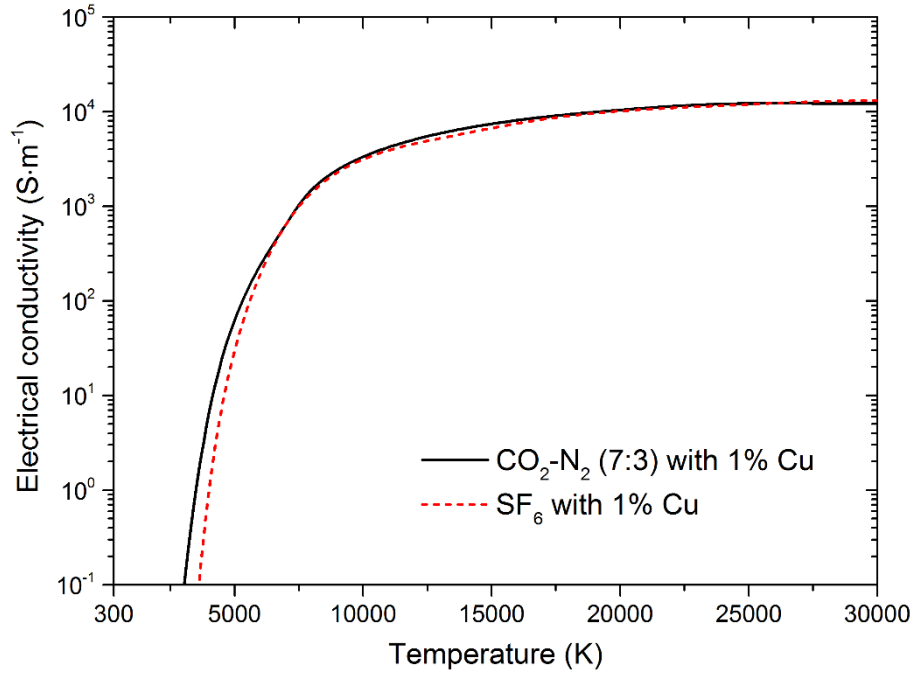
(a) Electrical conductivity
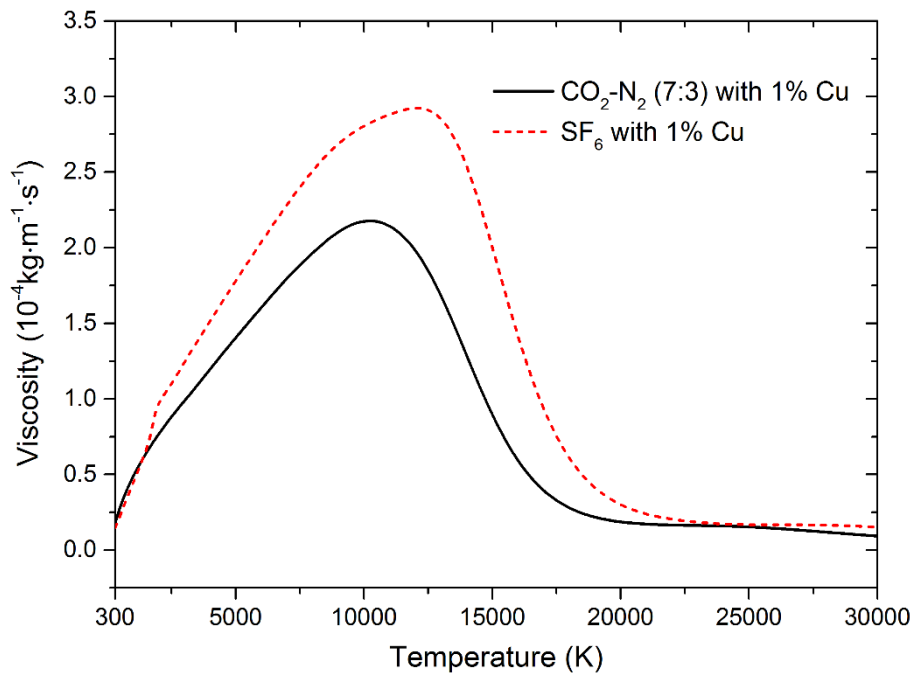
(b) Viscosity
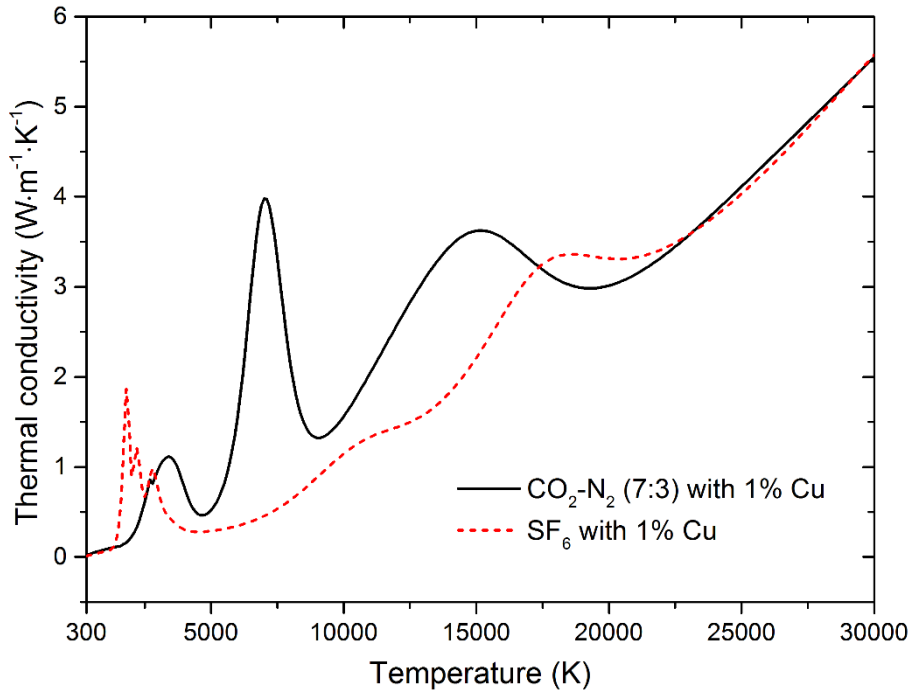
(c) Thermal conductivity
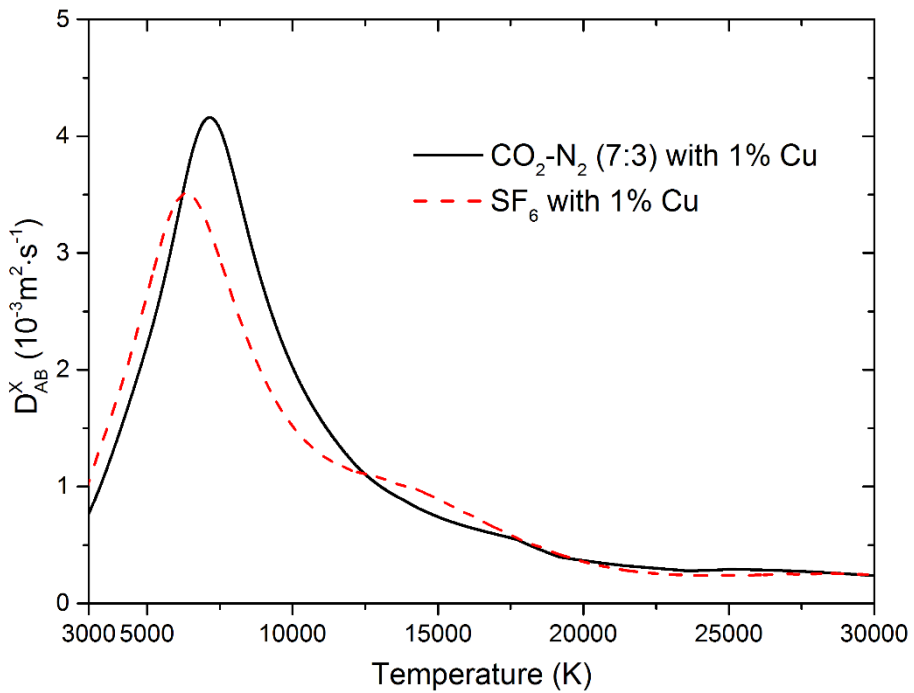
(d) Combined ordinary diffusion coefficient

Figure 3-22. Transport coefficients and combined ordinary diffusion coefficient of CO_2-N_2 (mixing ratio 7:3) mixture and SF_6 gas contaminated by 1% copper at temperatures up to 3000 K and at 1 bar

3.5 Summary

In this chapter, we perform the calculation of transport coefficients and combined diffusion coefficients of CO_2-N_2-Cu mixtures at various temperatures and pressures based on the Chapman-Enskog theory. In this theory, the collision integrals are the key point of the calculation, and to determine these collision integrals, four kinds of interactions, namely neutral-neutral, neutral-ion, electron-neutral, and charged-charged interactions, are taken into account. The influences of copper contamination, mixing ratios between CO_2 and N_2, and gas pressures on the transport and combined diffusion coefficients are discussed.

The newly developed Lennard-Jones like phenomenological model potential is adopted to describe the neutral-neutral and neutral-ion interactions. The results show that Cu-Cu pair has much larger collision integrals than C-C, N-N and O-O pairs. This predictably can affect the transport and diffusion coefficients of CO_2-N_2-Cu mixtures.

Copper has large mass and low ionization potential, which thus shows remarkable effects on the transport and combined diffusion coefficients of CO_2-N_2-Cu mixtures. With the increase of copper, the viscosity and thermal conductivity are both reduced while the influence of copper on electrical conductivity varies in three different temperature ranges. For the combined diffusion coefficients, with the increase of copper, $\overline{D_{AB}^x}$ is raised sharply after it reaches the peak value; $\overline{D_{AB}^E}$ shows the similar observation as electrical conductivity and should be considered in three temperature ranges; In general, $\overline{D_{AB}^T}$ and $\overline{D_{AB}^P}$ are both raised when the proportion of copper is below 90% and reduced otherwise. Copper contamination also changes the number and position of peaks in thermal conductivity as it does in specific heat.

Similar to the observation in specific heat, copper evaporation at low temperatures also affects the thermal conductivity significantly, leading to a hump in the thermal conductivity when the phase transition occurs. Moreover, increasing copper shifts the hump to a higher temperature.

The mixing ratio of CO_2 and N_2 shows very slight effect on the electrical conductivity and viscosity. For the thermal conductivity, the addition of N_2 diminishes the first peak gradually, changes the value of the second peak slightly, and reduces the third peak considerably.

The influence of gas pressure is clear, i.e. reducing or increasing the values, and shifting the peaks. All of these can be attributed to the delay of dissociation and ionization reactions according to the Le Chatelier's principle.

Compared with SF_6-Cu mixtures, CO_2-N_2-Cu mixtures present large difference in transport and diffusion coefficients. For example, CO_2-N_2-Cu mixtures have lower and higher thermal conductivity than SF_6-Cu mixtures in low (below 2800 K) and medium (2800 – 17,000 K) temperature range respectively.

CHAPTER 4 NET EMISSION COEFFICIENTS OF CO_2-N_2-CU PLASMAS

4.1 Introduction

The radiation plays an important role in the energy transport of thermal plasmas. For example, the radiation of electric arc in circuit breakers especially in high-voltage circuit breakers is an essential energy-loss term during the operating process, and has several effects on the operation: [9] Firstly, the radiation energy transfer in arc plasmas may result in an increase of pressure in the upstream area of circuit breakers. Secondly, the radiation is responsible for the ablation of electrodes and nozzle in circuit breakers. Thirdly, the energy loss due to radiation also raises the cooling rate of arc during the current zero in circuit breakers. Consequently, not only the thermodynamic and transport coefficients but also the radiation properties are required to understand the characteristics of thermal plasmas, especially in the numerical modellings.

Moreover, according to the works by Gleizes et al. [68], Cressault et al. [84, 85], Aubrecht et al. [91] and Billoux et al. [82], the metallic vapours resulting from electrode surfaces or walls in arc apparatuses strongly increase the radiation in arc plasmas because of the low ionization potential of metallic species and the high intensities of metallic lines. Therefore, to model the arc plasmas at high current which interacts strongly with electrodes or walls, the influence of metallic contamination must be taken into account.

The radiation transfer is usually taken to be as a function of wavelength spanning from the infrared to the far ultraviolet region of the spectrum [91]. The exact calculation of radiation properties are thus very complicated and time consuming. As we introduced in Chapter 1, several numerical models were proposed to simplify the description of the radiation in thermal plasmas, such as the semi-empirical model based on the net emission coefficients (NEC) [70, 71], the P1 model [72], and the method of partial characteristics [73, 74]. Among these models, the NEC-based model proposed by Lowke [70] is widely used because of its good estimation ability and lowest

computation cost. Therefore, this chapter is dedicated to the calculation and discussion of the NEC in CO_2-N_2-Cu plasmas.

The rest of the sections is organized as follows. In section 4.2, the calculation method of NEC is introduced, and the determinations of atomic lines, atomic continuum, and molecular bands and continuum are presented respectively in section 4.2.1 – 4.2.3. In section 4.3, the results for the NEC of CO_2-N_2-Cu mixtures are discussed and the influences of copper contamination, plasma size, and gas pressure on the NEC are analyzed. In section 4.4, in order to show the difference between CO_2-N_2 mixtures and SF_6 gas, we make a comparison of the NEC between CO_2-N_2-Cu and SF_6-Cu mixtures. In the end, a summary of this chapter is presented in section 4.5.

4.2 Calculation method

4.2.1 General description

In an isothermal and homogeneous plasma, the radiation energy loss can be represented as the divergence of radiation flux $\overrightarrow{F_R}$ [91]:

$$\nabla \cdot \overrightarrow{F_R} = 4\pi\varepsilon_N \tag{4-1}$$

Where ε_N is the net emission coefficient (NEC) defined by Lowke [70].

In Lowke's theory, ε_N corresponds to the effective radiation emitted from the axis of the isothermal cylinder, i.e. the fraction of the total power that is radiated per unit volume and unit solid angle into a volume element surrounding the axis of the cylinder and escaping from the cylinder after crossing a thickness R of the isothermal plasma [108].

Assuming an isothermal sphere instead of cylinder, ε_N can be approximated as [9, 108]

$$\varepsilon_N = \int_0^\infty B_\lambda \kappa_\lambda \exp\left(-\kappa_\lambda R\right) d\lambda \tag{4-2}$$

Where B_λ is Planck's function, and κ_λ is the monochromatic absorption coefficient corrected by the induced emission.

The calculation of κ_λ is the main difficulty in determining ε_N because κ_λ varies with wavelength λ, and both continuum emission and line profiles should be taken into account [108]. To simplify the calculation, the lines are assumed to be isolated, which means that the overlapping of lines is ignored and thus each line can be dealt with separately [108]. Under such assumption together with the local thermodynamic equilibrium (LTE), κ_λ can be further expressed as [108]

$$\kappa_\lambda = \left[\kappa_c^{'} + \kappa_0^{'} P(v) \right]\left[1 - \exp\left(-\frac{hc}{k\lambda T} \right) \right] \tag{4-3}$$

Where $\kappa_c^{'}$ is the absorption coefficient of the continuum close to the line, $\kappa_0^{'}$ is the absorption coefficient at the line center, and $P(v)$ characterizes the line profile. The upper index " ' " indicates that the induced emission is not considered, but in equation (4-3), this induced emission is taken into account by multiplying the factor [1 - exp(-$hc/k\lambda T$)] according to Kirchhoff's law [79, 85, 108].

To further simplify the calculation, let us consider the net emission coefficient associated with the central wavelength λ_0 of a line, which is denoted as $\varepsilon_{N\lambda 0}$. The spectral band $\Delta\lambda$ relating to λ_0 is very narrow compared with the whole spectrum, and thus the Planck's function B_λ and the exponent factor exp(-$hc/k\lambda T$) can be considered constant within this band [108]. Moreover, the net emission coefficient due only to the continuum can be calculated independently and does not need to be accounted for as an emission term. Therefore, $\varepsilon_{N\lambda 0}$ can be determined as follows. [9, 108]

$$\varepsilon_{N\lambda_0} = B_{\lambda_0}\kappa_0^{'}\left[1 - \exp\left(-\frac{hc}{k\lambda_0 T} \right) \right]\int_0^\infty P(\lambda)\exp(-\kappa_\lambda R)d\lambda \tag{4-4}$$

Combining the equations (4-3) and (4-4) and assuming that the continuum absorption coefficient $\kappa_c^{'}$ keeps constant within the line spectral band width, the net emission coefficient of a line becomes [108]

$$\varepsilon_{N\lambda_0} = B_{\lambda_0}\kappa_0^{'}\left[1 - \exp\left(-\frac{hc}{k\lambda_0 T} \right) \right]\exp(-\kappa_c^{'}R)\Lambda_{ul} \tag{4-5}$$

Where Λ_{ul} is the escape factor for the transition λ_{ul} and defined as [108]

84

$$\Lambda_{ul} = \int_0^\infty P(\lambda) \exp\left(-\kappa_0' P(\lambda) R\right) d\lambda \qquad (4\text{-}6)$$

As we can see from equation (4-5), the calculation of NEC consists of three parts, i.e. the calculations of escape factors, absorption coefficients due to lines, and absorption coefficients due to continuum radiation. The escape factors can be calculated provided the line profiles and the temperature distribution functions [108]. Usually, three kinds of profiles, namely Gaussian profile, Lorentzian profile and Voigt profile are used. The detailed description about line profiles will be presented in the next section 4.2.2. The absorption coefficients can be derived from the emission coefficients based on the Kirchhoff's law. We will therefore discuss the calculation of emission coefficients due to atomic lines, atomic continuum, and molecules in sections 4.2.2 – 4.2.4 respectively.

4.2.2 Atomic lines

For an atomic line corresponding to a transition between an upper level u and a lower level l, the volumetric emission coefficient is written as [9]

$$\varepsilon_{ul}(\lambda) = \frac{hc}{4\pi\lambda_{ul}} A_{ul} N_u P(\lambda) \qquad (4\text{-}7)$$

Where λ_{ul} and A_{ul} are the wavelength and spontaneous emission coefficient of the line, N_u is the number density of the atoms at level u, and $P(\lambda)$ is the normalized profile of the line.

As introduced in the previous section 4.2.1, line profile $P(\lambda)$ describing the shape of line is used to define the escape factor Λ_{ul} which plays an important role in determining the net emission coefficient. We re-express the escape factor using the optical depth of the line τ_{ul}. [9]

$$\Lambda_{ul} = \int_0^\infty P(\lambda) \exp\left(-\tau_{ul} \frac{P(\lambda)}{P(\lambda = \lambda_{ul})}\right) d\lambda \qquad (4\text{-}8)$$

The optical depth τ_{ul} is calculated as [9]

$$\tau_{ul} = \frac{\pi e^2}{m_e c} f_{lu} N_l R P \left(\lambda = \lambda_{ul} \right) \tag{4-9}$$

Where f_{lu} is the corresponding absorption oscillator strength, N_l the number density of atoms at level l, m_e the electron mass, e the elementary charge, and c the speed of light.

As we can see above, the calculation of an escape factor requires the corresponding line profile (also known as spectral line shape). Line profile describes the form of a feature associated with an energy change in a spectroscopic transition. The ideal line profiles include Gaussian, Lorentzian, and Voigt profiles. In spectroscopy, different line profiles depend on different line broadening. Generally, there are four kinds of broadenings, including pressure broadening, Stark broadening, Doppler broadening, and natural broadening.

At higher pressures, due to higher number densities of species, the radiating atoms collide more frequently with each other, resulting in so-called pressure broadening [108]. The derivation of the pressure-broadening line shape is a difficult problem because it depends on the interatomic potentials between the colliding atoms or their ions [155]. However, two simplified models within the semi-classical picture give some estimation of the effect: Van der Waals broadening and resonance broadening. The former one is applied when the perturber is a neutral atom different from the emitter or when the two atoms are the same but the upper level of the emitter is not linked to the ground state [9]. The latter one is applied when the perturber and the emitting atom are of the same type and the upper level of the emitter is linked to the ground state [9]. Both of the broadenings lead to a Lorentzian profile.

In Van der Waals broadening, the interaction between an emitting atom and a disturber is usually described by the C_6/r^6 Lennard-Jones potential, where C_6 is the Van der Waals constant and r is the distance between two colliding particles [79]. According to the work by Walkup et al. [156], the full width at half maximum (FWHM) of Van der Waals broadening for a line centered in λ_0 is approximated by [79]

$$\delta_V = 8.16 \cdot C_6^{2/5} \overline{V}^{3/5} N^* \frac{\lambda_0^2}{2\pi c} \qquad (4\text{-}10)$$

Where $\overline{V}$ is the mean velocity of the two colliding particles and N^* is the number density of the perturber.

In the resonance broadening, the interaction between an emitting atom and a disturber is described by the C_3/r^3 potential, where C_3 is the potential constant [79]. The resonance broadening will become important if the higher energy level of the atom is coupled with its ground state. The FWHM of the resonance broadening is written as [9, 79]

$$\delta_R = 5.48 \cdot \sqrt{\frac{g_0}{g_r}} N_0 \frac{e^2}{4\varepsilon_0} \frac{f_r}{m_e} \frac{\lambda_0^3}{(2\pi c)^2} \qquad (4\text{-}11)$$

Where g_0 and g_r are the statistical weights of the ground state and resonance state respectively, N_0 the number density of the atoms at ground level, f_r the oscillator strength of the resonance state, and ε_0 is the permittivity of free space.

When the electric field resulting from the charged species becomes significant, it perturbs the normal energy levels of the spectral lines via Stark broadening [108]. The interactions between atoms or ions are described by the C_4/r^4 potential, where C_4 is the potential constant [9, 79]. For neutral atoms, the FWHM of Stark broadening can be expressed as [9, 79]

$$\delta_S^{atom} = 11.37 \cdot C_4^{2/3} V_e^{1/3} N_e \frac{\lambda_0^2}{2\pi c} \qquad (4\text{-}12)$$

For atomic ions,

$$\delta_S^{ion} = \frac{200.8}{631} \cdot C_4^{2/5} Z^{4/5} \frac{N_e}{\sqrt{T}} \frac{\lambda_0^2}{2\pi c} \qquad (4\text{-}13)$$

Where V_e and N_e are the mean velocity and number density of electrons respectively, and Z is the charge of the emitter ion. According to the work of Griem [157, 158], the influence of ions on Stark broadening is often considered as a correction term using a quasi-static approach.

When the pressure is progressively reduced, the effects arising from the pressure broadening and Stark broadening will be weakened, and the line width will asymptotically approach a temperature-dependent finite value [108]. The remaining width of the line is due to the random motion of radiating atoms, which is described as Doppler broadening [108]. Assuming that the velocity distribution of atoms is Maxwellian, the FWHM of Doppler broadening is written as [9]

$$\delta_D = \lambda_0 \sqrt{\frac{8\ln 2 \cdot kT}{mc^2}} \tag{4-14}$$

Where k is the Boltzmann constant and m is the mass of the emitting atom.

When the thermal velocities of radiating atoms are reduced until the Doppler width is decreased to negligible, the remaining width is known as the natural width [108].The natural broadening is ultimately related to the uncertainty principle [159], and the natural width is generally much narrower than Doppler width [108]. Therefore, the natural broadening is not taken into account in this work.

4.2.3 Atomic continuum

As described in section 4.2.1, the calculation of net emission coefficients requires not only atomic lines but also atomic continuum. According to the works of Gleizes et al. [76], Liani et al. [77], Cressault et al. [79, 85] and Hannachi et al. [160], the continuum radiation of atoms is described by radiative attachment, radiative recombination, and Bremsstrahlung.

For radiative attachment, an atom can capture an electron to form a negative ion with a photon emission: $A + e^- \leftrightarrow A^- + h\nu$ [77]. The monochromatic emission coefficient of this mechanism is formulated as [85]

$$\varepsilon_{att} = \frac{2hc^2}{\lambda^5} \exp\left(-\frac{hc}{\lambda kT}\right) N_{A^-} \sigma_{det}(\lambda) \tag{4-15}$$

Where N_{A^-} is the number density of the atomic species A^- and σ_{det} is the photodetachment cross section of A^-.

For radiative recombination, an atomic ion with charge Z+ can capture an electron

to form an ion with charge (Z-1)+ and emit a photon: $A^{Z+} + e^- \leftrightarrow A^{(Z-1)+} + h\nu$ [77]. The monochromatic emission coefficient of this process is written as [85]

$$\varepsilon_{rec} = \frac{16\pi \left(e^2/4\pi\varepsilon_0\right)^3}{3c^3\sqrt{6\pi k m_e^3}} \frac{c}{\lambda^2} \frac{N_e N_{Z+}}{Q_{Z+}^{int}} \frac{Z^2}{\sqrt{T}} \left[1 - \exp\left(-\frac{hc}{\lambda kT}\right)\right] g_0^{Z+} \xi^{(Z-1)+}(\lambda, T) \quad (4\text{-}16)$$

Where N_e is the number density of electrons, N_{Z+}, Q_{Z+}^{int} and g_0^{Z+} are the number density, the internal partition function and statistical weight of the ground level of A^{Z+} respectively, and $\xi^{(Z-1)+}$ is the Bibermann-Schlüter factor accounting for the non-hydrogenic structure of $A^{(Z-1)+}$, and is derived from a summation of the photoionization cross section over all the levels of the atom considered [76]. When $\xi^{(Z-1)+}$ is unavailable, the emission coefficient ε_{rec} is usually approximated by taking the species as a hydrogen-like atom and using the formula presented in [85].

For Bremsstrahlung, a free electron in the field of an ion or an atom can be slowed down and therefore loses energy through radiation [76]. The monochromatic emission coefficients due to Bremsstrahlung are given in equations (4-17) and (4-18) for atoms and atomic ions respectively [76, 77, 85].

$$\varepsilon_{ea} = \frac{32}{3c^3} \frac{e^2}{4\pi\varepsilon_0} \left(\frac{k}{2\pi m_e}\right)^{3/2} \frac{c}{\lambda^2} N_A N_e T^{3/2} \exp\left(-\frac{hc}{\lambda kT}\right) G_{ea}(\lambda, T) \quad (4\text{-}17)$$

$$\varepsilon_{ei} = \frac{16\pi \left(e^2/4\pi\varepsilon_0\right)^3}{3c^3\sqrt{6\pi k m^3}} \frac{c}{\lambda^2} \frac{Z^2 N_{A+} N_e}{\sqrt{T}} \exp\left(-\frac{hc}{\lambda kT}\right) G_{ei}(\lambda, T) \quad (4\text{-}18)$$

Where N_A and N_{A+} are, respectively, the number densities of neutral atoms and atomic ions, G_{ea} is a factor proportional to the cross sections of electron-atom collisions, and G_{ei} is the Gaunt factor of atomic ion originating from the cross sections of free-free transitions.

4.2.4 Molecular roles

In the thermal plasma initially composed of molecular gases at low temperatures, the predominant molecules show effects of molecular bands and continuum. These

effects were ignored in the early study of the net emission coefficients. For example, in Gleizes's et al. works [9, 76] for N_2, SF_6 and SF_6-N_2 mixtures, the radiation of N_2 and the dissociative products of SF_6 was not taken into account, and only atoms and atomic ions were considered.

Compared with atoms, molecules have not only electronic but also vibrational and rotational energy levels, resulting in large quantities of molecular bands and thus making the calculation much more complicated and time-consuming. Moreover, lacking spectroscopic data is also one of large difficulties for molecules especially for polyatomic molecules. In the works of Naghizadeh-Kashani et al. [78], Hannachi et al. [160], Aubrecht et al. [91] and Jan et al. [86], only diatomic molecules (except for CO_2) were taken into account in the calculation of the radiation of molecular bands, and the role of polyatomic molecules is only considered in the molecular continuum.

For a diatomic molecule, the monochromatic emission coefficient of a transition between tow rotational levels $J^{'}$ and $J^{''}$ can be written as [78, 108]

$$\varepsilon_{band} = \frac{hc}{4\pi\lambda} A_{n^{''},v^{''},K^{''},J^{''}}^{n^{'},v^{'},K^{'},J^{'}} N\left(n^{'},v^{'},K^{'},J^{'}\right) \tag{4-19}$$

Where $N(n^{'}, v^{'}, K^{'}, J^{'})$ is the number density of the given particle in the emitting state $(n^{'}, v^{'}, K^{'}, J^{'})$, and $A_{n^{''},v^{''},K^{''},J^{''}}^{n^{'},v^{'},K^{'},J^{'}}$ is the corresponding transition probability which can be calculated using the method described in [78] or obtained through experiments.

The molecular continuum is mainly associated with the two reactions involving photons, namely photo-dissociation reaction ($hv + AB \leftrightarrow A + B$) and photo-ionization reaction ($hv + AB \leftrightarrow AB^+ + e^-$). Accordingly, the total molecular continuum absorption coefficient of gas mixtures is determined by summing the contribution of each molecule with considering their roles in photo-dissociation and photo-ionization reactions [86].

$$\kappa_{molecule} = \sum_i N_i \sigma_i \tag{4-20}$$

Where N_i is the number density of particle i and σ_i is its cross sections for photo-dissociation or photo-ionization reactions.

In practical computation, the photo-dissociation and photo-ionization cross

90

sections are usually assumed to be independent of temperature as such cross sections are difficult to obtain above room temperature. As a result, the cross sections at 300 K are used in this work. This method was also adopted in the previous works [78, 79, 86, 160] to yield reasonable results for molecular continuum.

4.3 Results and discussion

In this calculation of NEC, the equilibrium compositions of CO_2-N_2-Cu mixtures are obtained according to the work presented in chapter 2. The condensed species are considered in the determination of compositions, but they are ignored in the calculation of NEC. This only affects the results at temperatures below 3000 K because the condensed species evaporate into gaseous ones above this temperature. The atomic species including C, C^+, C^{2+}, C^{3+}, O, O^+, O^{2+}, O^{3+}, N, N^+, N^{2+}, N^{3+}, Cu, Cu^+, Cu^{2+} and Cu^{3+} are taken into account in the calculation of atomic lines and atomic continuum. The source data (energy levels and lines) were compiled from NIST database [119] and the tables provided by Kurucz and Peytremann [161-163]. The molecules including CO_2, CO, O_2, N_2, NO, CN and C_2 are considered in the molecular lines and continuum. The corresponding source data were compiled from HITRAN database [164]. Cu_2 and CuO are ignored in the calculation as the corresponding spectroscopic data are unavailable and their contents are not so high. The other molecules and ions as listed in chapter 2 are not taken into account because of their very low concentration.

Figure 4-1 shows the NEC of CO_2-N_2 (mixing ratio 7:3) mixtures contaminated by 10% Cu with different plasma radii at ambient pressure. Compared with the optically thick plasmas ($R > 0$), the optically thin plasma ($R = 0$) presents larger values of NEC at temperatures above 2200 K. Moreover, with the increase of the plasma size, the values of NEC drop dramatically. This can be attributed to the strong absorption of the lines, especially the resonance lines. However, at low temperatures, molecules dominate the mixtures, and thus the absorption of radiation is so weak that the NEC is nearly independent of plasma radius.
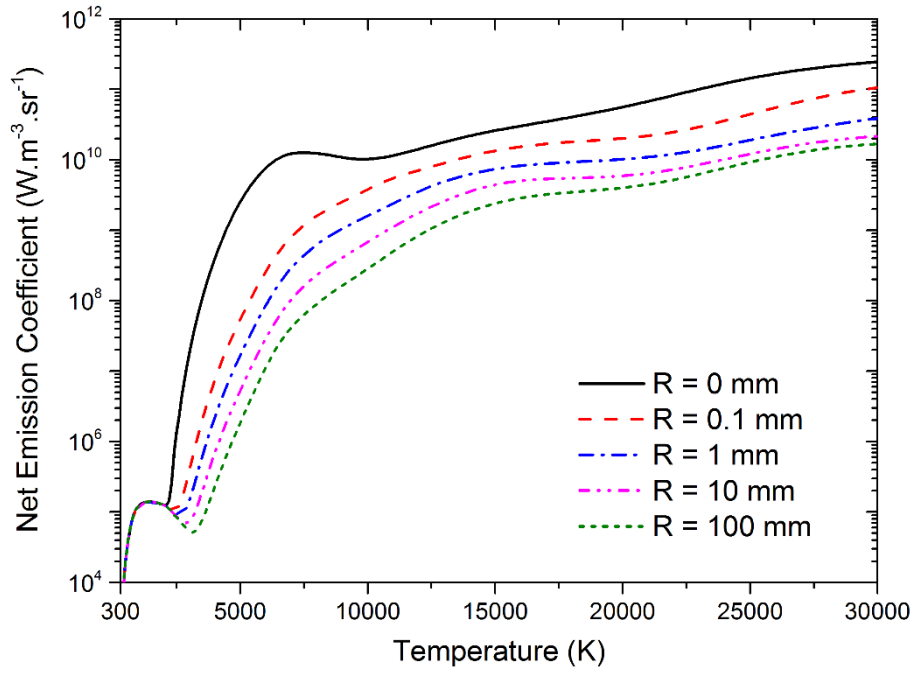
Figure 4-1. NEC of CO_2-N_2 (mixing ratio 7:3) mixtures contaminated by 10% Cu
with different plasma radii at temperatures of 300 – 30,000 K and at 1 bar
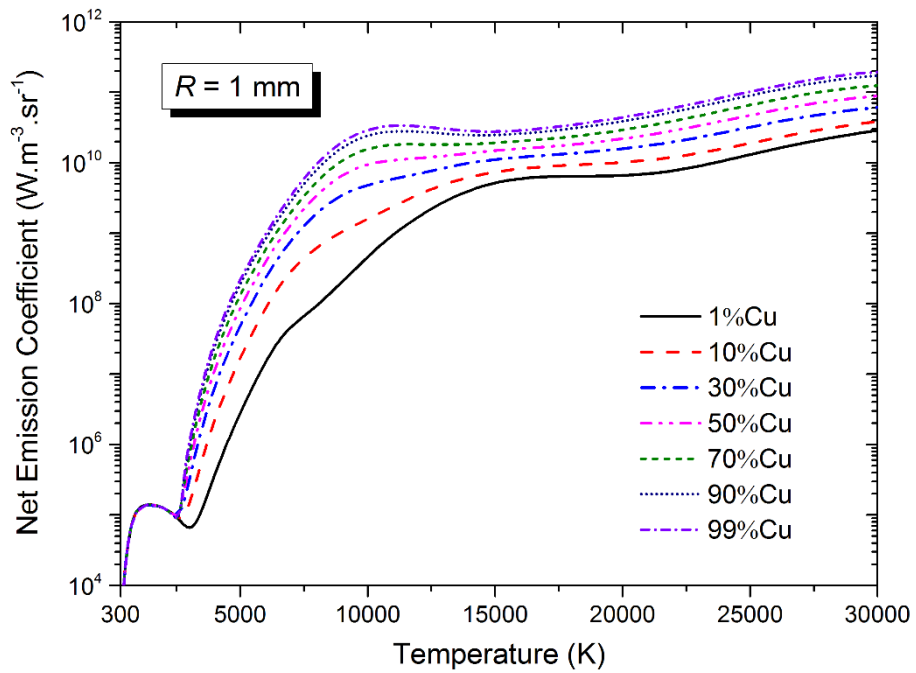

Figure 4-2. NEC of CO_2-N_2 (mixing ratio 7:3) mixtures contaminated by different
proportions of Cu at temperatures of 300 – 30,000 K and at 1 bar

92

The influence of copper contamination is shown in Figure 4-2 for CO_2-N_2-Cu mixtures with R = 1 mm. Obviously, the copper vapour results in a strong increase of NEC at temperatures above 2500 K. This is because copper has lower ionization potential and is easier to excite than the other atoms (carbon, oxygen, and nitrogen), which leads to the increase of line intensities when the copper proportion is raised. However, at temperatures below 2500 K, since elemental copper exists mainly in the form of condensed species which is not taken into account in the calculation of NEC, the influence arising from copper is negligible.

Figure 4-3 describes the NEC of pure CO_2, pure N_2 and their different mixtures contaminated by 10% Cu with R = 1 mm at ambient pressure. As we can see, the addition of N_2 into CO_2-N_2 mixtures only has a slight effect at temperatures above 3000 K because the line intensities of different types of atoms are close to each other, whereas at low temperatures the mixing of N_2 causes the significant decrease of NEC of CO_2-N_2-Cu mixtures as the emission of CO_2 is much stronger than that of N_2.
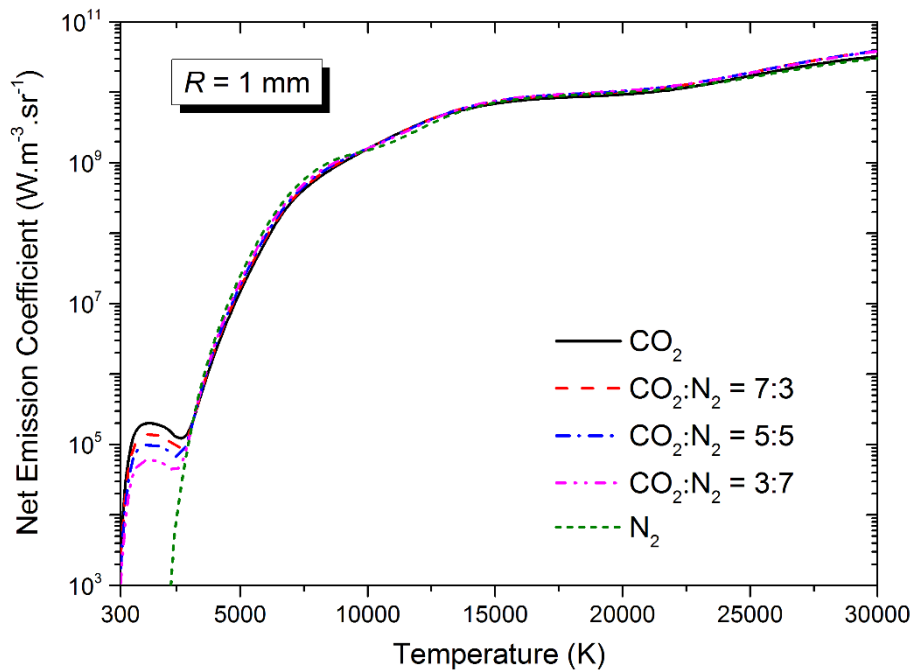

Figure 4-3. NEC of CO_2, N_2, and their different mixtures contaminated by 10% Cu at temperatures of 300 – 30,000 K and at 1 bar

Lastly, the influence of gas pressure on the NEC of CO_2-N_2-Cu mixtures is shown in Figure 4-4. The volume proportion of copper contamination and the mixing ratio of CO_2 and N_2 are set to be 10% and 7:3 respectively. Clearly, due to the compression of gas with the increase of pressure, the particle number densities are raised, resulting in the enhancement of radiation. Additionally, the NEC of CO_2-N_2-Cu plasma mixtures experiences a trough when the molecules do not play an essential role any more, and this trough is shifted to a higher temperature given a higher pressure because the dissociations of molecules are suppressed.
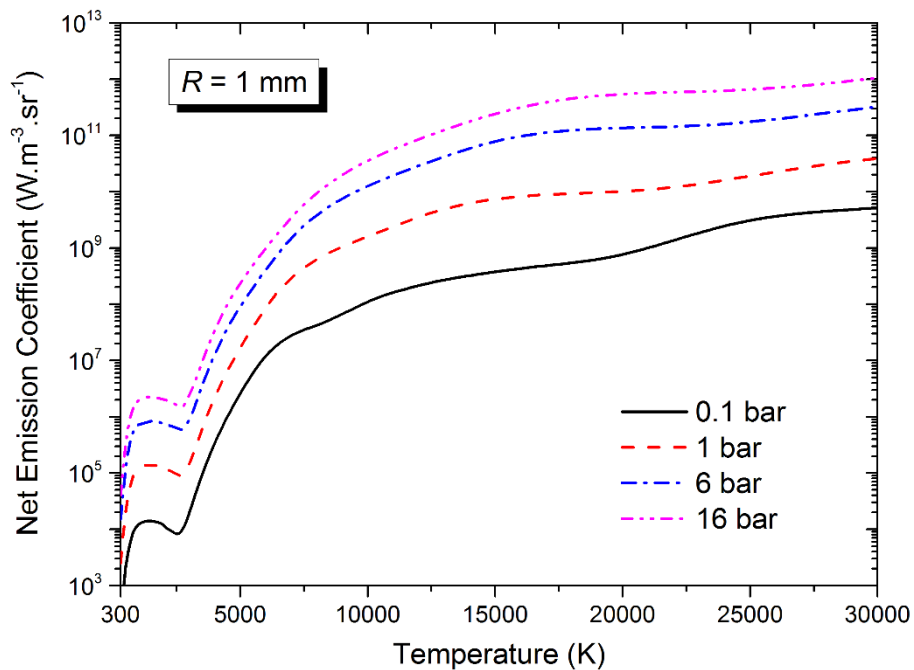
Figure 4-4. NEC of CO_2-N_2 (mixing ratio 7:3) mixtures contaminated by 10% Cu at temperatures of 300 – 30,000 K and at different pressures

4.4 Comparison with SF_6-Cu mixtures

In order to present the difference of NEC between SF_6 and CO_2-N_2 mixtures, we calculated the NEC of SF_6-Cu mixtures. Considering that the basic data for the molecules and condensed species are not sufficient and they mainly exist at low temperatures, they are ignored so as to highlight the roles of atoms at high temperatures.

94

Figure 4-5 shows the NEC of CO_2-N_2 (mixing ratio 7:3) mixture and SF_6 gas contaminated by 1% copper at ambient pressure. Compared with SF_6-Cu mixtures, CO_2-N_2-Cu mixtures present higher NEC below 17,000 K while lower NEC above 17,000 K. This difference will result in the different rates of energy loss between SF_6-Cu arc and CO_2-N_2-Cu arc during the arc interruption.
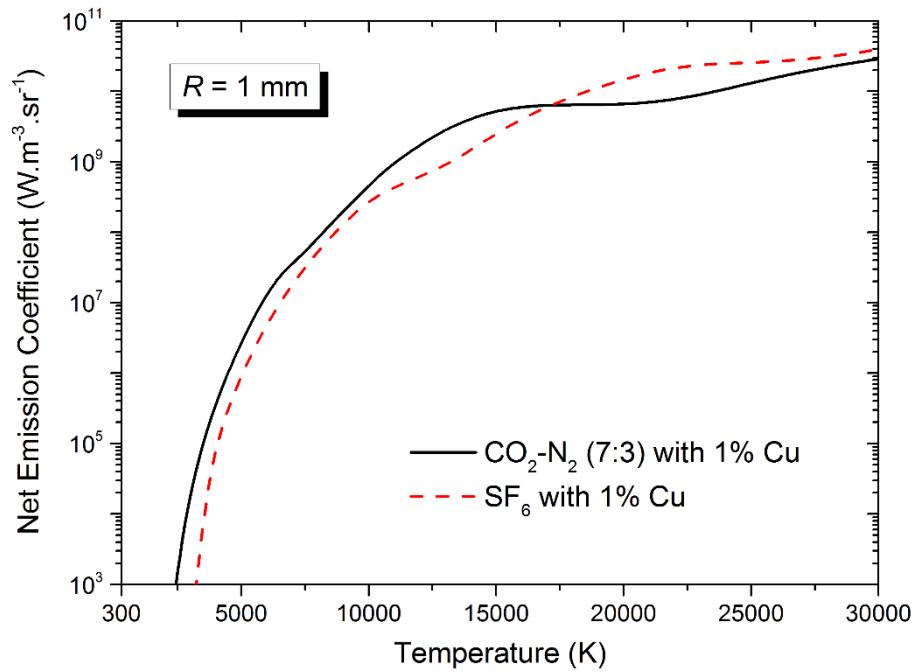
Figure 4-5. Comparison of NEC of CO_2-N_2 (mixing ratio 7:3) mixture and SF_6 gas contaminated by 1% copper at 1 bar

4.5 Summary

In this chapter, we present a calculation of net emission coefficients of CO_2-N_2-Cu mixtures. The atomic lines, atomic continuum, molecular bands, and molecular continuum are all taken into account. In the calculation of atomic lines, four kinds of broadenings including Van der Waals broadening, resonance broadening, Stark broadening and Doppler broadening are considered. In the determination of atomic continuum, three kinds of mechanism including radiative attachment, radiative recombination and Bremsstrahlung (including neutral atoms and atomic ions) are

considered. For molecules, their bands are considered with the available spectroscopic data, and the molecular continuum is approximated using the cross sections of photo-dissociation and photo-ionization reactions.

According to the results and discussion in this chapter, five conclusions can be drawn as follows.

(i) Due to the absorption of lines, the NEC of an optically thin plasma ($R = 0$) is much larger than that of an optically thick plasma ($R > 0$).

(ii) Copper contamination strongly raises the values of NEC after the condensed copper evaporates to gaseous species, because copper is easier to ionize and excite.

(iii) N_2 shows a significant effect on the NEC of CO_2-N_2-Cu mixtures at low temperatures as the emission of CO_2 is much stronger than that of N_2, whereas the influence arising from N_2 becomes slight at high temperatures because the line intensities of different types of atoms are close to each other.

(iv) With the increase of pressure, the NEC of gas mixtures is dramatically raised because of the increasing number densities of species.

(v) Compared with SF_6-Cu mixtures, CO_2-N_2-Cu mixtures present higher NEC below 17,000 K while lower NEC above 17,000 K.

CHAPTER 5 DIELECTRIC BREAKDOWN PROPERTIES OF CO_2-N_2-CU PLASMAS

5.1 Introduction

To be applied in circuit breakers, a good arc quenching gas must not only present high specific heat and thermal conductivity to rapidly cool the arc down, but also have high electron attachment ability to enable a rapid transition between the conducting state and the dielectric state at low temperatures [30]. In the previous chapters 2-4, the thermodynamic, transport, combined diffusion, and radiation properties of CO_2-N_2-Cu mixtures were discussed. These data are necessarily required in the physical modellings of thermal plasmas, such as Magnetohydrodynamics (MHD) modelling. In circuit breakers, the MHD model is capable of describing the physical fields, such as temperature field, pressure field, electric field, and magnetic field of arc plasma during the interruption process, by solving the Navier–Stokes equations combined with the equations describing electric and magnetic fields [165, 166]. However, such model is not capable of determining the dielectric breakdown performance of gaseous medium during the current zero. Actually, a high electric field strength caused by a transient recovery voltage (TRV) in the current interruption process is applied to the hot arc quenching gas between the electrodes and between the exhaust tube and grounded tank [43, 92]. If the hot gas has a lower dielectric strength than the applied electric field strength, the gas breakdown known as 'dielectric failure' will occur, leading to the re-ignition of the arc [43, 44, 92].

In order to better understand the gas breakdown occurring in circuit breakers, this chapter is dedicated to the dielectric breakdown properties of hot gas mixtures during the dielectric recovery phase. According to the works by Tanaka [44] and Wang et al. [43], copper vapour has a significant effect on the critical electric field strength of gas medium. Therefore, the dielectric breakdown properties of CO_2-N_2 mixtures contaminated by copper, including electron energy distribution function (EEDF),

ionization coefficient, electron attachment coefficient, and critical electric field strength, are calculated and discussed under various conditions.

The rest sections are organized as follows. In section 5.2, the calculation procedure and necessary input data for dielectric breakdown properties are introduced. Next, the results for EEDF, reduced ionization and electron attachment coefficients, and reduced critical electric field strength are discussed in sections 5.3.1 – 5.3.3 respectively. In section 5.4, a comparison between CO_2-N_2-Cu and SF_6-Cu mixtures are performed. Lastly, a summary is given in section 5.5.

5.2 Calculation method and basic data

5.2.1 Determination of dielectric breakdown properties

For the sake of convenience, we refer to the gas mixtures at room temperature (300 K) as "cold gas" and the mixture above room temperature as "hot gas". In the past few decades, the electron swarm parameters of many kinds of gas mixtures have been calculated or measured at room temperature in order to evaluate the insulating ability of cold gases [1, 6-8, 13, 26, 95, 102, 103, 167-169]. However, when the gas temperature increases above room temperature, the dielectric performance of hot gas will be different from that of cold gas as the compositions of mixtures change with temperature mainly due to the dissociations of molecules. Consequently, the plasma compositions need to be determined firstly when calculating the dielectric breakdown properties of hot gases. The method presented in chapter 2 is adopted here with the consideration of condensed species. Following our previous publications [1, 43], the upper limit of temperature is set to be 3500 K.

During the current zero period, a dielectric breakdown will occur if the overall balance between the electron generation and electron loss is in favor of the former [94]. In order to determine the dielectric breakdown properties, the electron swarm coefficients (i.e. ionization coefficient and electron attachment coefficient) which depend on the EEDF have to be obtained [1]. For the theoretical investigation of

98

electron swarm coefficients in cold gases, the Monte Carlo method [26, 103, 170] and Boltzmann equation method [5, 101, 104, 171] are usually used. For hot gases, however, only the Boltzmann equation method was used [1, 2, 8, 13-15, 43, 172-175]. In this method, the EEDF which in general is not Maxwellian is derived from the solution of the Boltzmann equation for an ionized gas [176].

$$\frac{\partial f}{\partial t} + \vec{v} \cdot \nabla f - \frac{e}{m} \vec{E} \cdot \nabla_v f = C[f] \tag{5-1}$$

Where f is the electron distribution in six-dimensional phase space, $\vec{v}$ the velocity coordinates, e the elementary charge, m the electron mass, $\vec{E}$ the electric field, ∇_v the velocity-gradient operator, and C represents the rate of change in f due to the elastic and inelastic collisions.

Assuming that the electric field and the collision probabilities are spatially uniform, a common approach to solve Boltzmann equation is to expand the electron distribution function in two terms of Legendre polynomials of spherical harmonics expansion [176].

$$f(v, \cos\theta, z, t) = f_0(v, z, t) + f_1(v, z, t) \cos\theta \tag{5-2}$$

Where f_0 and f_1 are the isotropic and anisotropic parts of f respectively, and θ is the angle between the velocity and the field direction.

In high precision cases, six or more expansion terms are needed to solve the Boltzmann equation numerically, but in many cases a two-term approximation can provide sufficient accuracy [176]. Yousfi et al. [95] compared the reduced critical electric field strength of hot SF_6 gas calculated by the two-term and multi-term Boltzmann equation. Their result shows that the maximal deviation (nearly 5%) between these two methods was observed in the temperature range of 300-1200K and the deviation became completely negligible when the temperature was above 2000 K. Therefore, following our previous works [1, 2, 43], the two-term Boltzmann equation is adopted in this work.

To further simplify the Boltzmann equation, the velocity-dependent distribution functions f_0 and f_1 are both assumed to be independent of time and space. As a result,

they are expressed as [176, 177]

$$f_0(\varepsilon, z, t) = \frac{1}{2\pi\gamma^3} F_0(\varepsilon) N_e(z, t) \tag{5-3}$$

$$f_1(\varepsilon, z, t) = \frac{1}{2\pi\gamma^3} F_1(\varepsilon) N_e(z, t) \tag{5-4}$$

With

$$\gamma = \sqrt{\frac{2e}{m}}, \quad \varepsilon = \left(\frac{v}{\gamma}\right)^2 \tag{5-5}$$

Where ε and N_e are the electron energy and electron number density respectively, and the energy distribution F_0 and F_1 are both constant in time and space, and are normalized by [176]

$$\int_0^\infty F_0 \sqrt{\varepsilon} d\varepsilon = 1 \tag{5-6}$$

In order to determine the time and space dependence of electron density, two simple models corresponding to the specific swarm experiments are usually used. One is the model of exponential temporal growth without space dependence, which corresponds to the pulsed Townsend experiments [176, 178]. The other is the model of exponential spatial growth without time dependence, which corresponds to the steady state Townsend experiments [176, 178]. To be consistent with the state of dielectric breakdown in circuit breakers, we adopt the previous model.

In this model, the temporal growth rate of electrons equals is associated with the sum over the ionization and electron attachment processes.

$$\frac{1}{N_e}\frac{\partial N_e}{\partial t} = \gamma N \int_0^\infty \left(\sum_{k=ionization} x_k \sigma_k - \sum_{k=attachment} x_k \sigma_k \right) \varepsilon F_0 d\varepsilon \tag{5-7}$$

Where x_k and σ_k are, respectively, the mole fraction of the target species and the corresponding cross section in the electron-impact collision process k, and N is the number density of the gas.

In the above model, the energy distribution F_1 can be derived from F_0 [176] according to the following formula.

100

$$F_1 = \frac{E}{N} \frac{1}{\tilde{\sigma}_m} \frac{\partial F_0}{\partial \varepsilon} \tag{5-8}$$

With

$$\tilde{\sigma}_m = \sum_k x_k \sigma_k + \frac{1}{N_e N \gamma \sqrt{\varepsilon}} \frac{\partial N_e}{\partial t} \tag{5-9}$$

Here, for elastic collisions, σ_k is the effective momentum-transfer cross section; for inelastic collisions, σ_k is the total cross section, assuming all momentum are lost in the collision.

Therefore, solving the Boltzmann equation turns out to be the determination of the energy distribution F_0. As comprehensively described in [176], the equation describing F_0 can be transformed into a convection-diffusion continuity equation, which can be solved numerically by discretizing the energy space on a grid.

After obtaining the EEDF, the reduced ionization coefficient α/N (also known as Townsend ionization coefficient) and reduced electron attachment coefficient η/N (also known as Townsend attachment coefficient) are calculated according to the following definitions.

$$\alpha/N = \frac{E/N}{P/N} \gamma \int_0^\infty \sum_{k=ionization} x_k \sigma_k \varepsilon f_0 d\varepsilon \tag{5-10}$$

$$\eta/N = \frac{E/N}{P/N} \gamma \int_0^\infty \sum_{k=attachment} x_k \sigma_k \varepsilon f_0 d\varepsilon \tag{5-11}$$

Where E/N is the reduced electric field and P/N is the reduced power gained by the electrons from the electric field.

The reduced critical electric field strength $(E/N)_{cr}$ is therefore determined when the formation and loss of electrons reach a balance. This means that the effective ionization coefficient $(\alpha-\eta)/N$ equals to zero.

5.2.2 Electron impact cross sections

As introduced above, the electron impact collision cross sections are needed to solve the Boltzmann equation, and thus to obtain the EEDF and the electron swarm

coefficients. The collisions between heavy particles as well as the photo-detachment and photo-ionization collisions are not considered in this work due to their negligible effects on the dielectric breakdown properties of gas mixtures according to our previous work [1, 2, 43]. As for the electron-electron collision, its influence become significant only when the ionization degree n/N (the proportion of gas species that are ionized into charged particles) is above 10^{-6} [179]. However, the ionization degree of hot CO_2-N_2-Cu mixtures at temperatures of $300 - 3500$ K is so low that the electron-electron collisions can also be neglected. Therefore, only the interactions, including elastic, excitation, ionization, and attachment collisions, between electrons and neutral species are taken into account. It should be noted that the total momentum transfer cross sections needed in solving Boltzmann equation should include the components both from elastic and inelastic collisions [1, 176].

Based on the compositions of hot CO_2-N_2-Cu mixtures ($300 - 3500$ K), 11 neutral particles with high molar fraction (i.e. $>10^{-5}$), namely CO, CO_2, N, N_2, NO, NO_2, O, O_2, Cu, Cu_2 and CuO, are dealt as main species in the calculation. The electron impact cross sections of CO, CO_2, O, and O_2 were presented in our previous publication [1]. The cross sections of N, N_2, NO, and NO_2 were compiled from the online database [180-184]. As for Cu_2 and CuO, no corresponding cross sections could be found in literatures. They were therefore ignored in the previous works (e.g. Tanaka's work for Air-Cu [44] and Li's et al. work for CO_2-Cu [106]).

However, Cu_2 (7.90 eV [145]) and CuO (9.41 eV [185]) have low ionization potential which inevitably affects the ionization coefficient of gas mixtures. Moreover, as discussed in Chapter 2, the concentrations of Cu_2 and CuO are not low enough to be ignored. Therefore, we took the ionization cross sections of Cu_2 and CuO into account in this work, which are calculated using the Deutsch–Märk (DM) formalism according to our previous work [1, 2, 43]. The required molecular orbital data in terms of the atomic orbital of the constituent atoms are obtained using a standard quantum chemistry code. The calculated results for the ionization cross sections of Cu_2 and CuO are
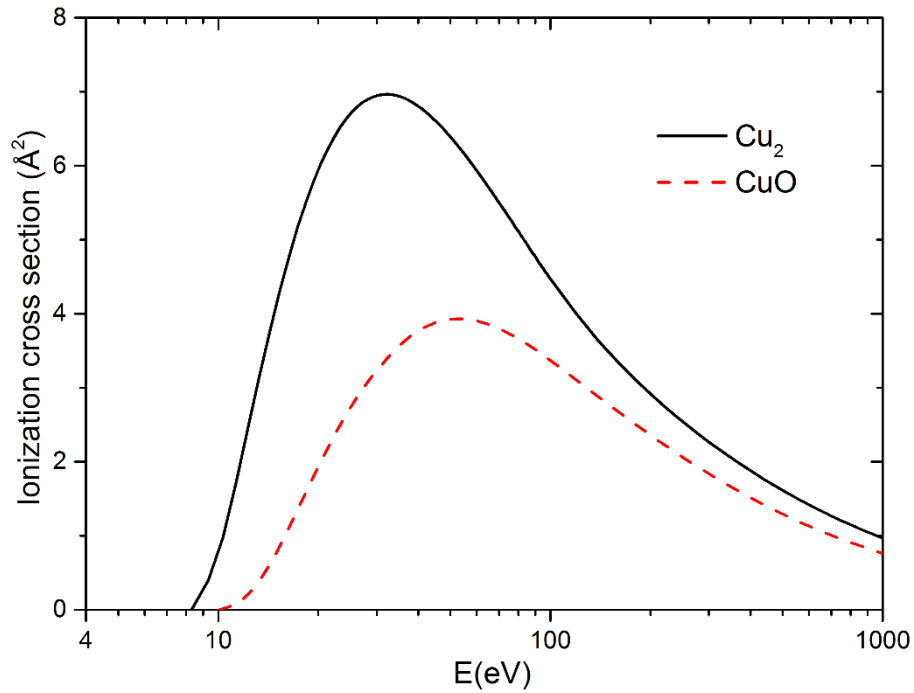
illustrated in Figure 5-1.

Figure 5-1. Ionization cross sections of Cu_2 and CuO calculated using DM method

5.3 Results and discussion

5.3.1 Electron energy distribution function (EEDF)

Figure 5-2 shows the EEDF of the hot CO_2-N_2 (mixing ratio 7:3) mixtures contaminated by 1% Cu for various temperatures at a constant E/N of 100 Td and ambient pressure.

The temperature dependence of the quantity of high-energy electrons can be divided into three parts: at $300 - 1500$ K, due to the weak ionization, the gas temperature shows no effect on EEDF; at $1500 - 3000$ K, the number of high-energy electrons deceases with temperature because of the generation of CO which has large excitation cross section, resulting in the decay of electron kinetic energy; above 3000 K, the copper vapour resulting from the phase transition of condensed copper starts to increase the probability density of electrons, because copper has relatively low ionization potential as described in the previous chapters.
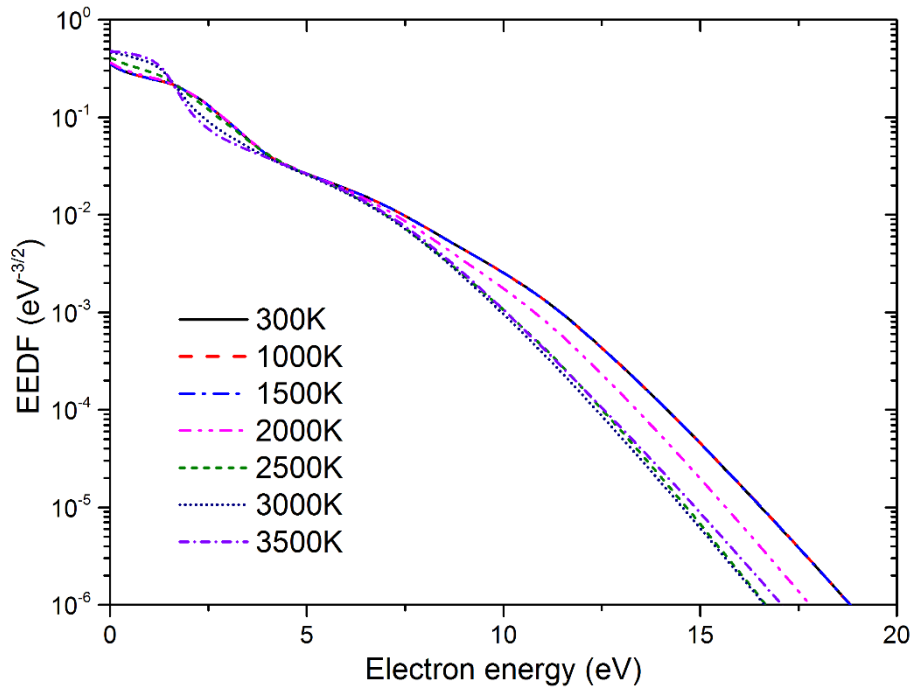
103

Figure 5-2. EEDF of CO_2-N_2 (mixing ratio 7:3) mixtures contaminated by 1% Cu for various temperatures at E/N of 100 Td and pressure of 1 bar.
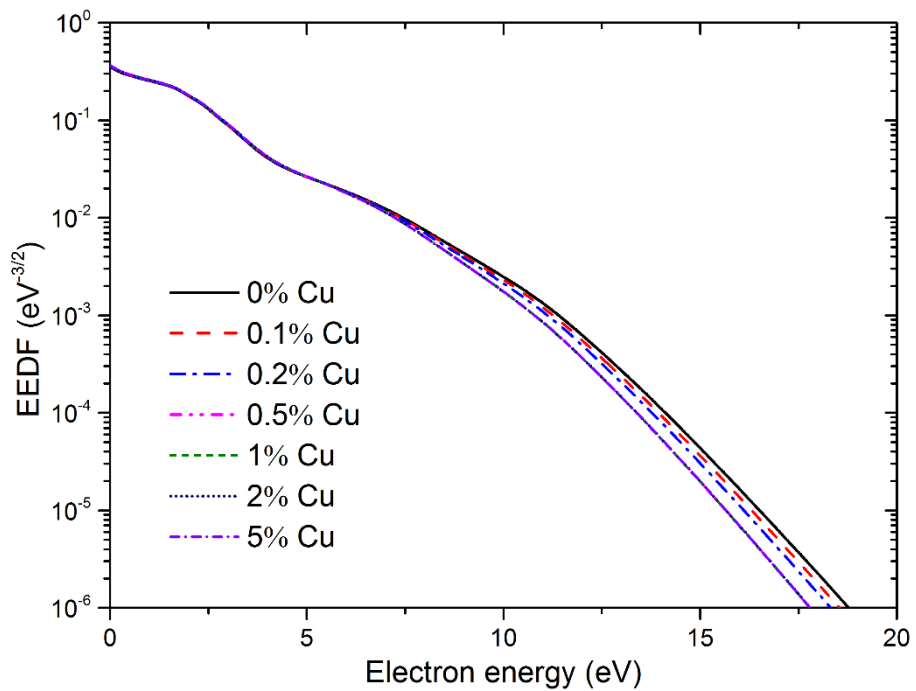

Figure 5-3. EEDF of CO_2-N_2 (mixing ratio 7:3) mixtures contaminated by different proportions of Cu at temperature of 2000 K, pressure of 1 bar and E/N of 100 Td.

Figure 5-3 describes the influence of copper contamination on the EEDF of hot CO_2-N_2-Cu mixtures at temperature of 2000 K, pressure of 1 bar and reduced electric field strength E/N of 100 Td.

As we can see from Figure 5-3, the existence of copper at 2000 K generally reduces the concentration of high-energy electrons significantly even for very low percentage (e.g. 0.1 %) of Cu, although copper is easier to ionize than the other species. This is because copper has larger electron impact cross sections to consume much kinetic energy during colliding with electrons.

Figure 5-4 shows the EEDF of pure CO_2 and various CO_2- N_2 mixtures (mixing ratios of 9:1, 7:3, 5:5, 3:7 and 1:9) contaminated by 1% Cu at temperature of 2000 K, pressure of 1 bar and E/N of 100 Td.

As illustrated in Figure 5-4, the mixing ratio between CO_2 and N_2 shows a marked effect on the EEDF of the hot CO_2-N_2-Cu mixtures. The addition of N_2 raises the quantity of electrons with low energy (< 2.4 eV) while reduces the quantity of electrons with high energy (> 2.4 eV). This the consequence of the difference of excitation cross sections between CO_2 and N_2. In general, the excitation cross sections with low threshold values for CO_2 are larger than those for N_2, whereas the excitation cross sections with high threshold values for CO_2 are smaller than those for N_2. The high excitation cross sections provide extra energy dissipation channels and thus restrain the ionization processes [2], leading to the reduction of electron amount.

The influence of gas pressure on the EEDF of the hot CO_2-N_2 (mixing ratio 7:3) mixtures contaminated by 1% Cu at E/N of 100Td and temperature of 2000 K is shown in Figure 5-5.

It is observed in Figure 5-5 that a higher pressure generally results in a higher probability density of electrons especially the high-energy electrons. These changes of the EEDF are mainly attributed to the different gas compositions, i.e. the pressure increase opposes the dissociation of molecules [1]. However, a change of pressure hardly affects the EEDF when the pressure is above 6 bar.
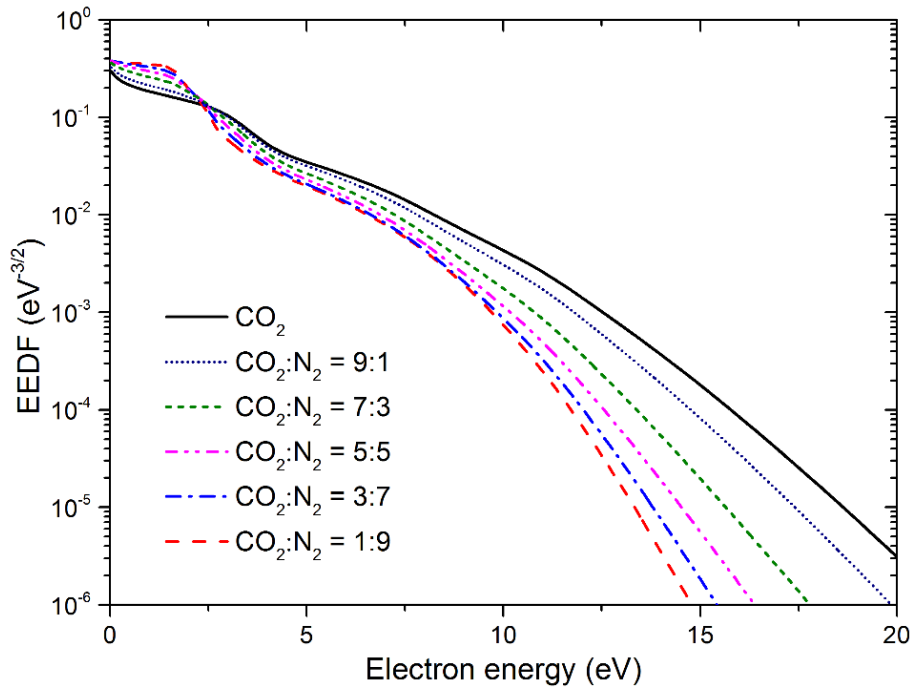
105

Figure 5-4. EEDF of CO_2 and different CO_2-N_2 mixtures contaminated by 1% Cu at temperature of 2000 K, pressure of 1 bar and E/N of 100 Td.
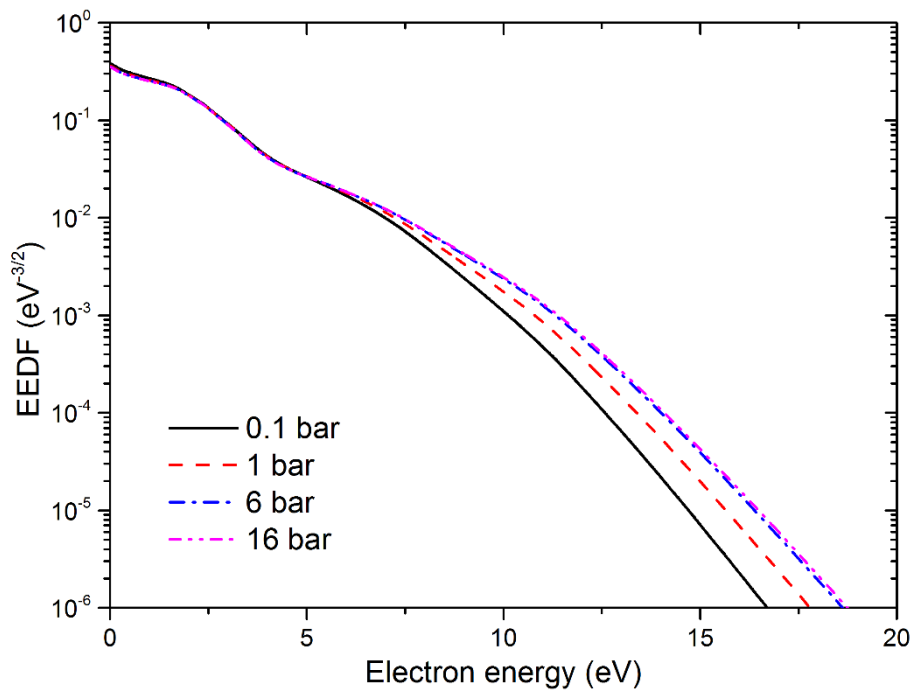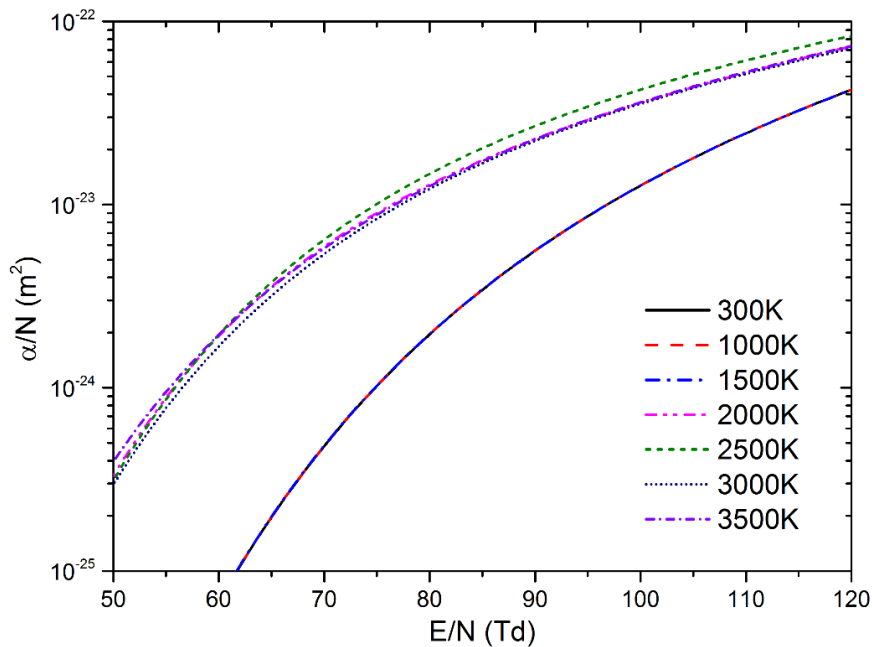

Figure 5-5. EEDF of CO_2-N_2 (mixing ratio 7:3) mixtures contaminated by 1% Cu for various pressures at temperature of 2000 K and E/N of 100 Td.

*5.3.2 Reduced ionization and electron attachment coefficients*

Collision ionization and electron attachment processes play an important role in calculating dielectric breakdown properties [43]. Based on the EEDF, the reduced ionization coefficient α/N, electron attachment coefficient η/N and effective ionization coefficient $(\alpha-\eta)/N$ of hot CO_2-N_2-Cu mixtures are calculated in this section.

Parts (a)-(c) in Figure 5-6 show the temperature dependence of α/N, η/N and $(\alpha-\eta)/N$ respectively in hot CO_2-N_2 (mixing ratio 7:3) mixtures contaminated by 1% Cu as a function of E/N at ambient pressure.

From 300 to 1500 K, α/N and η/N is almost independent of temperature because the composition does not change too much in this temperature range, considering that CO_2 and N_2 dominate the mixtures and copper exits in the form of condensed species. From 1500 to 2500 K, the condensed copper evaporates and increases the values of α/N abruptly. Above 2500 K, the dissociation of CO_2 reduces copper concentration and raises CO and O_2. This results in the decrease of α/N and increase of η/N respectively not only because copper has better ionization ability but also because CO and O_2 have better electron attachment ability than CO_2.

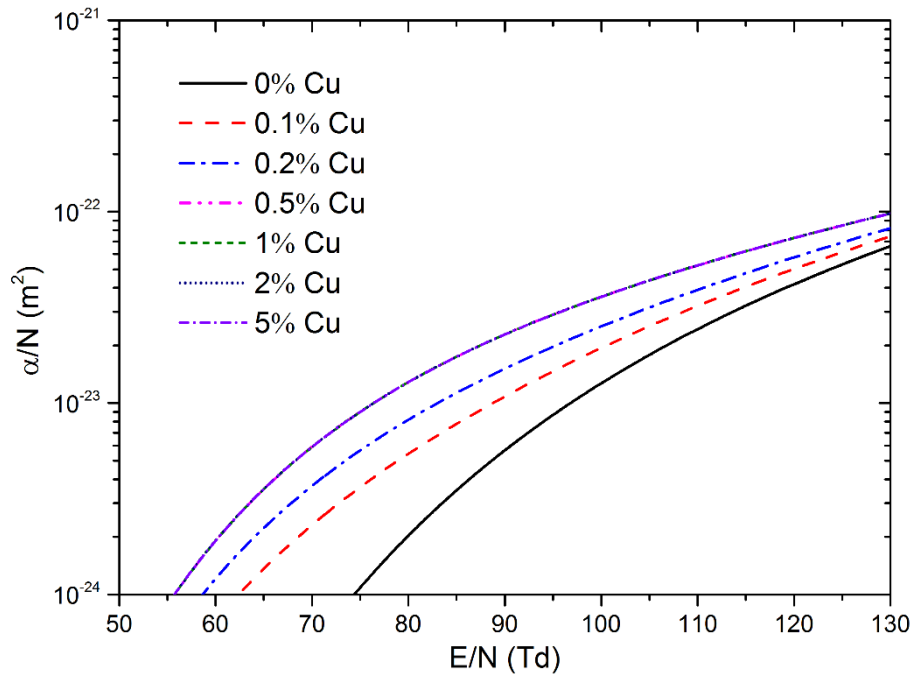(a) α/N
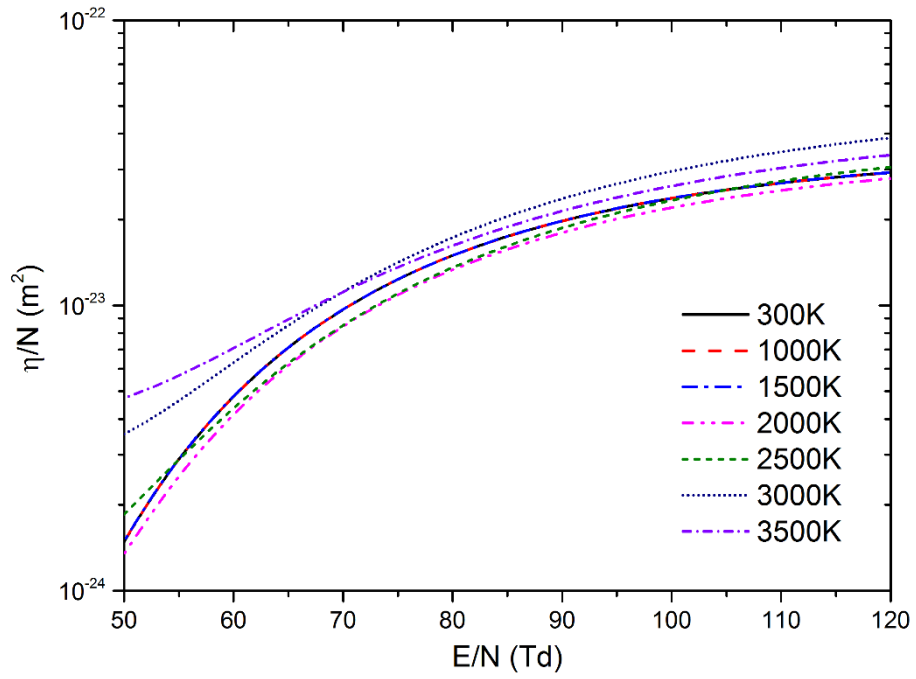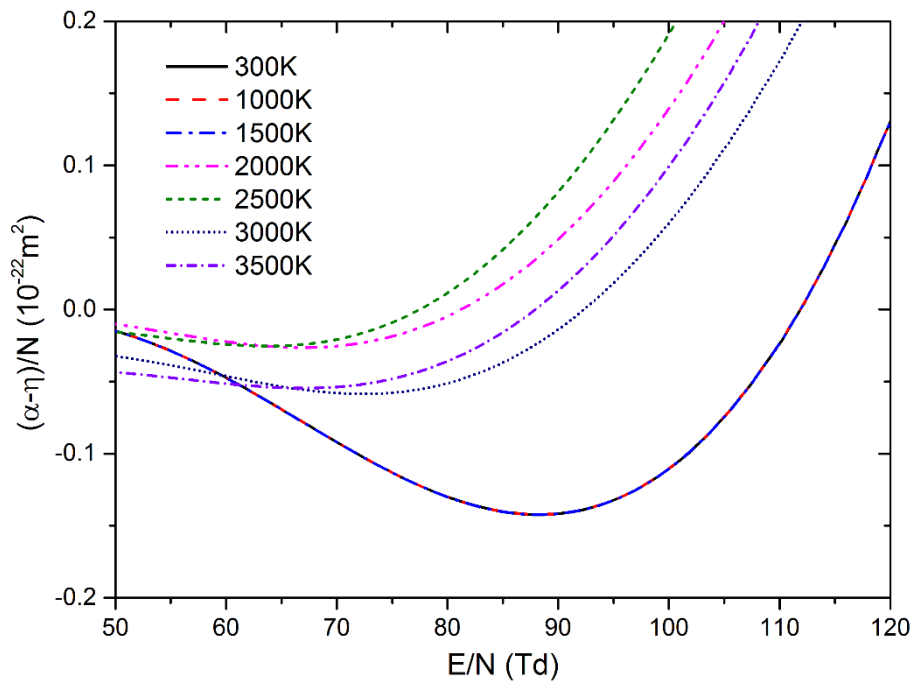
107

(b) η/N

(c) $(\alpha\text{-}\eta)/N$

Figure 5-6. α/N, η/N and $(\alpha\text{-}\eta)/N$ of CO_2-N_2 (mixing ratio 7:3) mixtures contaminated by 1% Cu for various temperatures as a function of E/N at 1 bar.

The influence of copper contamination on the values of α/N, η/N and $(\alpha-\eta)/N$ in CO_2-N_2-Cu mixtures is shown in parts (a)-(c) of Figure 5-7 respectively as a function of E/N at temperature of 2000 K and pressure of 1 bar. The mixing ratio of CO_2 and N_2 is set to be 7:3. The proportion of the copper contamination ranges from 0% to 5% in volume.

It is observed in Figure 5-7 that the copper contamination affects the ionization process significantly, i.e. enhancing the ionization in the mixtures even when the copper proportion is very low (e.g. 0.1%). This can be attributed to the better ionization performance of Cu than that of CO_2, N_2 and their dissociated products.

In the electron attachment processes, due to the poor electron affinity performance of Cu, the values of η/N fall with the increase of copper content. However, the further increase of Cu percentage (i.e. > 0.5%) raises the values of α/N and reduces η/N slightly. This observation can be partly explained by the slight increase of species with relatively small ionization cross sections and large electron attachment cross sections (e.g. CO and O_2) in CO_2-N_2-Cu plasma mixtures.
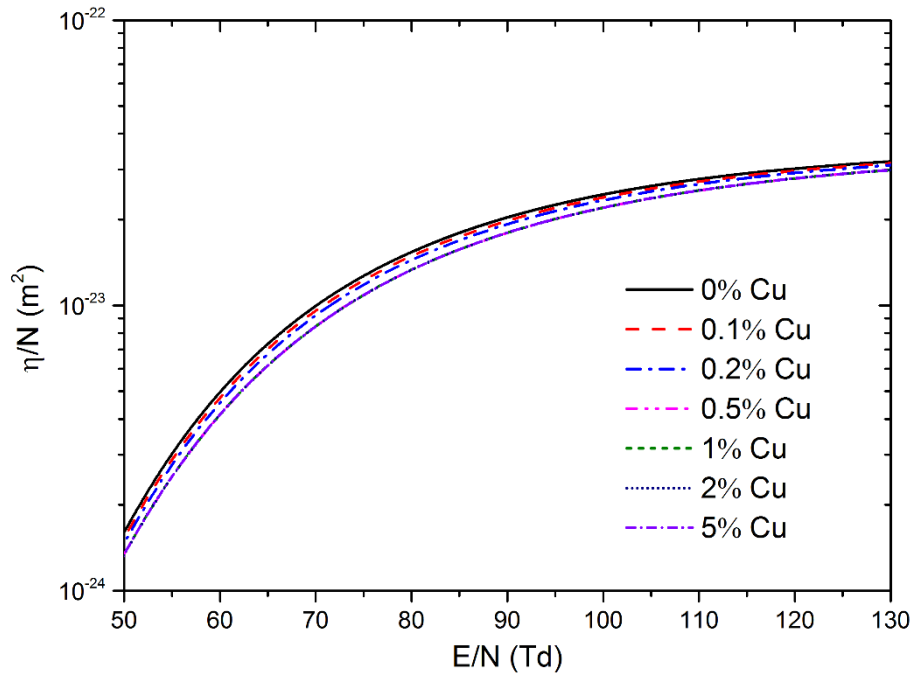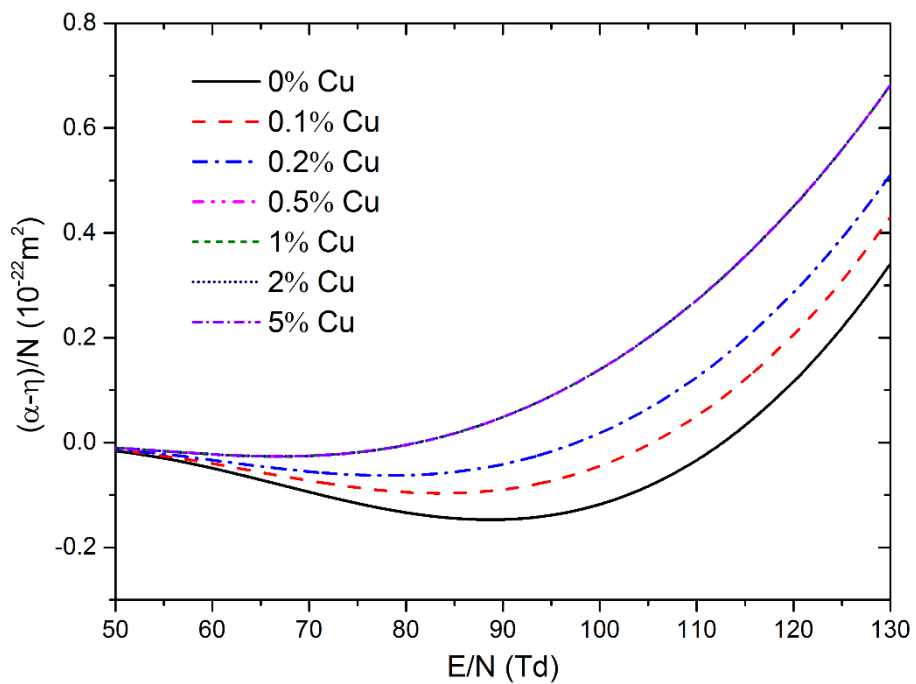
(a) α/N

109

(b) η/N

(c) $(\alpha-\eta)/N$

Figure 5-7. α/N, η/N and $(\alpha-\eta)/N$ of CO_2-N_2 (mixing ratio 7:3) mixtures contaminated by different proportions of Cu as a function of E/N at temperature of 2000 K and pressure of 1 bar.

Figure 5-8 (a)-(c) describe the behavior of α/N, η/N and $(\alpha\text{-}\eta)/N$ in pure CO_2, pure N_2 and CO_2-N_2 mixtures contaminated by 1% Cu as a function of E/N at temperature of 2000 K and ambient pressure.

As clearly seen from Figure 5-8, the addition of N_2 results in the remarkable decrease of α/N and η/N because N_2 has high excitation cross sections which provide extra energy dissipation channels. Since both the values of α/N and η/N are reduced at 2000 K, the $(\alpha\text{-}\eta)/N$ do not vary monotonously with the percentage of N_2.

Lastly, the effect of gas pressure on α/N, η/N and $(\alpha\text{-}\eta)/N$ of CO_2-N_2-Cu mixtures is illustrated in Figure 5-9 as a function of E/N at 2000 K. Similar to the observation in our previous works [1, 43], the values of α/N and $(\alpha\text{-}\eta)/N$ decrease with pressure while the dependence of η/N is opposite. According to Le Chatelier's law, the increase of pressure opposes changes to the original state of equilibrium that increases the number of molecules, so that the dissociation of molecules with high electron attachment cross sections and the ionization of atoms with high ionization ability are suppressed and shifted to higher temperatures, leading to lower α/N and higher η/N.

(a) α/N

(b) η/N

(c) $(\alpha\text{-}\eta)/N$
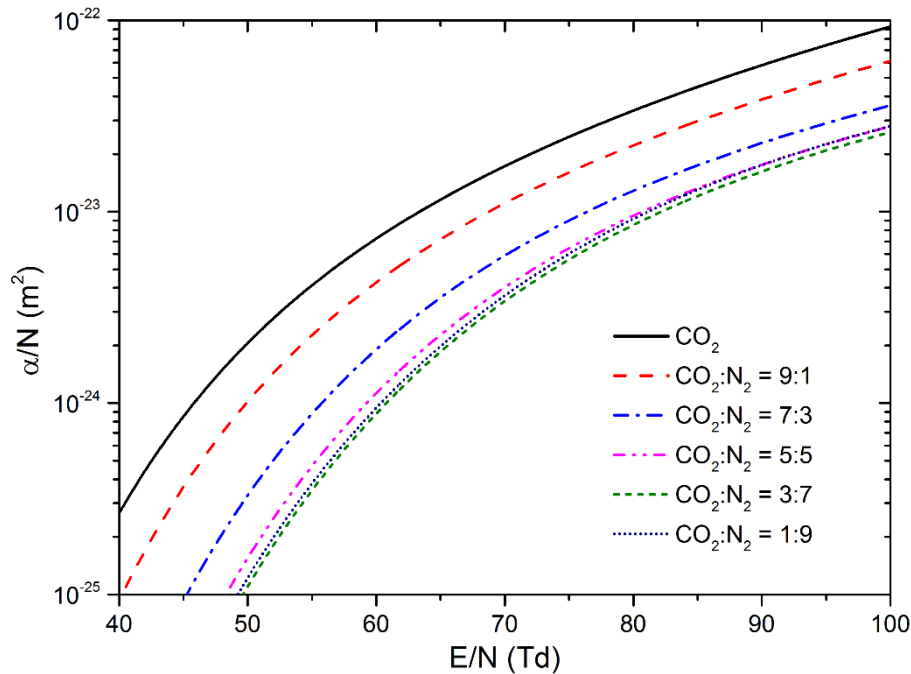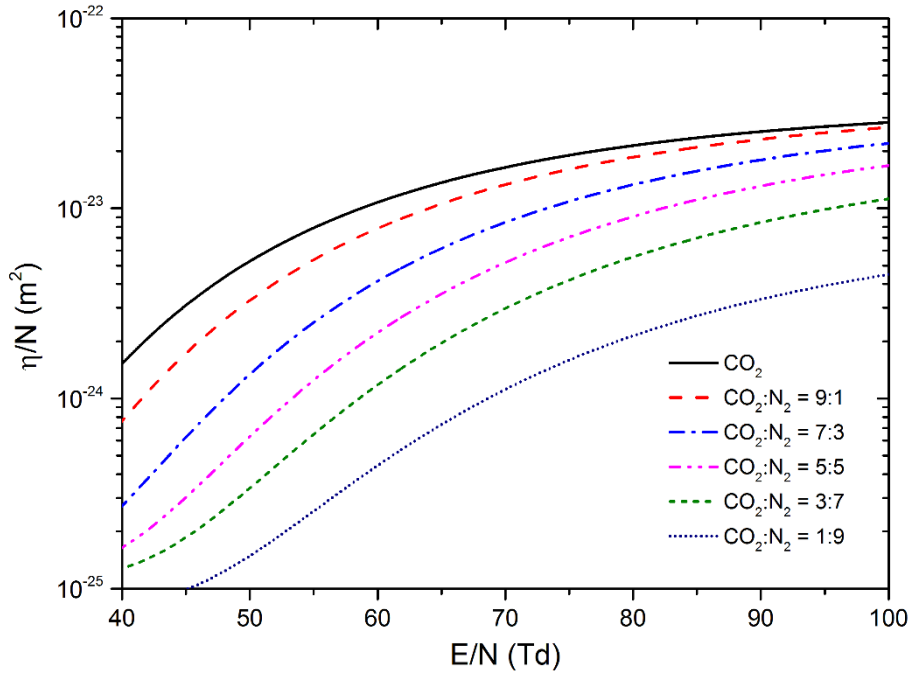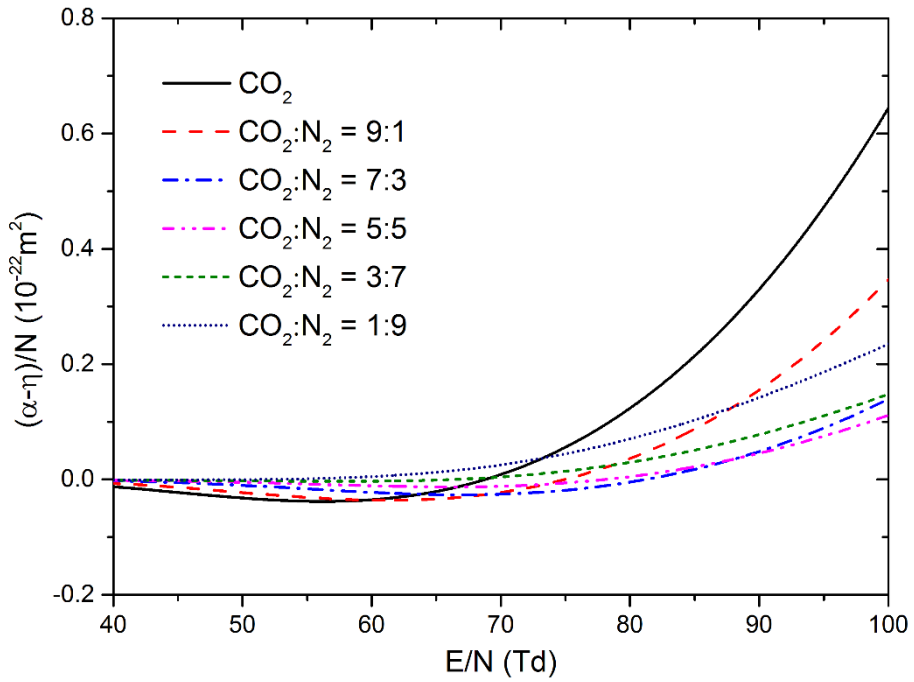
Figure 5-8. α/N, η/N and $(\alpha\text{-}\eta)/N$ of CO_2, N_2 and their different mixtures contaminated by 1% Cu as a function of E/N at temperature of 2000 K and pressure of 1 bar.

(a) α/N
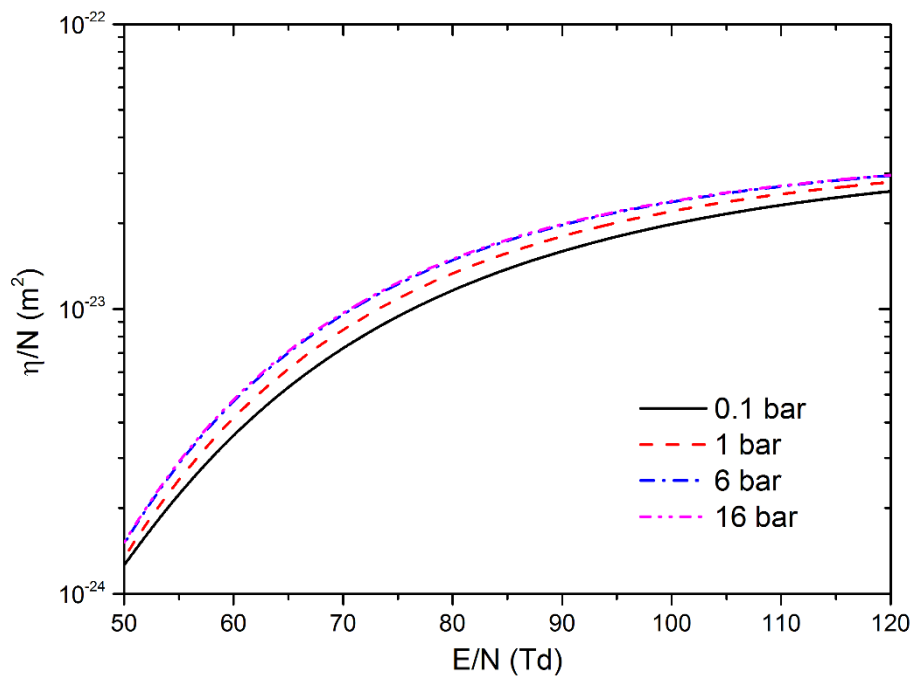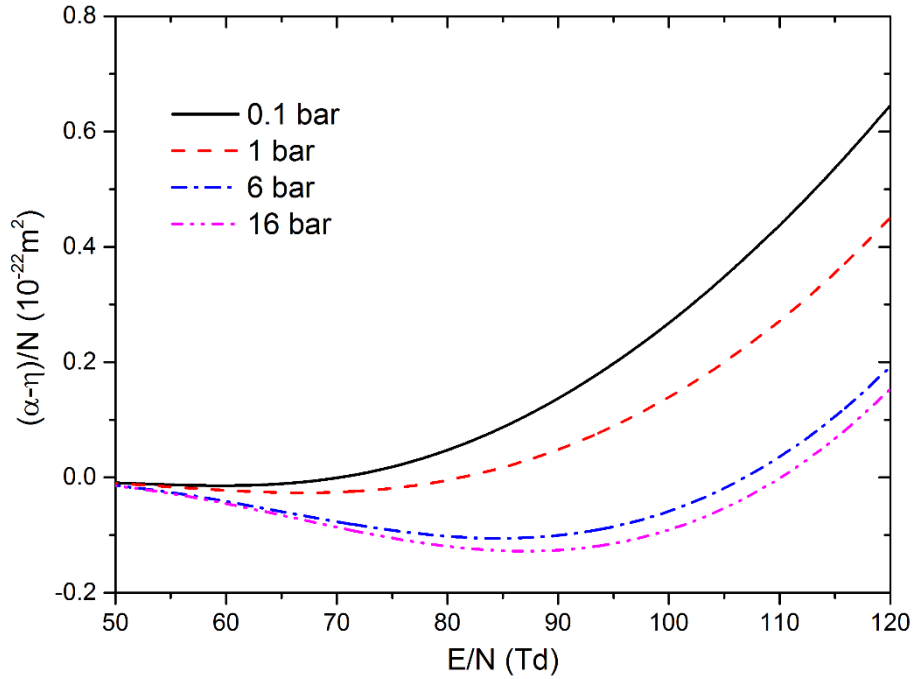
(b) η/N

113

(c) $(\alpha\text{-}\eta)/N$

Figure 5-9. α/N, η/N, and $(\alpha\text{-}\eta)/N$ of CO_2-N_2 (mixing ratio 7:3) mixtures contaminated by 1% Cu for various pressures as a function of E/N at temperature of 2000 K.

5.3.3 Reduced critical electric field strength

The reduced critical electric field strength $(E/N)_{cr}$ is determined when the ionization of mixtures is completely balanced by the electron attachment [43]. Figure 5-10 shows the $(E/N)_{cr}$ of CO_2-N_2 (mixing ratio 7:3) mixtures contaminated by different proportions of Cu as a function of temperature at ambient pressure.

As observed in Figure 5-10, the values of $(E/N)_{cr}$ are almost independent of copper proportion at temperatures below 1600 K because the compositions (CO_2, N_2, and condensed copper) are nearly constant. When the temperature increases above 1600 K, the values of $(E/N)_{cr}$ in CO_2-N_2-Cu mixtures is witnessed to drop firstly and then go up with temperature. This can be attributed to the evaporation of condensed copper and the dissociation of CO_2 as discussed for the ionization coefficients in Figure 5-6. Generally, increasing copper reduces the $(E/N)_{cr}$ of CO_2-N_2-Cu mixtures significantly

after the evaporation of condensed copper.
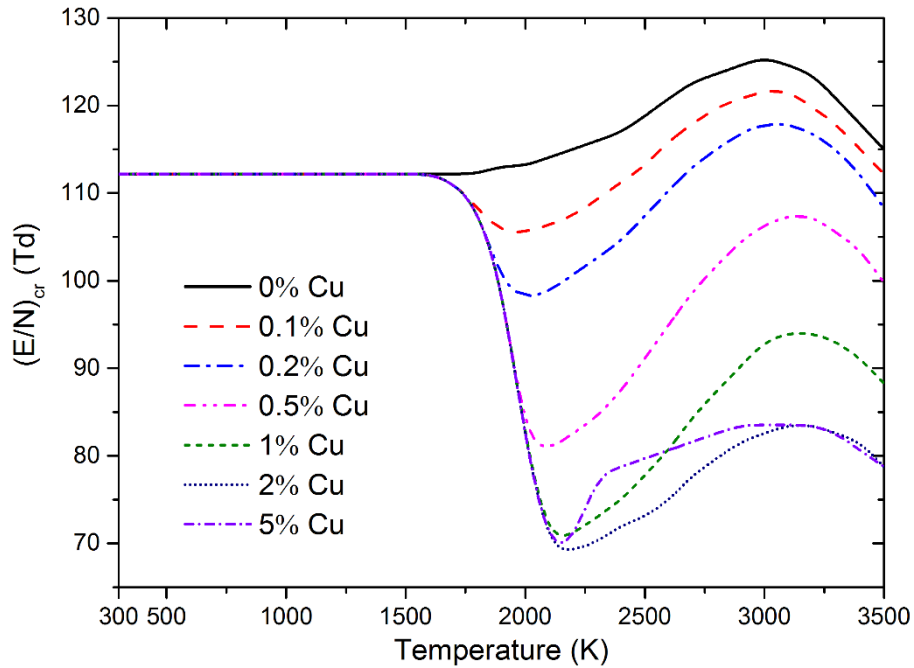
Figure 5-10. $(E/N)_{cr}$ of CO_2-N_2 (mixing ratio 7:3) mixtures contaminated by different proportions of Cu as a function of temperature at 1 bar.

The influence of the mixing ratio between CO_2 and N_2 on the $(E/N)_{cr}$ is described in Figure 5-11. The copper contamination and gas pressure are fixed to be 1% and 1 bar respectively in the calculation.

It is obvious that the addition of N_2 enhances the dielectric breakdown strength of CO_2-N_2-Cu mixtures at low temperatures but reduces it at high temperatures. The compositions of CO_2-N_2 mixtures can help us to understand this. At low temperatures, CO_2 and N_2 dominate the mixtures while at high temperatures CO and O_2 start to show their influences due to the dissociation of CO_2. Considering that N_2 has large excitation cross sections which provide energy dissipation channels to slow down electrons, the mixing of N_2 enhances the dielectric breakdown strength at low temperatures. However, the addition of N_2 also decreases the content of CO and O_2 which have better dielectric performance than CO_2. This addition therefore reduces the values of $(E/N)_{cr}$.
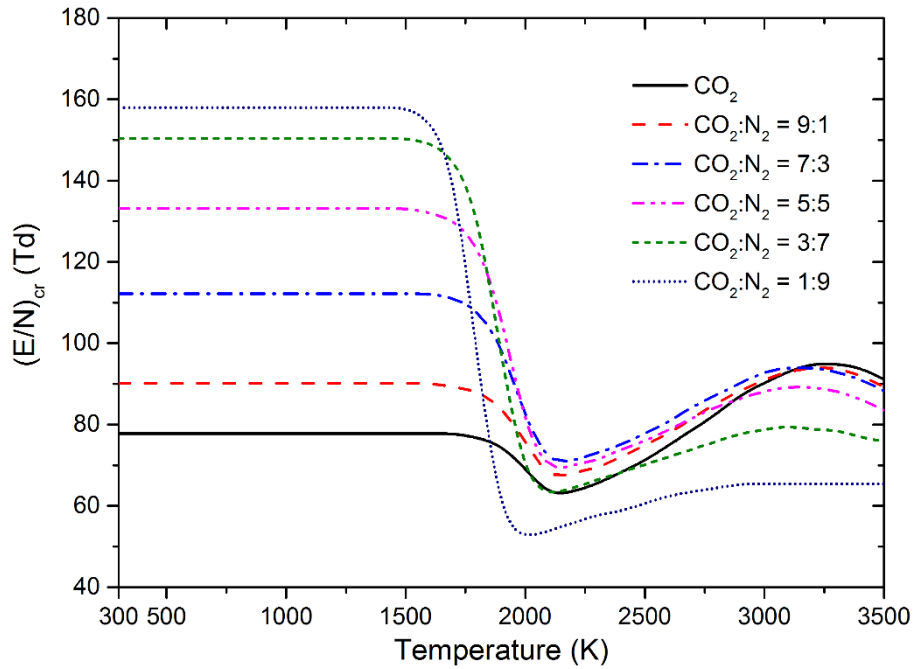
Figure 5-11. $(E/N)_{cr}$ of CO_2, N_2, and their different mixtures contaminated by 1% Cu as a function of temperature at 1 bar.

Figure 5-12 presents the $(E/N)_{cr}$ of CO_2-N_2 (mixing ratio 7:3) mixtures contaminated by 1% Cu as a function of temperature at different pressures of 0.1, 1, 6 and 16 bar.

It can be seen that the value of $(E/N)_{cr}$ is almost independent of pressure at temperatures below 1500 K because the decomposition of molecular species is so weak that the mole fractions of dominant particles (i.e. CO_2 and N_2) are almost constant in this temperature range. The similar result observed in SF_6-CO_2 and SF_6-Cu mixtures has been reported in our previous works [1, 43].

However, at high temperatures above 1500 K, increasing pressure can shift the curves of $(E/N)_{cr}$ right to higher temperatures. This can be attributed to the suppression of dissociation of molecular species because of the pressure compression. The influence of pressure on the values of $(\alpha-\eta)/N$ as shown in Figure 5-9 can also explain this qualitative feature.

116
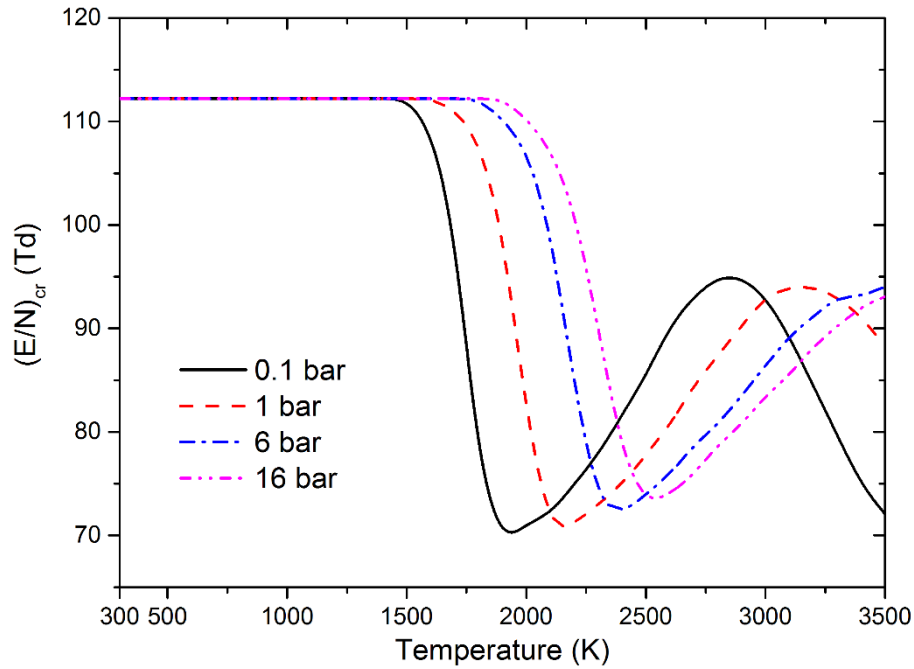
Figure 5-12. $(E/N)_{cr}$ of CO_2-N_2 (mixing ratio 7:3) mixtures contaminated by 1% Cu as a function of temperature at various pressures.

5.4 Comparison with SF_6-Cu mixtures

In order to investigate the difference of dielectric breakdown performance between SF_6 and CO_2-N_2 mixtures, we performed a calculation of dielectric breakdown properties of SF_6-Cu mixtures.

Figure 5-13 compares the results of $(E/N)_{cr}$ for CO_2-N_2-Cu and SF_6-Cu mixtures at ambient pressure. The mixing ratio of CO_2 and N_2 is set to be 7:3. The copper proportions in both mixtures are fixed to be 1%.

As obviously seen on the graph, the hot CO_2-N_2-Cu mixtures have much poorer dielectric strength than SF_6-Cu mixtures when the temperature is below 2000 K. However, at temperatures above 2000 K, the hot CO_2-N_2-Cu mixtures present better dielectric breakdown performance. This indicates that CO_2-N_2 mixtures are more suitable to be applied in medium-voltage circuit breakers rather than high-voltage circuit breakers.
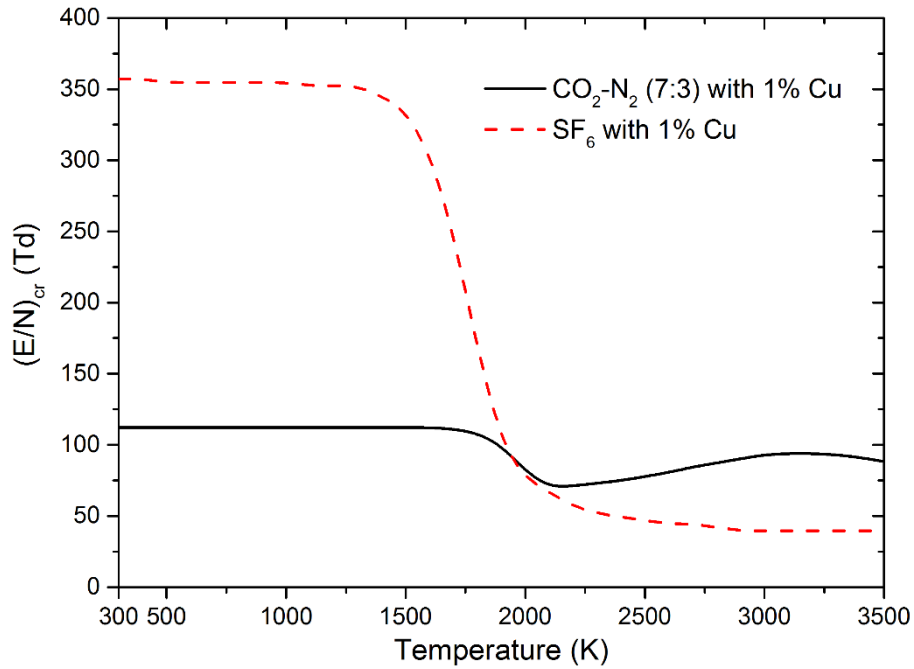
Figure 5-13. Comparison of $(E/N)_{cr}$ for CO_2-N_2 (mixing ratio 7:3) mixture and SF_6 gas contaminated by 1% copper at 1 bar

5.5 Summary

In this chapter, we perform the calculation of dielectric breakdown properties (including electron energy distribution function (EEDF), reduced ionization coefficient α/N, reduced electron attachment coefficient η/N, reduced effective ionization coefficient $(\alpha-\eta)/N$, and reduced critical electric field strength $(E/N)_{cr}$) in CO_2-N_2-Cu mixtures. The EEDF of the mixtures at a given reduced electric field is determined by solving the Boltzmann equation in a two-term approximation. The interactions, including elastic, excitation, ionization and attachment collisions, between electrons and neutral species are taken into account. The ionization cross sections of Cu_2 and CuO which are unavailable in literatures are calculated using the DM method. Based on the results of EEDF, the influences of temperatures, copper contamination, mixing ratio (CO_2:N_2), and gas pressure on the EEDF, α/N, η/N, $(\alpha-\eta)/N$ and $(E/N)_{cr}$ of CO_2-N_2-Cu mixtures are discussed.

Even small quantity of copper (e.g. 0.1% Cu) has a large effect on the dielectric

breakdown properties after the evaporation of condensed copper because of its low ionization potential. Generally, the copper vapour reduces the dielectric performance of gas mixtures.

The addition of N_2 also affects the dielectric breakdown performance of CO_2-N_2-Cu mixtures significantly, i.e. raising the $(E/N)_{cr}$ at low temperatures but reducing the $(E/N)_{cr}$ at high temperatures. This is because N_2, CO and O_2 have the higher dielectric strength than CO_2.

Increasing gas pressure suppresses the dissociation of molecules (e.g. CO_2, O_2 and N_2), resulting in the shift of $(E/N)_{cr}$ towards higher temperatures.

Compared with SF_6-Cu mixtures, CO_2-N_2-Cu mixtures have poorer dielectric strength below 2000 K but better dielectric performance from 2000 K to 3500 K.

CHAPTER 6 CONCLUSIONS AND FUTURE WORKS

6.1 Conclusions

CO_2, N_2 and their mixtures are potential alternatives to SF_6 which is a greenhouse gas designated by the Kyoto Protocol because of its extremely high global warming potential (GWP). What determines whether a gas can replace SF_6 in certain applications is its thermophysical and dielectric properties. In circuit breakers, a successful interruption requires that the arc quenching gas must have high specific heat and thermal conductivity to remove energy quickly from itself. Also, the high dielectric strength characterizes a good interrupting medium. Moreover, when the gas mixtures are applied as insulating and arc quenching medium in circuit breakers, the copper vapour resulting from the heating of electrode surfaces can modify the characteristics of arc plasmas, which have to be taken into account when setting up physical models. Therefore, this dissertation is devoted to the comprehensive investigation of the thermodynamic, transport, radiation, and dielectric breakdown properties of CO_2-N_2-Cu mixtures at temperatures of $300 - 30,000$ K and pressures of $0.1 - 16$ bar.

In Chapter 2, the equilibrium compositions and thermodynamic properties of CO_2-N_2-Cu mixtures with considering condensed species are calculated and discussed. It is found that copper condenses at temperatures below 3000 K and the concentration of other condensed species (e.g. graphite and solid CuO) is negligible. The phase transition of condensed copper inevitably affects the thermodynamic properties of CO_2-N_2-Cu mixtures, e.g. causing the specific heat to increase sharply and drop steeply. Copper also leads to the remarkable increase of mass density and the decease of specific enthalpy in the mixtures containing copper. For the specific heat, the copper contamination makes its three peaks diminish gradually. The three peaks correspond to the decomposition of O_2, dissociation of CO and N_2, and ionization of O and N respectively. Instead, the peaks due to the first and second ionization of copper are observed more and more clearly with the increase of copper proportion. The mixing

ratio between CO_2 and N_2 has a slight or even negligible effect on the mass density and specific enthalpy of the mixtures. For the specific heat, the peak values are affected by the mixing of N_2.

In Chapter 3, the transport coefficients and combined diffusion coefficients of CO_2-N_2-Cu mixtures are calculated based on the Chapman-Enskog theory. The newly developed Lennard-Jones like phenomenological model potential is adopted to describe the neutral-neutral and neutral-ion interactions in determining collision integrals. Due to the large mass, low ionization potential and large collision integrals of Cu-Cu pair, copper contamination shows remarkable effects on the transport and combined diffusion coefficients of CO_2-N_2-Cu mixtures. With the increase of copper, the viscosity and thermal conductivity are both reduced while the influence of copper on the electrical conductivity varies in three temperature ranges. Copper vapour also changes the number and position of peaks in thermal conductivity as it does in specific heat. For the combined diffusion coefficients, with the increase of copper, $\overline{D_{AB}^x}$ is raised sharply after it reaches the peak; $\overline{D_{AB}^E}$ shows the similar observation as electrical conductivity and should be discussed in three temperature ranges; $\overline{D_{AB}^T}$ and $\overline{D_{AB}^P}$ are generally raised when the copper proportion is below 90%, and reduced otherwise. Similar to the observation in specific heat, the copper evaporation at low temperatures also affects the thermal conductivity significantly, leading to a hump in thermal conductivity when the phase transition occurs. Moreover, increasing copper shifts the hump to a higher temperature. The mixing ratio of CO_2 and N_2 shows very slight effect on the electrical conductivity and viscosity. For thermal conductivity, the addition of N_2 diminishes the first peak gradually, changes the value of the second peak slightly, and reduces the third peak considerably.

In Chapter 4, the calculation and discussion for the net emission coefficients (NEC) of CO_2-N_2-Cu mixtures are presented with the consideration of atomic lines, atomic continuum, molecular bands, and molecular continuum. Due to the absorption of lines,

the NEC of an optically thin plasma ($R = 0$) is much larger than that of an optically thick plasma ($R > 0$). Copper contamination strongly raises the values of NEC after the condensed copper evaporates to gaseous species. The addition of N_2 shows a significant effect on the NEC of CO_2-N_2-Cu mixtures at low temperatures, whereas the influence arising from N_2 becomes slight at high temperatures. Increasing the gas pressure dramatically raises the NEC of gas mixtures.

In Chapter 5, the dielectric breakdown properties (including electron energy distribution function (EEDF), reduced ionization coefficient α/N, reduced electron attachment coefficient η/N, reduced effective ionization coefficient $(\alpha-\eta)/N$, and reduced critical electric field strength $(E/N)_{cr}$) of CO_2-N_2-Cu mixtures are calculated and discussed based on the two-term approximation of the Boltzmann equation. The ionization cross sections of Cu_2 and CuO which are unavailable in literatures are calculated using the DM method. It is found that even small quantity of copper (e.g. 0.1% Cu) has a large effect on dielectric breakdown properties after the evaporation of condensed copper. Generally, copper vapour reduces the dielectric performance of gas mixtures. The mixing of N_2 also affects the dielectric breakdown performance of CO_2-N_2-Cu mixtures significantly, i.e. raising the $(E/N)_{cr}$ at low temperatures but reducing the $(E/N)_{cr}$ at high temperatures. Increasing gas pressure suppresses the dissociation of molecules (e.g. CO_2, O_2 and N_2), resulting in the shift of $(E/N)_{cr}$ towards higher temperatures.

Compared with SF_6-Cu mixtures, CO_2-N_2-Cu mixtures present much different thermophysical, radiation, and dielectric breakdown properties. As an arc quenching gas, CO_2-N_2-Cu mixtures have lower $\rho \cdot C_p$ and thermal conductivity at low temperatures but present higher $\rho \cdot C_p$, thermal conductivity, and NEC in the medium temperature range. As an insulating medium, the hot CO_2-N_2-Cu mixtures have much poorer dielectric strength below 2000 K, whereas from 2000 K to 3500 K, they present better dielectric breakdown performance than SF_6-Cu mixtures.

6.2 Future works

This work is conducted under the assumption of local thermodynamic equilibrium (LTE) which means electron temperature (T_e) in thermal plasmas equals the temperature of heavy particles (T_h). However, the departure from thermal equilibrium arises when large temperature gradient exists (e.g. near the cold walls) and when electron concentration is not high enough to allow sufficient transfer of energy between electrons and heavy particles [186, 187], which results in the different values of T_e and T_h. To solve the problems where LTE is not valid, Devoto [132] derived the transport coefficients of two-temperature (2T) plasma mixtures assuming a complete decoupling between electrons and heavy particles. Rat et al. [188, 189] took the coupling into account and developed an improved 2T theory which can be applied in the calculation of combined diffusion coefficients. Using the above 2T plasma model, Colombo et al. [190, 191], Ghorui et al. [192] and Wang et al. [193] investigated the 2T compositions, thermodynamic, and/or transport properties of N_2 plasma, and Colombo et al. [186] studied the 2T properties of CO_2 plasma. However, no corresponding results for CO_2-N_2 plasma and CO_2-N_2-Cu plasma have been published. Therefore, the future work could focus on the 2T properties of CO_2-N_2-Cu plasmas, which will help us to understand this SF_6 replacement more deeply.

According to the discussion in the previous chapters, the condensed species show non-negligible effects on the thermodynamic and transport properties of plasmas at relatively low temperatures. The solid phases in form of powder also lower the dielectric performance of gas mixtures. However, the most simulation works, such as the modelling of electric arc in circuit breakers, used the thermophysical properties calculated without consideration of condensed phases. This is because it is very difficult to take condensed species into account in the modelling of thermal plasmas as they are not just a single-phase flow. The future work could contribute to the modelling of thermal plasmas as a multi-phase flow with consideration of condensed phases.

A suitable and environmentally sustainable replacement of SF_6 should have high

dielectric strength, good arc quenching capability, low boiling point, and low GWP. However, all the previous candidates display a deficiency in one category or another. Recently a specific compound, namely heptafluoro-iso-butyronitrile $(CF_3)_2$-CF-CN, was developed commercially available under the designation of 3M™ Novec™ 4710 Dielectric Fluid. It is the first material to combine all the required properties into one compound. The thermophysical properties of this new compound is still unknown when used as arc quenching medium, which also could be investigated in the future.

A. Comparison with literature data

In order to validate the calculation procedures for the thermodynamic, transport, radiation, and dielectric breakdown properties, the comparison between the present results and the literature data for the CO_2 plasma is presented as follows. It should be noted that the condensed species were not considered in the following calculation so as to be consistent with the setting in the literature.

The mass density, specific enthalpy, specific heat at constant pressure, electrical conductivity, viscosity, thermal conductivity, net emission coefficient, and effective ionization coefficient of CO_2 plasma at ambient pressure are illustrated from Figure A-1 to Figure A-8 respectively. Generally, the good and reasonable agreement is observed in these figures, proving that the calculation is valid. The disagreement in some plots can be attributed to the different data source used in the calculation.
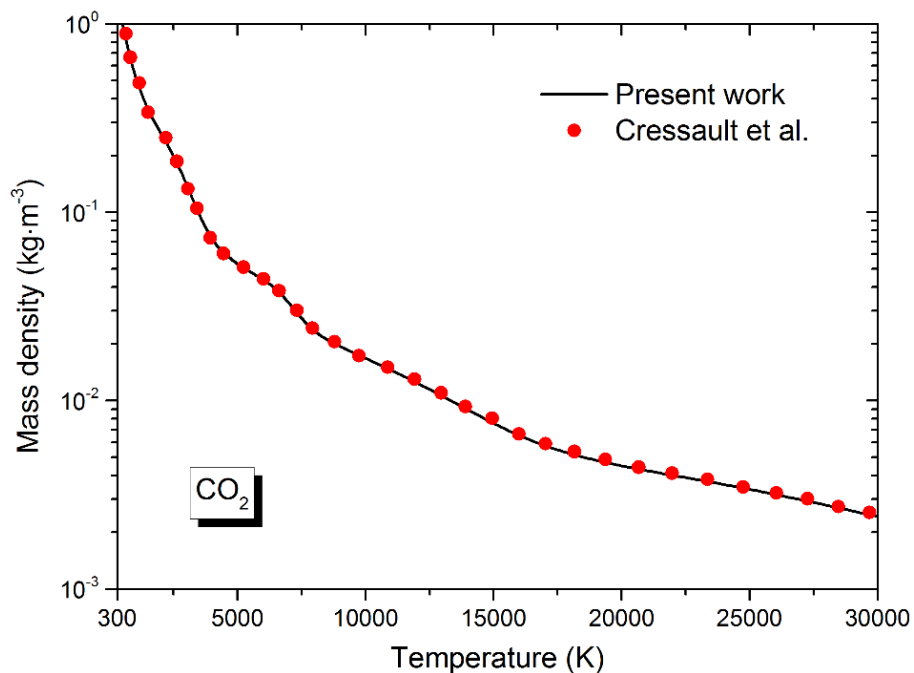
Figure A-1. Mass density of CO_2 plasma at 1 bar with comparison to the work by Cressault et al. [19]

125
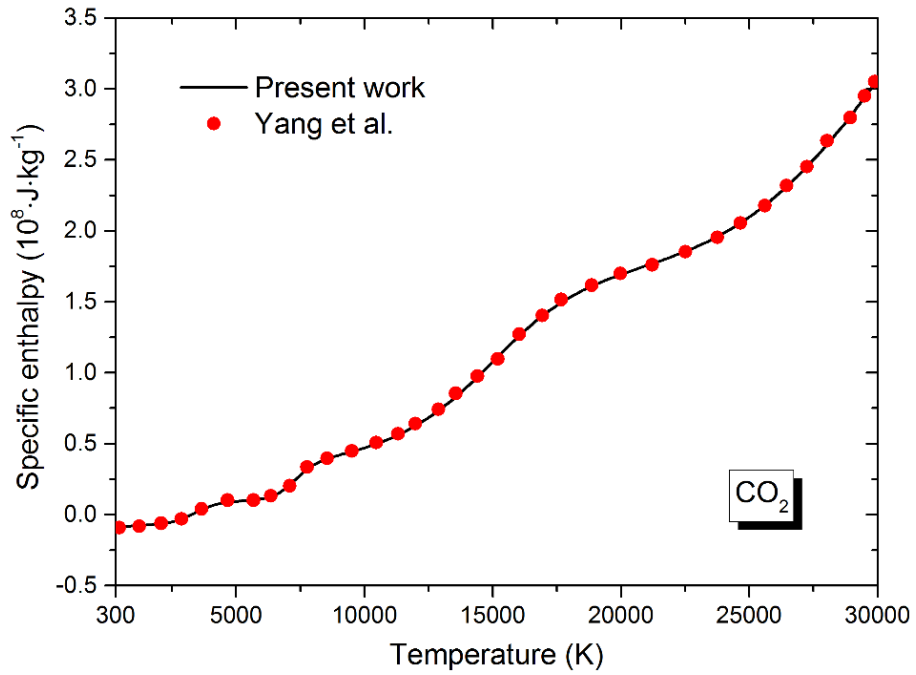
Figure A-2. Specific enthalpy of CO_2 plasma at 1 bar with comparison to the work by

Yang et al. [153]
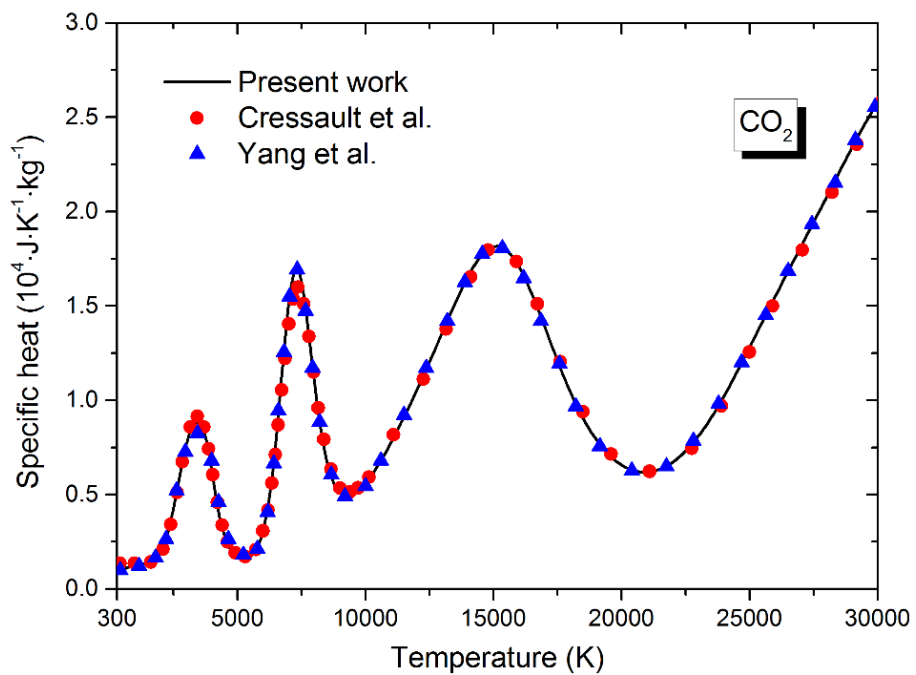
Figure A-3. Specific heat of CO_2 plasma at 1 bar with comparison to the works by

Cressault et al. [19] and Yang et al. [153]
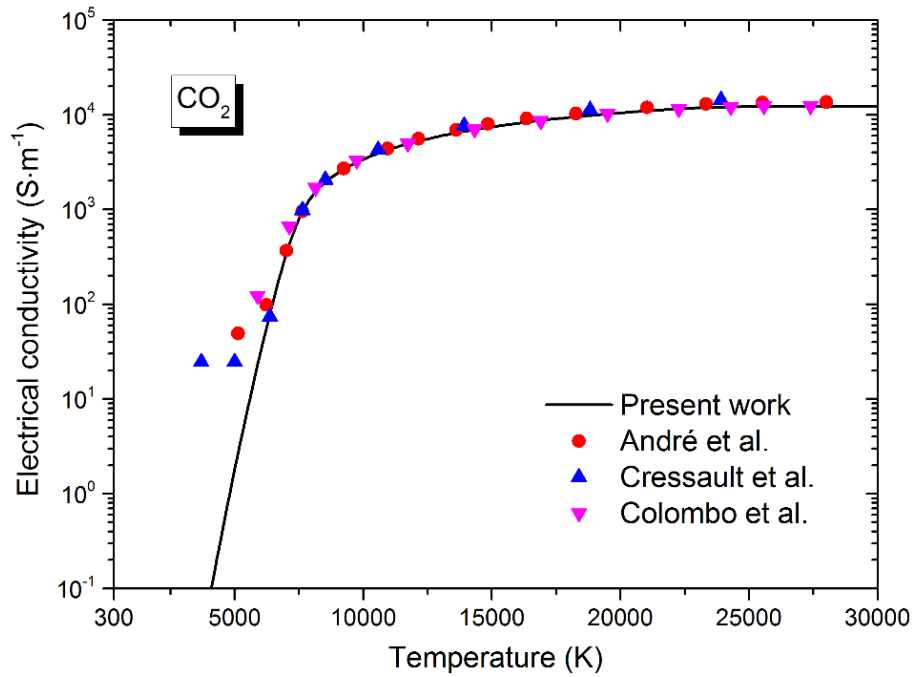
Figure A-4. Electrical conductivity of CO_2 plasma at 1 bar with comparison to the works by André et al. [148], Cressault et al. [19], and Colombo et al. [186]
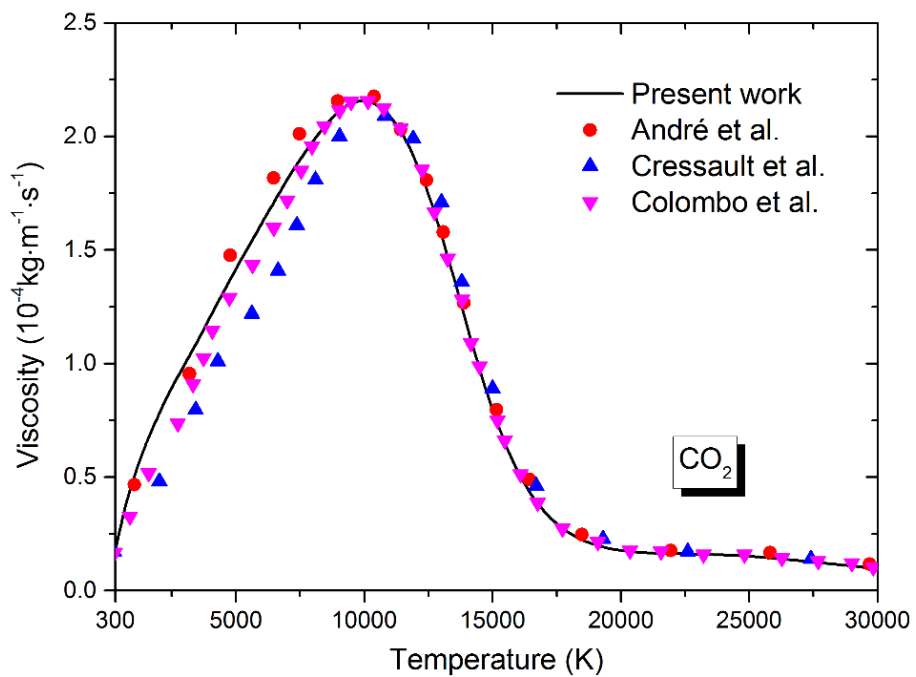
Figure A-5. Viscosity of CO_2 plasma at 1 bar with comparison to the works by André et al. [148], Cressault et al. [19], and Colombo et al. [186]
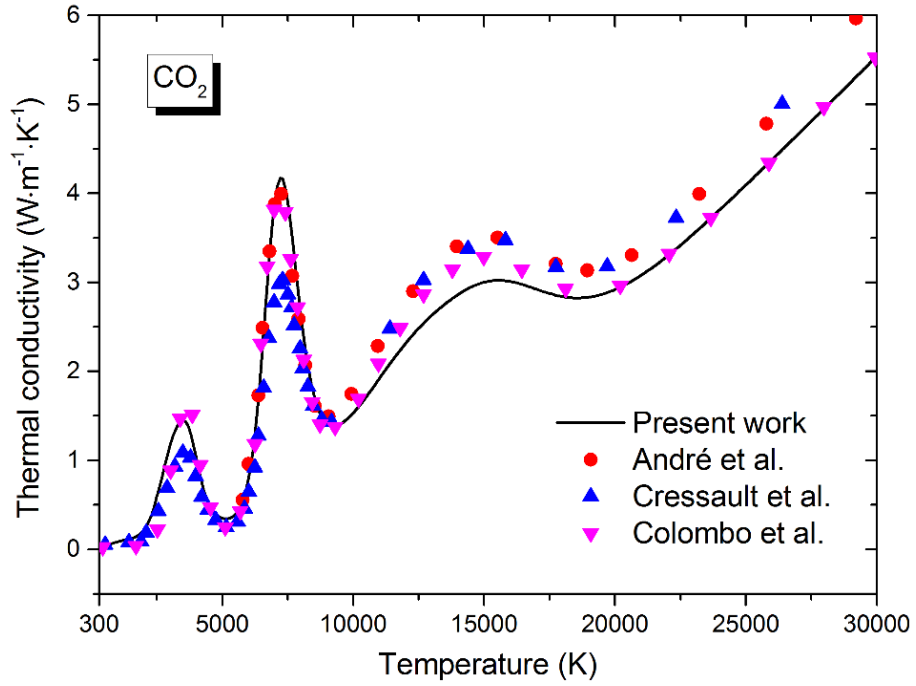
Figure A-6. Thermal conductivity of CO_2 plasma at 1 bar with comparison to the works by André et al. [148], Cressault et al. [19], and Colombo et al. [186]
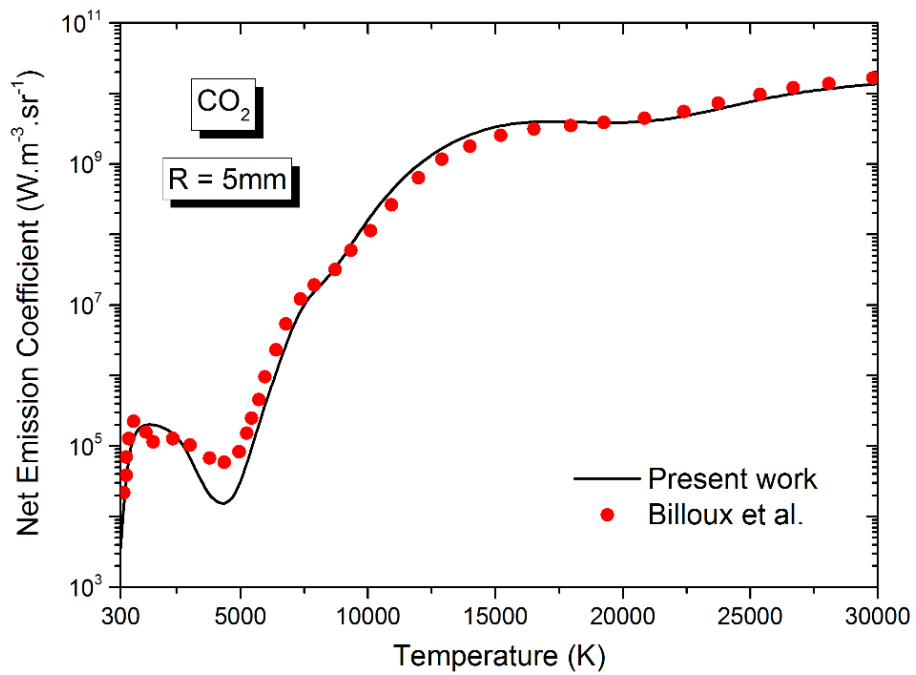
Figure A-7. Net emission coefficient of CO_2 plasma at 1 bar with comparison to the works by Billoux et al. [82]
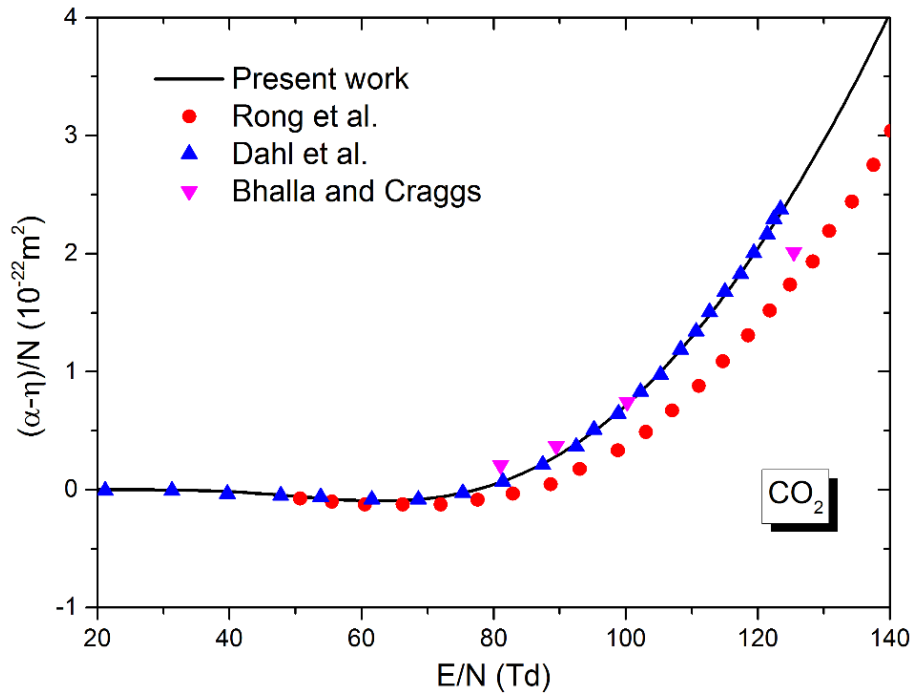
Figure A-8. Effective ionization coefficient of CO_2 gas as a function of E/N at room temperature and ambient pressure with comparison to the works by Rong et al. [105], Dahl et al. [194], and Bhalla and Creggs [195]

REFERENCES

[1]   L. Zhong, A. Yang, X. Wang, D. Liu, Y. Wu and M. Rong, *Phys. Plasmas* **21** (5), 053506 (2014).

[2]   X. Wang, L. Zhong, J. Yan, A. Yang, G. Han, G. Han, Y. Wu and M. Rong, *Eur. Phys. J. D* **69** (10) (2015).

[3]   F. Chu, *IEEE Transactions on Electrical Insulation* (5), 693-725 (1986).

[4]   M. Marland, ENG4111/4112 Dissertation, University of Southern Queensland, 2014.

[5]   M. Pinheiro and J. Loureiro, *J. Phys. D: Appl. Phys.* **35** (23), 3077 (2002).

[6]   Y. Qiu, Y. Liu, A. Sun and E. Kuffel, *J. Phys. D: Appl. Phys.* **21** (1), 208 (1988).

[7]   L. Laska, K. Mašek, J. Krasa and V. Peřina, *Czechoslovak Journal of Physics B* **34** (10), 1038-1047 (1984).

[8]   X. Li, H. Zhao and S. Jia, *J. Phys. D: Appl. Phys.* **45** (44), 445202 (2012).

[9]   A. Gleizes, B. Rahmani, J. Gonzalez and B. Liani, *J. Phys. D: Appl. Phys.* **24** (8), 1300 (1991).

[10]   A. Gleizes, I. Sakalis, M. Razafinimanana and S. Vacquie, *J. Appl. Phys.* **61** (2), 510 (1987).

[11]   J. Hern ández-Ávila, E. Basurto and J. De Urquijo, *J. Phys. D: Appl. Phys.* **35** (18), 2264 (2002).

[12]   W. Wang, M. Rong, Y. Wu and J. D. Yan, *J. Phys. D: Appl. Phys.* **47** (25), 255201 (2014).

[13]   W. Wang, A. B. Murphy, M. Rong, H. M. Looe and J. W. Spencer, *J. Appl. Phys.* **114** (10), 103301 (2013).

[14]   X. Li, H. Zhao, S. Jia and A. B. Murphy, *J. Appl. Phys.* **114** (5), 053302 (2013).

[15]   W. Wang, X. Tu, D. Mei and M. Rong, *Phys. Plasmas* **20** (11), 113503 (2013).

[16]   W. Wang, M. Rong and Y. Wu, *Plasma Chemistry and Plasma Processing* **34** (4), 899-916 (2014).

[17] Y. Wu, W. Wang, M. Rong, L. Zhong, J. Spencer and J. Yan, *IEEE Trans. Dielectr. Electr. Insul.* **21** (1), 129-137 (2014).

[18] H. Kasuya, Y. Kawamura, H. Mizoguchi, Y. Nakamura, S. Yanabu and N. Nagasaki, *IEEE Trans. Dielectr. Electr. Insul.* **17** (4), 1196-1203 (2010).

[19] Y. Cressault, V. Connord, H. Hingana, P. Teulet and A. Gleizes, *J. Phys. D: Appl. Phys.* **44** (49), 495202 (2011).

[20] Y. Yokomizu, R. Ochiai and T. Matsumura, *J. Phys. D: Appl. Phys.* **42** (21), 215204 (2009).

[21] Y. Yokomizu, M. Suzuki and T. Matsumura, *IEEJ Transactions on Electrical and Electronic Engineering* **1** (3), 268-275 (2006).

[22] X. Zhang, S. Xiao, Y. Han and Y. Cressault, *Appl. Phys. Lett.* **108** (9), 092901 (2016).

[23] M. Hikita, S. Ohtsuka, S. Okabe and G. Ueta, *IEEE Trans. Dielectr. Electr. Insul.* **16** (5), 1413-1419 (2009).

[24] M. Koch and C. M. Franck, *J. Phys. D: Appl. Phys.* **47** (40), 405203 (2014).

[25] O. Yamamoto, T. Takuma, S. Hamada, Y. Yamakawa and M. Yashima, *IEEE Trans. Dielectr. Electr. Insul.* **8** (6), 1075-1081 (2001).

[26] B.-T. Wu, D.-M. Xiao, Z.-S. Liu, L.-C. Zhang and X.-L. Liu, *J. Phys. D: Appl. Phys.* **39** (19), 4204-4207 (2006).

[27] J. Mantilla, N. Gariboldi, S. Grob and M. Claessens, *Investigation of the insulation performance of a new gas mixture with extremely low GWP*, 2014 IEEE Electrical Insulation Conference (EIC), (Philadelphia, Pennsylvania, USA, 2014).

[28] P. Simka and N. Ranjan, *Dielectric Strength of C5 Perfluoroketone*, The 19th International Symposium on High Voltage Engineering, (Pilsen, Czech Republic, 2015).

[29] M. Saxegaard, M. Kristoffersen, P. Stoller, M. Seeger, M. Hyrenbach and H. Landsverk, *Dielectric Properties of Gases Suitable for Secondary Medium*

Voltage Switchgear, 23rd International Conference on Electricity Distribution, (Lyon, France, 2015).

[30] L. G. Christophorou, J. K. Olthoff and D. S. Green, *Gases for electrical insulation and arc interruption: possible present and future alternatives to pure SF₆.* (US Department of Commerce, Technology Administration, National Institute of Standards and Technology, 1997).

[31] *Gaseous Dielectrics, X*, Proceedings of the Tenth International Symposium on Gaseous Dielectrics, (Athens, Greece, 2004).

[32] K. Brand, *IEEE Transactions on Electrical Insulation* (5), 451-456 (1982).

[33] L. G. Christophorou, J. K. Olthoff and M. V. V. S. Rao, *Journal of Physical and Chemical Reference Data* **25** (5), 1341 (1996).

[34] S. Ohtsuka, S. Nagara, M. Koumura, Y. Hashimoto, M. Nakamura and M. Hikita, *Electrical Engineering in Japan* **140** (3), 34-43 (2002).

[35] P. C. Stoller, M. Seeger, A. A. Iordanidis and G. V. Naidis, *IEEE Transactions on Plasma Science* **41** (8), 2359-2369 (2013).

[36] J. L. Zhang, J. D. Yan and M. T. Fang, *IEEE Trans. Plasma Sci.* **32** (3), 1352-1361 (2004).

[37] M. Rong, L. Zhong, Y. Cressault, A. Gleizes, X. Wang, F. Chen and H. Zheng, *J. Phys. D: Appl. Phys.* **47** (49), 495202 (2014).

[38] B. Chervy, A. Gleizes and M. Razafinimanana, *J. Phys. D: Appl. Phys.* **27** (6), 1193 (1994).

[39] K. Paul, T. Sakuta, T. Takashima and M. Ishikawa, *J. Phys. D: Appl. Phys.* **30** (1), 103 (1997).

[40] X. Wang, L. Zhong, Y. Cressault, A. Gleizes and M. Rong, *J. Phys. D: Appl. Phys.* **47** (49), 495201 (2014).

[41] L. Zhong, X. Wang, M. Rong, Y. Wu and A. B. Murphy, *Phys. Plasmas* **21** (10), 103506 (2014).

[42] Y. Cressault and A. Gleizes, *J. Phys. D: Appl. Phys.* **43** (43), 434006 (2010).

[43] X. Wang, L. Zhong, M. Rong, A. Yang, D. Liu, Y. Wu and S. Miao, *J. Phys. D: Appl. Phys.* **48** (15), 155205 (2015).

[44] Y. Tanaka, *IEEE Trans. Dielectr. Electr. Insul.* **12** (3), 504-512 (2005).

[45] A. B. Murphy, *J. Phys. D: Appl. Phys.* **43** (43), 434001 (2010).

[46] J.-C. Lee and Y. J. Kim, *Vacuum* **81** (7), 875-882 (2007).

[47] V. K. Liau, B. Y. Lee, K. D. Song and K. Y. Park, *J. Phys. D: Appl. Phys.* **39** (10), 2114-2123 (2006).

[48] J. M. Yos, *Transport properties of nitrogen, hydrogen, oxygen, and air to 30,000 K* Report No. RAD-TM-63-7, 1963.

[49] M. Capitelli, *Physics of Fluids* **16** (11), 1835 (1973).

[50] A. B. Murphy and C. Arundelli, *Plasma Chemistry and Plasma Processing* **14** (4), 451-490 (1994).

[51] J. S. Lee and P. J. Bobbitt, *Transport properties at high temperatures of CO2-N2-O2-Ar gas mixtures for planetary entry applications*. (National Aeronautics and Space Administration, 1969).

[52] G. N. Freeman and C. C. Oliver, *AIAA Journal* **8** (9), 1687-1693 (1970).

[53] G. Romanov, Y. A. Stankevich, L. Stanchits and K. Stepanov, *Journal of Engineering Physics and Thermophysics* **68** (2), 255-268 (1995).

[54] M. Capitelli, D. Cappelletti, G. Colonna, C. Gorse, A. Laricchiuta, G. Liuti, S. Longo and F. Pirani, *Chemical Physics* **338** (1), 62-68 (2007).

[55] A. Laricchiuta, D. Bruno, M. Capitelli, C. Catalfamo, R. Celiberto, G. Colonna, P. Diomede, D. Giordano, C. Gorse, S. Longo, D. Pagano and F. Pirani, *The European Physical Journal D* **54** (3), 607-612 (2009).

[56] C. Catalfamo, D. Bruno, G. Colonna, A. Laricchiuta and M. Capitelli, *The European Physical Journal D* **54** (3), 613-621 (2009).

[57] P. Shayler and M. Fang, *J. Phys. D: Appl. Phys.* **10** (12), 1659 (1977).

[58] A. Yang, Y. Liu, L. Zhong, X. Wang, C. Niu, M. Rong, G. Han, Y. Zhang, Y. Lu and Y. Wu, *Plasma Chemistry and Plasma Processing* **36** (4), 1141-1160 (2016).

[59] A. B. Murphy, *The Journal of Chemical Physics* **99** (2), 1340 (1993).

[60] A. B. Murphy, *Physical Review E* **48** (5), 3594-3603 (1993).

[61] A. B. Murphy, *Phys Rev Lett* **73** (13), 1797-1800 (1994).

[62] A. B. Murphy, *J. Phys. D: Appl. Phys.* **29** (7), 1922 (1996).

[63] A. B. Murphy, *J. Phys. D: Appl. Phys.* **31** (23), 3383 (1998).

[64] A. B. Murphy, *Scientific Report* **4**, 4304 (2014).

[65] J. Hu and H. L. Tsai, *International Journal of Heat and Mass Transfer* **50** (5-6), 833-846 (2007).

[66] F. Yang, M. Rong, Y. Wu, A. B. Murphy, J. Pei, L. Wang, Z. Liu and Y. Liu, *J. Phys. D: Appl. Phys.* **43** (43), 434011 (2010).

[67] M. Rong, Q. Ma, Y. Wu, T. Xu and A. B. Murphy, *J. Appl. Phys.* **106** (2), 023308 (2009).

[68] A. Gleizes, J. Gonzalez, B. Liani and G. Raynal, *J. Phys. D: Appl. Phys.* **26** (11), 1921 (1993).

[69] C. M. Dixon, J. D. Yan and M. T. C. Fang, *J. Phys. D: Appl. Phys.* **37** (23), 3309-3318 (2004).

[70] J. Lowke, *Journal of Quantitative Spectroscopy and Radiative Transfer* **14** (2), 111-122 (1974).

[71] J. Zhang, M. Fang and D. Newland, *J. Phys. D: Appl. Phys.* **20** (3), 368 (1987).

[72] S. Eby, J. Trepanier and X. Zhang, *J. Phys. D: Appl. Phys.* **31** (13), 1578 (1998).

[73] V. Sevast'yanenko, *Journal of Engineering Physics and Thermophysics* **36** (2), 138-148 (1979).

[74] V. Aubrecht and J. Lowke, *J. Phys. D: Appl. Phys.* **27** (10), 2066 (1994).

[75] R. Liebermann and J. Lowke, *Journal of Quantitative Spectroscopy and Radiative Transfer* **16** (3), 253-264 (1976).

[76] A. Gleizes, M. Gongassian and B. Rahmani, *J. Phys. D: Appl. Phys.* **22** (1), 83 (1989).

[77] B. Liani, M. Rahmouni, A. Belbachir, H. Riad and A. Gleizes, *J. Phys. D: Appl.*

Phys. **30** (21), 2964 (1997).

[78] Y. Naghizadeh-Kashani, Y. Cressault and A. Gleizes, *J. Phys. D: Appl. Phys.* **35** (22), 2925 (2002).

[79] Y. Cressault, M. E. Rouffet, A. Gleizes and E. Meillot, *J. Phys. D: Appl. Phys.* **43** (33), 335204 (2010).

[80] A. Gleizes, Y. Cressault and P. Teulet, *Plasma Sources Science and Technology* **19** (5), 055013 (2010).

[81] H. Z. Randrianandraina, Y. Cressault and A. Gleizes, *J. Phys. D: Appl. Phys.* **44** (19), 194012 (2011).

[82] T. Billoux, Y. Cressault, V. F. Boretskij, A. N. Veklich and A. Gleizes, *Journal of Physics: Conference Series* **406**, 012027 (2012).

[83] T. Billoux, Y. Cressault, P. Teulet and A. Gleizes, *Journal of Physics: Conference Series* **406**, 012010 (2012).

[84] Y. Cressault, A. Gleizes and G. Riquel, *J. Phys. D: Appl. Phys.* **45** (26), 265202 (2012).

[85] Y. Cressault and A. Gleizes, *J. Phys. D: Appl. Phys.* **46** (41), 415206 (2013).

[86] C. Jan, Y. Cressault, A. Gleizes and K. Bousoltane, *J. Phys. D: Appl. Phys.* **47** (1), 015204 (2014).

[87] Y. Cressault and A. Gleizes, *High Temperature Material Processes: An International Quarterly of High-Technology Plasma Processes* **10** (1) (2006).

[88] D. Vacher, M. Lino da Silva, P. André, G. Faure and M. Dudeck, *Plasma Sources Science and Technology* **17** (3), 035012 (2008).

[89] M. Lino da Silva, D. Vacher, M. Dudeck, P. André and G. Faure, *Plasma Sources Science and Technology* **17** (3), 035013 (2008).

[90] J. Menart and S. Malik, *J. Phys. D: Appl. Phys.* **35** (9), 867 (2002).

[91] V. Aubrecht, M. Bartlova and O. Coufal, *J. Phys. D: Appl. Phys.* **43** (43), 434007 (2010).

[92] Y. Tanaka, *J. Phys. D: Appl. Phys.* **37** (6), 851-859 (2004).

[93] J. Yan, M. Fang and Q. Liu, *IEEE Trans. Dielectr. Electr. Insul.* **4** (1), 114-119 (1997).

[94] G. Cliteur, Y. Hayashi, E. Haginomori and K. Suzuki, *IEEE Trans. Dielectr. Electr. Insul.* **5** (6), 843-849 (1998).

[95] M. Yousfi, P. Robin-Jouan and Z. Kanzari, *IEEE Trans. Dielectr. Electr. Insul.* **12** (6), 1192-1200 (2005).

[96] L. Rothhardt, J. Mastovsky and J. Blaha, *J. Phys. D: Appl. Phys.* **14** (12), L215 (1981).

[97] L. Rothhardt, J. Mastovsky and J. Blaha, *J. Phys. D: Appl. Phys.* **18** (10), L155 (1985).

[98] A. E. Dubinov, V. Letyagin, K. E. Mikheev, B. G. Ptitsyn, S. A. Sadovoi and V. D. Selemir, *High Temperature* **39** (1), 31-36 (2001).

[99] A. E. Dubinov, V. Letyagin, K. E. Mikheev, B. G. Ptitsyn, S. A. Sadovoi and V. D. Selemir, *High Temperature* **39** (2), 205-208 (2001).

[100] A. E. Dubinov, V. Letyagin, K. E. Mikheev, B. G. Ptitsyn, S. A. Sadovoi and V. D. Selemir, *High Temperature* **39** (3), 338-341 (2001).

[101] Y. Ohmori, M. Shimozuma and H. Tagashira, *J. Phys. D: Appl. Phys.* **21** (5), 724 (1988).

[102] D. M. Xiao, X. G. Li and X. Xu, *J. Phys. D: Appl. Phys.* **34** (24), L133 (2001).

[103] D.-M. Xiao, X. Xu and J.-L. Yang, *Japanese Journal of Applied Physics* **43** (2), 703-704 (2004).

[104] M. Yousfi, J. de Urquijo, A. Juarez, E. Basurto and J. L. Hernandez-Avila, *IEEE Trans. Plasma Sci.* **37** (6), 764-772 (2009).

[105] M. Rong, H. Sun, F. Yang, Y. Wu, Z. Chen, X. Wang and M. Wu, *Phys. Plasmas* **21** (11), 112117 (2014).

[106] X. Li, X. Guo, H. Zhao, S. Jia and A. B. Murphy, *J. Appl. Phys.* **117** (14), 143302 (2015).

[107] A. Gleizes, J. J. Gonzalez and P. Freton, *J. Phys. D: Appl. Phys.* **38** (9), R153-

R183 (2005).

[108] M. I. Boulos, P. Fauchais and E. Pfender, *Thermal Plasmas: Fundamentals and Applications*. (Springer Science & Business Media, 1994).

[109] O. Coufal and O. Živný, *The European Physical Journal D* **61** (1), 131-151 (2011).

[110] S. Gordon and B. J. McBride, *Computer program for calculation of complex chemical equilibrium compositions and applications. Part 1: Analysis*. (NASA Reference Publication, 1994).

[111] B. J. McBride, M. J. Zehe and S. Gordon, *NASA Glenn coefficients for calculating thermodynamic properties of individual species* Report No. NASA/TP—2002-211556, 2002.

[112] M. Capitelli, G. Colonna and A. D'Angola, *Fundamental Aspects of Plasma Chemical Physics: Thermodynamics*. (Springer Science & Business Media, 2011).

[113] W. Wang, M. Rong, A. B. Murphy, Y. Wu, J. W. Spencer, J. D. Yan and M. T. C. Fang, *J. Phys. D: Appl. Phys.* **44** (35), 355207 (2011).

[114] W. Wang, M. Rong and J. W. Spencer, *Phys. Plasmas* **20** (11), 113504 (2013).

[115] G. D'Ammando, G. Colonna and M. Capitelli, *Phys. Plasmas* **20** (3), 032108 (2013).

[116] K. S. Drellishak, D. P. Aeschliman and A. B. Cambel, *Physics of Fluids* **8** (9), 1590 (1965).

[117] D. McQuarrie and J. Simon, *Physical Chemistry: A Molecular Approach*. (University Science Books, 1997).

[118] Y. Wu, Z. Chen, F. Yang, Y. Cressault, A. B. Murphy, A. Guo, Z. Liu, M. Rong and H. Sun, *J. Phys. D: Appl. Phys.* **48** (41), 415205 (2015).

[119] A. Kramida, Y. Ralchenko, J. Reader and NIST ASD Team. NIST Atomic Spectra Database (version 5.3) [Online]. Available: http://physics.nist.gov/asd

[120] J. Malcolm W. Chase, *NIST-JANAF Thermochemical Tables (Fourth Edition)*. (American Chemical Society and American Institute of Physics, 1998).

[121] T. L. Cottrell, *The strengths of chemical bonds*. (Academic Press, 1958).

[122] W. Z. Wang, A. B. Murphy, J. D. Yan, M. Z. Rong, J. W. Spencer and M. T. C. Fang, *Plasma Chemistry and Plasma Processing* **32** (1), 75-96 (2012).

[123] S. Gordon and B. J. McBride, *Thermodynamic data to 20,000 K for monatomic gases*. (NASA, 1999).

[124] R. S. Devoto, *Physics of Fluids* **16** (5), 616 (1973).

[125] A. B. Murphy, *Plasma Chemistry and Plasma Processing* **20** (3), 279-297 (2000).

[126] A. Gleizes, M. Mitiche and P. Van Doan, *IEEE Trans. Plasma Sci.* **19** (1), 12-19 (1991).

[127] M. Capitelli, D. Bruno and A. Laricchiuta, *Transport* **74** (2013).

[128] W. Wang, J. D. Yan, M. Rong, A. B. Murphy and J. W. Spencer, *Plasma Chemistry and Plasma Processing* **32** (3), 495-518 (2012).

[129] M. Capitelli, G. Colonna, C. Gorse and A. d'Angola, *The European Physical Journal D-Atomic, Molecular, Optical and Plasma Physics* **11** (2), 279-289 (2000).

[130] Y. Cressault and A. Gleizes, *J. Phys. D: Appl. Phys.* **37** (4), 560-572 (2004).

[131] P. André, W. Bussière and D. Rochette, *Plasma Chemistry and Plasma Processing* **27** (4), 381-403 (2007).

[132] R. S. Devoto, *Physics of Fluids* **10** (10), 2105 (1967).

[133] J. N. Butler and R. S. Brokaw, *The Journal of Chemical Physics* **26** (6), 1636 (1957).

[134] M. Capitelli, R. Celiberto, G. Colonna, F. Esposito, C. Gorse, K. Hassouni, A. Laricchiuta and S. Longo, *Fundamental Aspects of Plasma Chemical Physics: Kinetics*. (Springer Science & Business Media, 2015).

[135] S. Chapman and T. G. Cowling, *The Mathematical Theory of Non-Uniform Gases: an Account of the Kinetic Theory of Viscosity, Thermal Conduction and Diffusion in Gases*. (Cambridge University Press, Cambridge, 1970).

[136] R. S. Devoto, *J. Plasma Phys* **2**, 617-631 (1968).

[137] F. J. Smith and R. J. Munn, *The Journal of Chemical Physics* **41** (11), 3560 (1964).

[138] P. D. Neufeld, A. Janzen and R. Aziz, *The Journal of Chemical Physics* **57** (3), 1100-1102 (1972).

[139] L. Monchick, *Physics of Fluids* **2** (6), 695 (1959).

[140] J. C. Rainwater, *The Journal of Chemical Physics* **77** (1), 434 (1982).

[141] A. D. S. Mesa, C. Quesne and Y. F. Smirnov, *Journal of Physics A: Mathematical and General* **31** (1), 321 (1998).

[142] A. Laricchiuta, G. Colonna, D. Bruno, R. Celiberto, C. Gorse, F. Pirani and M. Capitelli, *Chemical Physics Letters* **445** (4-6), 133-139 (2007).

[143] W. Wang, Y. Wu, M. Rong, L. Éhn and I. Černušák, *J. Phys. D: Appl. Phys.* **45** (28), 285201 (2012).

[144] W.-Z. Wang, M.-Z. Rong, F. Yang and Y. Wu, *Chinese Physics Letters* **31** (3), 035202 (2014).

[145] R. D. Johnson. NIST Computational Chemistry Comparison and Benchmark Database [Online]. Available: http://cccbdb.nist.gov/

[146] A. B. Murphy, *Plasma Chemistry and Plasma Processing* **15** (2), 279-307 (1995).

[147] A. B. Murphy, *Chemical Physics* **398**, 64-72 (2012).

[148] P. André, J. Aubreton, S. Clain, M. Dudeck, E. Duffour, M. F. Elchinger, B. Izrar, D. Rochette, R. Touzani and D. Vacher, *The European Physical Journal D* **57** (2), 227-234 (2010).

[149] Y. Cressault, R. Hannachi, P. Teulet, A. Gleizes, J. P. Gonnet and J. Y. Battandier, *Plasma Sources Science and Technology* **17** (3), 035016 (2008).

[150] Y. Cressault, A. B. Murphy, P. Teulet, A. Gleizes and M. Schnick, *J. Phys. D: Appl. Phys.* **46** (41), 415207 (2013).

[151] F. Copeland and D. Crothers, *Atomic Data and Nuclear Data Tables* **65** (2), 273-288 (1997).

[152] J. Aubreton, M. F. Elchinger, A. Hacala and U. Michon, *J. Phys. D: Appl. Phys.* **42** (9), 095206 (2009).

[153] A. Yang, Y. Liu, B. Sun, X. Wang, Y. Cressault, L. Zhong, M. Rong, Y. Wu and C. Niu, *J. Phys. D: Appl. Phys.* **48** (49), 495202 (2015).

[154] T. Kihara, M. H. Taylor and J. O. Hirschfelder, *Physics of Fluids* **3** (5), 715 (1960).

[155] P. F. Bernath, *Spectra of Atoms and Molecules*, 2nd ed. (Oxford University Press, 2005).

[156] R. Walkup, B. Stewart and D. Pritchard, *Physical Review A* **29** (1), 169 (1984).

[157] H. R. Griem, *Spectral line broadening by plasmas*. (Academic Press, New York and London, 1974).

[158] H. R. Griem, *Principles of Plasma Spectroscopy*. (Cambridge University Press, Cambridge, 2005).

[159] E. L. Degl'Innocenti and G. Del Zanna, *Atomic Spectroscopy and Radiative Processes*. (Springer, 2014).

[160] R. Hannachi, Y. Cressault, P. Teulet, Z. Ben Lakhdar and A. Gleizes, *J. Phys. D: Appl. Phys.* **41** (20), 205212 (2008).

[161] R. L. Kurucz and E. Peytremann, *A table of semiempirical gf values. Part 1: Wavelengths: 5.2682 nm to 272.3380 nm* Report No. 0081-0320, 1975.

[162] R. L. Kurucz and E. Peytremann, *A table of semiempirical gf values. Part 2: Wavelengths: 272.3395 nm to 599.3892 nm.*, 1975.

[163] R. L. Kurucz and E. Peytremann, *A table of semiempirical gf values. Part 3: Wavelengths: 599.4004 nm to 9997.2746 nm*, 1975.

[164] L. S. Rothman, I. E. Gordon, Y. Babikov, A. Barbe, D. C. Benner, P. F. Bernath, M. Birk, L. Bizzocchi, V. Boudon and L. R. Brown, *Journal of Quantitative Spectroscopy and Radiative Transfer* **130**, 4-50 (2013).

[165] J.-J. Gonzalez, P. Freton, F. Reichert and D. Randrianarivao, *IEEE Trans. Plasma Sci.* **40** (3), 936-945 (2012).

[166] J. J. Gonzalez, F. Lago, P. Freton, M. Masquère and X. Franceries, *J. Phys. D: Appl. Phys.* **38** (2), 306-318 (2005).

[167] J. Lucas and H. Saelee, *J. Phys. D: Appl. Phys.* **8** (6), 640 (1975).

[168] L. E. Kline, D. K. Davies, C. L. Chen and P. J. Chantry, *J. Appl. Phys.* **50** (11), 6789 (1979).

[169] Y. Qiu and Y. Feng, *Investigation of SF6-N2, SF6-CO2 and SF6-air as substitutes for SF6 insulation*, Conference Record of the 1996 IEEE International Symposium on Electrical Insulation, 1996 (unpublished).

[170] M. Dincer, O. C. Ozerdem and S. Bektas, *IEEE Trans. Plasma Sci.* **35** (5), 1210-1214 (2007).

[171] H. Itoh, Y. Miura, N. Ikuta, Y. Nakao and H. Tagashira, *J. Phys. D: Appl. Phys.* **21** (6), 922 (1988).

[172] X. Li, H. Zhao, S. Jia and A. B. Murphy, *J. Phys. D: Appl. Phys.* **47** (42), 425204 (2014).

[173] X. Li, H. Zhao, J. Wu and S. Jia, *J. Phys. D: Appl. Phys.* **46** (34), 345203 (2013).

[174] H. Zhao, X. Li, S. Jia and A. B. Murphy, *J. Appl. Phys.* **113** (14), 143301 (2013).

[175] H. Zhao, X. Li, S. Jia and A. B. Murphy, *J. Phys. D: Appl. Phys.* **47** (32), 325203 (2014).

[176] G. J. M. Hagelaar and L. C. Pitchford, *Plasma Sources Science and Technology* **14** (4), 722-733 (2005).

[177] G. J. M. Hagelaar, *Plasma Sources Science and Technology* **25** (1), 015015 (2016).

[178] H. Tagashira, Y. Sakai and S. Sakamoto, *J. Phys. D: Appl. Phys.* **10** (7), 1051 (1977).

[179] L. Pitchford, S. ONeil and J. Rumble Jr, *Physical Review A* **23** (1), 294 (1981).

[180] QUANTEMOL database [Online]. Available: www.lxcat.net

[181] IST-Lisbon database [Online]. Available: www.lxcat.net

[182] Morgan database [Online]. Available: www.lxcat.net

[183] Itikawa database [Online]. Available: www.lxcat.net

[184] Hayashi database [Online]. Available: www.lxcat.net

[185] R. B. Metz, C. Nicolas, M. Ahmed and S. R. Leone, *The Journal of chemical physics* **123** (11), 114313 (2005).

[186] V. Colombo, E. Ghedini and P. Sanibondi, *Plasma Sources Science and Technology* **20** (3), 035003 (2011).

[187] W. Wang, M. Rong, Y. Wu, J. W. Spencer, J. D. Yan and D. Mei, *Phys. Plasmas* **19** (8), 083506 (2012).

[188] V. Rat, P. Andre, J. Aubreton, M. F. Elchinger, P. Fauchais and A. Lefort, *Phys Rev E Stat Nonlin Soft Matter Phys* **64** (2 Pt 2), 026409 (2001).

[189] V. Rat, J. Aubreton, M. F. Elchinger, P. Fauchais and A. B. Murphy, *Phys Rev E Stat Nonlin Soft Matter Phys* **66** (5 Pt 2), 056407 (2002).

[190] V. Colombo, E. Ghedini and P. Sanibondi, *Progress in Nuclear Energy* **50** (8), 921-933 (2008).

[191] V. Colombo, E. Ghedini and P. Sanibondi, *J. Phys. D: Appl. Phys.* **42** (5), 055213 (2009).

[192] S. Ghorui, J. V. R. Heberlein and E. Pfender, *Plasma Chemistry and Plasma Processing* **28** (4), 553-582 (2008).

[193] W. Wang, M. Rong, J. D. Yan and Y. Wu, *IEEE Trans. Plasma Sci.* **40** (4), 980-989 (2012).

[194] D. A. Dahl, T. H. Teich and C. M. Franck, *J. Phys. D: Appl. Phys.* **45** (48), 485201 (2012).

[195] M. Bhalla and J. Craggs, *Proceedings of the Physical Society* **76** (3), 369 (1960).

PUBLICATION LIST

Journals (international)

1. **L. Zhong**, X. Wang, M. Rong, and Y. Cressault, "Effects of Copper Vapour on Thermophysical Properties of CO_2-N_2 Plasma", *Eur. Phys. J. D* 70, 233 (2016)

2. **L. Zhong**, X. Wang, Y. Cressault, Ph. Teulet, and M. Rong, "Influence of metallic vapours on thermodynamic and transport properties of two-temperature air plasma", *Phys. Plasmas* 23, 093514 (2016)

3. **L. Zhong**, X. Wang, M. Rong, Y. Wu and A. B. Murphy, "Calculation of combined diffusion coefficients in SF_6-Cu mixtures", *Phys. Plasmas* 21, 103506 (2014)

4. **L. Zhong**, A. Yang, X. Wang, D. L, Y. Wu and M. Rong, "Dielectric breakdown properties of hot SF_6-CO_2 mixtures at temperatures of 300–3500K and pressures of 0.01–1.0MPa", *Phys. Plasmas* 21, 053506 (2014)

5. X. Wang, **L. Zhong**, J. Yan, A. Yang, G. Han, G. Han, Y. Wu, and M. Rong, "Investigation of dielectric properties of cold C_3F_8 mixtures and hot C_3F_8 gas as Substitutes for SF_6", *Eur. Phys. J. D* 69, 240 (2015)

6. X. Wang, **L. Zhong**, M. Rong, A. Yang, D. Liu, and Song Miao, "Dielectric breakdown properties of hot SF_6 gas contaminated by copper at temperatures of 300–3500K", *J. Phys. D: Appl. Phys.* 48, 155205 (2015)

7. M. Rong, **L. Zhong**, Y. Cressault, A. Gleizes, X. Wang, F. Chen, and H. Zheng, "Thermophysical properties of SF_6-Cu mixtures at temperatures of 300-30,000 K and pressures of 0.01-1.0 MPa. Part I. Equilibrium compositions and thermodynamic properties considering condensed phases", *J. Phys. D: Appl. Phys.* 47, 495202 (2014)

8. X. Wang, **L. Zhong**, Y. Cressault, A. Gleizes and M. Rong, "Thermophysical properties of SF_6-Cu mixtures at temperatures of 300-30,000 K and pressures of 0.01-1.0 MPa. Part II. Collision integrals and transport coefficients", *J. Phys. D:*

Appl. Phys. 47, 495201 (2014)

9. A. Yang, Y. Liu, **L. Zhong**, X. Wang, C. Niu, M. Rong, G. Han, Y. Zhang, Y. Lu, and Y. Wu, "Thermodynamic Properties and Transport Coefficients of CO_2– Cu Thermal Plasmas", *Plasma Chem. Plasma Process*, 36, 1141 (2016)

10. A. Yang, Y. Liu, B. Sun, X. Wang, Y. Cressault, **L. Zhong**, M. Rong, Y. Wu, and C. Niu, "Thermodynamic properties and transport coefficients of high-temperature CO_2 thermal plasmas mixed with C_2F_4", *J. Phys. D: Appl. Phys.* 48, 495202 (2015)

11. Y. Wu, W. Z. Wang, M. Z. Rong, **L. L. Zhong**, J. W. Spencer, and J. D. Yan, "Prediction of Critical Dielectric Strength of Hot CF_4 Gas in the Temperature Range of 300–3500 K", *IEEE Trans. Dielectr. Electr. Insul.* vol. 21, no. 1 (2014)

Journals (Chinese)

12. M. Rong, **L. Zhong**, X. Wang, Q. Gao, Y. Fu, Y. Liu, and D. Liu, "Review of Studies of Equilibrium and Non-Equilibrium Arc Plasma", *Transactions of China Electrotechnical Society*, vol. 31, no. 19 (2016) in Chinese

13. S. Hao, **L. Zhong**, X. Wang, G. Li, M Rong, "Mechanical Life Prognosis of High Voltage GIS Based on Support Vector Machine", *High Voltage Apparatus*, vol. 51, No. 7 (2015) in Chinese

14. W. Wang, M. Rong, J. D. Yan, Y. Wu, **L. Zhong**, "Investigation of the Dynamic Characteristics and Decaying Behavior of SF_6 Arcs in High Voltage Circuit Breakers during Current-zero Period: a Review", *Proceedings of The Chinese Society for Electrical Engineering (CSEE)*, vol. 35, no. 8 (2015) in Chinese

Conferences

15. **L. Zhong**, Y. Cressault, X. Wang, M. Rong, and Ph. Teulet, "Effects of Copper on Thermophysical Properties and Net Emission Coefficients of CO_2-N_2 Mixtures in High-Voltage Circuit Breakers", The 14th High-Tech Plasma Processes Conference (HTPP 14), Munich, **Germany**, 2016

16. **L. Zhong**, X. Zhang, Z. Xiang, Y. Zhao, S. Liu, X. Wang, Y. Wu, M. Rong,

"Influence of Copper Contamination on Equilibrium Compositions, Thermodynamic Properties, Transport Coefficients, and Combined Diffusion Coefficients of High-temperature SF_6 Gas", The 3rd International Conference on Electric Power Equipment - Switching Technology, Busan, **Korea**, 2015

17. **L. Zhong**, X Wang, A. Yang, D. Liu, Y. Wu and M. Rong, Predominant Particles in SF_6-Cu Mixture at Temperatures of 300-50,000 K, 20th International Conference on Gas Discharges and their Applications, Orléans, **France**, 2014

AUTHOR : Linlin ZHONG

TITLE : Influence of copper contamination on thermophysical, radiation, and dielectric breakdown properties of CO_2-N_2 **m**ixtures as Replacement of SF_6 in Circuit Breakers

THESIS SUPERVISOR : Yann CRESSAULT

SITE : LAPLACE UMR 5213 CNRS, Université Paul Sabatier, 118 route de Narbonne, Bât. 3R3, 31062 Toulouse Cedex 9

Abstract

Sulfur hexafluoride (SF_6) is a greenhouse gas designated by the Kyoto Protocol because of its extremely high global warming potential (GWP). CO_2, N_2, and their mixtures have the potential to replace SF_6 in certain applications, such as circuit breakers. In these electric apparatus, copper vapour resulting from the heating of electrodes can modify the characteristics of arc plasmas, which must be taken into account when setting up physical models. This dissertation, therefore, investigates the thermodynamic, transport, diffusion, radiation, and dielectric breakdown properties of CO_2-N_2 mixtures contaminated by copper at temperatures of $300 - 30,000$ K and pressures of $0.1 - 16$ bar.

The equilibrium compositions are calculated using the minimization of Gibbs free energy with consideration of condensed species. Copper vapour is found to condense at temperatures below 3000 K. Based on the compositions, the thermodynamic properties, including mass density, specific enthalpy, and specific heat at constant enthalpy, are determined according to their definitions. The Debye-Hückel corrections are also considered in the calculation of compositions and thermodynamic properties.

The transport coefficients (including electrical conductivity, viscosity, thermal conductivity) and combined diffusion coefficients (including the combined ordinary diffusion coefficient, combined electric field diffusion coefficient, combined temperature diffusion coefficient and combined pressure diffusion coefficient) are calculated based on the Chapman-Enskog theory. The newly developed Lennard-Jones like phenomenological model potential is adopted to describe the neutral-neutral and neutral-ion interactions in determining collision integrals.

The net emission coefficients (NEC) of gas mixtures are calculated with considering atomic lines and continuum and molecular bands and continuum. The pressure broadening (Van der Waals broadening and the resonance broadening), Stark broadening, and Doppler broadening are taken into account in the determination of escape factors. The continuum radiation of atoms is described by radiative attachment, radiative recombination, and Bremsstrahlung.

The dielectric breakdown properties (including EEDF, reduced ionization coefficient, reduced electron attachment coefficient, reduced effective ionization coefficient, and reduced critical electric field strength) of hot gas mixtures are calculated based on the two-term approximation of the Boltzmann equation. The interactions, including elastic, excitation, ionization and attachment collisions, between electrons and neutral species are taken into account in solving the Boltzmann equation. The ionization cross sections of Cu_2 and CuO which are unavailable in literatures are calculated using the DM method.

Compared with SF_6-Cu mixtures, CO_2-N_2-Cu mixtures present much different thermophysical, radiation, and dielectric breakdown properties. As an arc quenching gas, CO_2-N_2-Cu mixtures have lower $\rho \cdot C_p$ and thermal conductivity at low temperatures but present higher $\rho \cdot C_p$, thermal conductivity, and NEC in the medium temperature range. As an insulating medium, the hot CO_2-N_2-Cu mixtures have much poorer dielectric strength below 2000 K, whereas above 2000 K, they present better dielectric breakdown performance than SF_6-Cu mixtures.

Keywords

CO_2/N_2/Cu, circuit breakers, high voltage, transport properties, radiation properties, Chapman-Enskog method, Net emission coefficient, dielectric breakdown, SF_6 replacement.